Master's thesis

NTNU
Norwegian University of Science and Technology
Faculty of Engineering
Department of Energy and Process Engineering

Krister Aaen Pedersen

Numerical investigation of favorable injection strategies in a dual-fuel CI engine for an ammonia- and diesel-based fuel

Master's thesis in Energy and Environmental Engineering
Supervisor: Terese Løvås
Co-supervisor: Michał T. Lewandowski
June 2022

NTNU
Norwegian University of Science and Technology

Krister Aaen Pedersen

Numerical investigation of favorable injection strategies in a dual-fuel CI engine for an ammonia- and diesel-based fuel

Master's thesis in Energy and Environmental Engineering
Supervisor: Terese Løvås
Co-supervisor: Michał T. Lewandowski
June 2022

Norwegian University of Science and Technology
Faculty of Engineering
Department of Energy and Process Engineering

NTNU
Norwegian University of
Science and Technology

Problem description

The implementation of carbon-free fuels in the transport sector is a highly relevant research area, and ammonia is one of the promising fuels for implementation in compression ignition engines. The master thesis will investigate how different injection strategies of ammonia- and diesel-based fuel in a dual fuel CI engine application can be optimized to reduce the footprint of the combustion. The project will be linked up to the ongoing research of the ACTIVATE project at NTNU. It will be conducted numerical simulations with the purpose of identifying favorable injection strategies for a dual-fuel-based CI engine. In the process of identifying these strategies, an equivalence ratio vs. temperature map will be created. Here regions, where the soot, thermal NOx emission, and N_2O levels exceed a specific limit, will be identified. To surpass these regions, different injection strategies based on for example exhaust gas recirculation (EGR) and timing of fuel injection will be factors prominent for investigation. Detailed chemistry will be applied through the software LOGEsoft, and the investigation will be done by the use of a constant pressure reactor (CPR) and SMR.

Abstract

As the awareness of human-induced climate changes has grown, the quest for clean technologies has become a hot topic. Through agreements such as the Paris Agreement [73], countries have obligated themselves to reduce their greenhouse gas (GHG) emissions. The transport sector accounted for around 27 % of the GHG emissions in 2019, revealing a substantial potential for reduction. To pursue a less polluting transport sector, it was in this thesis investigated injection strategies and produced guidelines for dual fueled compression ignition engines. The two fuels used, with five different blending rations, was n-heptane and the novel fuel ammonia. The investigation provided maps depending on equivalence ratios and temperature where high concentrations of NOx, soot, and N_2O were highlighted. Lastly, to locate favorable injection timings, an investigation utilizing a stochastic reactor model was carried out. The results revealed a significant fuel dependency regarding soot and N_2O emissions, while the high NOx concentration region remained little affected by changing the fuel composition. The low fuel dependency for the high NOx concentrations was traced to the thermal NOx mechanism's contribution. Lower levels of NOx exhibited a fuel dependency to some extent, as the fuel NOx, prompt NOx, and thermal De-NOx mechanisms contributed differently to changing fuel compositions. The soot formation potential was of little concern for cases with more than 50 % of the energy in the fuel provided from ammonia. For these compositions, other emissions such as ammonia slip and N_2O became of greater importance. The N_2O emissions exhibit low formation potential for fully combusted conditions, yielding single digits or low double digits ppm levels. High N_2O levels were obtained in the ignition phase, defined as the region between no combustion and stabilized outlet combustion conditions. In this region, high levels were obtained creating an island shape located at lower temperatures. This region became more significant with increasing ammonia concentration in the fuel, with higher peak levels. This underpins the importance of N_2O consideration when ammonia is introduced into combustion applications. The SRM simulations backed up these findings. However, due to some uncertainties regarding the model, dual fuel operation results were considered preliminary and needs further investigation.

Abstract

Etter hvert som bevisstheten rundt menneskeskapte klimaendringer har vokst, har søken etter rene teknologier blitt et hett tema. Gjennom avtaler som Parisavtalen [73] har mange land forpliktet seg til å redusere sine klimagassutslipp (GHG). Transportsektoren sto for rundt 27 % av klimagassutslippene i 2019, noe som viser et betydelig potensial for forbedring. For å strebe etter en mindre forurensende transportsektor, ble det i denne oppgaven undersøkt injeksjonsstrategier og produsert veiledninger for kompresjonstenningsmotorer som går på to drivstoff. De to drivstoffene brukt i denne oppgaven, med fem forskjellige blandingsforhold, var n-heptan og det grønne alternative drivstoffet ammoniakk. Undersøkelsen ga figurer avhengig av ekvivalensforhold og temperatur der høye konsentrasjoner av NOx, sot og N_2O ble fremhevet. Til slutt ble det utført en undersøkelse med en stokastisk reaktormodell for å finne gunstige injeksjonstidspunkt. Resultatene viste en betydelig drivstoffavhengighet når det gjelder sot og N_2O-utslipp, mens området med høy NOx-konsentrasjon forble lite påvirket av endring av drivstoffsammensetningen. Den lave drivstoffavhengigheten for de høye NOx-konsentrasjonene ble sporet til bidraget til den termiske NOx-mekanismen. Lavere nivåer av NOx viste til en viss grad en drivstoffavhengighet, hvor drivstoff-NOx, prompt NOx og termiske De-NOx-mekanismer bidro i varierende grad til NOx når drivstoffsammensetningen ble endret. Sotdannelsespotensialet var lite bekymringsfullt i tilfeller med mer enn 50 % av energien i drivstoffet fra ammoniakk. For disse sammensetningene ble andre utslipp som ammoniakk-slip og N_2O av større betydning. N2O-utslippene viste lavt formasjonspotensial for fullt forbrente forhold, og gir enkeltsifrede eller lave tosifrede ppm-nivåer. Høye N_2O-nivåer ble oppnådd i antennelsesfasen, definert som området mellom ingen forbrenning og stabiliserte utløpsforbrenningsforhold. I denne regionen ble det oppnådd høye nivåer som skapte en øylignende form lokalisert ved lavere temperaturer. Denne regionen ble mer betydningsfull med økende ammoniakkkonsentrasjon i drivstoffet, med høyere toppnivåer. Resultaten underbygger viktigheten av å hensynta N_2O-utslipp når ammoniakk introduseres i forbrenningsapplikasjoner. SRM-simuleringene støttet også disse funnene. På grunn av noen usikkerhetsmomenter angående modellen, ble resultatene av dual fuel-drift ansett som innledende og trenger ytterligere undersøkelser.

Preface

I would like to start my master´s thesis with a quote from Arnold Sommerfeld. "Thermodynamics is a funny subject. The first time you go through it, you don't understand it at all. The second time you go through it, you think you understand it, except for one or two small points. The third time you go through it, you know you don't understand it, but by that time you are so used to it, it doesn't bother you anymore." This is a good summary of how I have felt through the process of working with combustion during my project- and master´s thesis. The project work started in the fall of 2021, and with the field of combustion being quite new to me, I felt a lot like the first stage of Arnold Sommerfeld´s quote. There were a lot of topics that were new to me, and to put my obtained knowledge during the other years of my degree together to form a scientific report, as well as understanding the results was a thought process requiring high computational brainpower. Through the fall and towards Christmas time, I slowly moved into Sommerfeld´s second stage. I felt that the pieces were coming together, and my knowledge of the subject had increased significantly. I felt like I started to truly understand the chemistry and physics behind combustion processes, yielding a good amount of self-esteem and motivation. When starting the master´s work after the holidays I had a lot of motivation and drive. By that time I understood why I was looking into this subject and what I was looking into. As I dug deeper and deeper into the material of combustion systems, I learned more and more, but at the same time, I realized how much I don´t know. It is like my girlfriend's father said. "Picture that your knowledge is like a balloon. As more knowledgeable air is introduced to the balloon, the surface of the balloon (representing the things you know, you do not know) is growing accordingly. So the more you know, the more you know that you do not know". This put me right back into Sommerfeld´s model, and I believe i have now moved into the third stage.

Either way, the process has been a pleasure, and i look foreword to continue into the world of combustion the next years.

Table of Contents

List of Figures

List of Tables

List of Abbreviations

ϕ Equivalence ratio

A/F Air to fuel ratio

ATDC After top dead center

BMEP Break man effective pressure

BP Brake power

BSFC Brake-specific fuel consumption

BTDC Before top dead center

BTE Brake thermal efficiency

BT Brake torque

CAD Crank angle degree

CFD Computational fluid dynamics

CFR Cooperative fuel research

CI Compression ignition

CNG Compressed natural gas

CN Cetane number

CPR Constant pressure reactor

CR Compression ratio

DICI Direct injection compression ignition

DI Direct injection

DME Dimethyl ether

EGR Exhaust gas recirculation

GHG Greenhouse gases

HACARC Hydrogen-Abstract-Carbon-Addition-Ring-Closure

HCCI Homogenous charge compression ignition

HC Hydrocarbon

HHV Higher heating value

ICE Internal combustion engine

IP Injection pressure

IT Injection timing

LHV Lower heating value

MK Modulated kinetics

PAH Polycyclic aromatic hydrocarbon

PDE Partial differential equation

PDF Probability density function

PM Particulate matter

ppm Parts per million

PSDF Prarticle size distribution function

rpm Rounds per minute

SI Spark ignition

SODI Start of direct injection

SOI Start of injection

SOV Start of vaporization

SRM Stochastic reactor model

TBC Top bottom center

TDC Top dead center

T Temperature

UHC Unburned hydrocarbons

1 Introduction

Ever since the industrial revolution, burning of fossil fuels has contributed to a continuously increasing amount of greenhouse gases (GHG) in the atmosphere. Despite the reduction in carbon dioxide (CO_2) emissions due to the Covid-19 pandemic, the highest ever average annual concentration in the atmosphere was recorded with 412.5 parts per million (ppm) in 2020 [22]. A CO_2 concentration around 50% higher than at the start of the industrial revolution.

To combat these human-induced deteriorated climate changes, 195 different countries signed in December 2015 the Paris Agreement [73]. This agreement commits its participating countries to take actions to reduce their GHG emissions. Several countries have taken further actions, committed themselves to pursue net-zero carbon emissions by 2050 to fulfill their obligations [48].

These actions are bold, however necessary, and the pursuit of meeting these targets has led to an increased interest in the search for novel and clean technologies in recent years. One sector that has attracted attention is the transport sector. This sector alone contributed in 2019 to around 27% of the total GHG emissions [23], revealing a huge potential for emission reduction. To do so, decarbonizing the transport sector, the search for carbon-free fuels such as hydrogen and ammonia, or electrification as an alternative approach, has been a hot topic. The challenge with electrification is the low energy densities in batteries, making them less suitable for heavy-duty long-distance transport [41]. For these applications, energy stored in carbon-free compounds such as hydrogen has shown promising results as an alternative fuel [4]. Hydrogen can either be used directly as a fuel or as an energy carrier. However, strict requirements for storing it as liquid result in high costs and a relatively low overall energy efficiency [25]. To avoid these negative qualities, hydrogen can be stored through a hydrogen carrier or chemical compound such as ammonia. Several studies regarding ammonia have previously been performed to pursue the utilization of ammonia as fuel feasible. Such studies date back to the second world war (or even earlier for steam engines) [18]. Back then, the main goal was to use ammonia as a substitute for fossil fuels for military vehicles due to low availability and supply. As the years passed and peace was restored, the investigation of utilizing ammonia dropped until more recently. It has now become an up-to-date topic, but with an environmental motivation.

In addition to the change towards novel fuels, optimizations of the combustion systems can contribute greatly. To achieve combustion systems suited to meet the future environmental requirements related to climate footprint, fuel flexibility and optimizations of engine systems are important topics to investigate. These optimizations are achieved by studying different engine parameters, whereas some have already been investigated with promising results [59, 45, 18]. When it comes to internal combustion engines (ICE), ammonia has been tested for usage both in spark ignition (SI) engines [31] and compression ignition (CI) engines [28]. In this thesis, blends of diesel and ammonia were numerically investigated in a CI engine. Thus, the focus was shifted toward these applications. CI engines, often called diesel engines, are ICE widely used in vehicles due to their high fuel efficiency and power density. Different after-treatment systems have been applied to reduce the combustion related emissions from the engines. The repercussions of applying these systems are typically decreased engine efficiency and higher cost. Another approach to prevent emissions and, at the same time, improve the effect of after-treatment systems, is to change the engine operating parameters. These include, amongst others, the compression ratio (CR), injection pressure (IP), injection timing (IT), air-fuel ratio (A/F), and exhaust gas recirculation (EGR). Investigating different injection strategies has been shown through several recent studies that can significantly affect the output emissions of NOx, unburned hydrocarbons (UHC), and engine performance as they influences the process of combustion either directly or indirectly [45].

In addition to the engine parameters, different fuel properties that come with different fuels can impact the combustion characteristics. This includes, i.e., different reactivity. As low reactivity fuels such as ammonia have combustion challenges related to low flame speed, narrow flammability limits, and high auto-ignition temperature, dual-fuel combustion can be a practical solution to burn these fuels in a CI engine. This strategy works with the principle of ammonia getting injected prior to the more reactive fuel or pilot fuel. This can happen through direct injection or through port injection, and allows the less reactive fuel to mix with the oxidizer. Then this ammonia-air mixture gets compressed during the compression stroke before the diesel, as a high reactivity fuel,

gets injected directly into the combustion chamber to initiate the combustion process at the desired crank angle.

To avoid engine strategies that result in high emissions, maps dependent on temperature and equivalence ratio (ϕ) have been made for various hydrocarbon fuels highlighting regions with high concentrations of NOx and soot emissions [27, 1]. The maps can be used as guidelines for investigating different injection strategies such as optimizing IP and IT to produce minimum emissions. Previous studies have focused on such maps mainly for hydrocarbon fuels, meaning that the influence novel fuels such as ammonia have on these maps remains uncertain. Another species that has not been included in these maps is the vital climate deteriorating gas nitrous oxide (N_2O) - a gas whose climate impact is around 300 times stronger than CO_2 [69].

For the transport sector, more precisely for road vehicles, the N_2O emissions were for an extended period considered to have an insignificant impact on the total N_2O emissions from a global perspective. A thought that originated because it was seen as unimportant compared to coal and oil combustion. Towards the end of the 20-th century however, the view on this climate deteriorating gas has received growing attention within this sector. An important reason for that is that after-treatment systems such as catalytic converters that aim to reduce other emissions, i.e., NOx, have proven to increase the N_2O emissions [8]. This has, amongst some other factors, resulted in requirements and restrictions for car manufacturers when it comes to N_2O emissions. For instance, the requirement for passenger cars and light-duty trucks is that they must not exceed 0.010 grams/mile during their lifetime [7].

To meet the requirements set by different legislation, optimization of the combustion system is crucial. This includes the geometry of the combustion chamber, the previously mentioned operating conditions, fuel properties, and further on. Obtaining these optimizations experimentally requires a lot of time and experiments, hence an impracticable path. Therefore, numerical alternatives have been applied to lower the cost and use of equipment. Perhaps the most common and accurate numerical methods are 3D computational fluid dynamics (CFD), where the use of Large Eddy Simulations (LES), Direct Numerical Simulations (DNS), etc., are essential. A problem using these methods to solve these complex problems regarding combustion systems is the detailed chemical models required to imitate the chemistry and behavior of the process. This results in high computational costs and resources. To overcome these challenges, the use of 0D/1D calculations has proven to be an effective method for predicting the phenomena that occur during combustion [13, 47, 5]. As an example the use of stochastic reactor models (SRM) has shown to reduce computational time without letting it deteriorate the prediction of the combustion to the point where it must be discarded.

This thesis addresses the uncertainty of N_2O emissions for different fuel blends containing ammonia. This was done by introducing the N_2O emissions into ϕ-T maps for five fuel blends containing ammonia and n-heptane. First, to obtain ϕ-T maps, kinetic calculations with a constant pressure reactor through the computational software LOGEresearch [35] were carried out. Secondly, SRM simulations performed with LOGEengine [34] was applied with the goal of identifying favorable IT. The goal was to avoid high emission-concentration regions and reduce the total emissions. The chemical mechanism applied in this investigation was the one from Seidel et al. [63]. The work aimed to provide a comprehensive guideline to enable clean utilization of ammonia in a dual-fueled compression ignition engine.

2 Literature review

The concept of compression ignition (CI) engines came to light in 1892 by Rudolf Diesel. Developing such technology was to ensure better utilization of heat and improve economic efficiency compared to the more common steam engines. Using diesel in CI engines proved to be more fuel-efficient than gasoline spark ignition (SI) engines, thereby decreasing the carbon footprint. In later years the search for other novel fuels with lower carbon footprints has started. This includes hydrogen, methane, bio-diesels, and ammonia, to name a few. This section will present and discuss a literature review about some of the aspects crucial in the search for a novel and clean combustion system.

For the present thesis, the injection timing (IT) of a dual-fueled engine application with ammonia and diesel as fuel will be addressed through a numerical investigation. By this investigation different combustion conditions can be identified for which one can minimize the pollution and emissions in the form of NOx, soot, and N_2O. Injection strategies have previously been studied and reviewed, and some of the essential findings, which can be of interest to the present investigation, will be provided in the following paragraphs.

2.1 Injection strategies and parameters

A study performed by Ramalingam et al. [59] reviewed several articles related to the effect of varying the operating parameters and antioxidant additives on the performance and emission in a CI engine running on biodiesel. They reviewed articles and summarized the findings up until 2018 on the topic of identifying non-fossil renewable fuels that could perform better than conventional diesel in terms of performance, emission, and combustion characteristics without any modifications to the system. By investigating the operating parameters compression ratio (CR), injection pressure (IP), and IT, the drawbacks, i.e., increased NOx emissions and decreased engine performance that bio-diesel contributes to, could be overcome. They reviewed studies with three approaches; different bio-diesels, bio-diesel with varying operating parameters, and finally, bio-diesel with additives. The present master thesis focuses on operating parameters. Hence the findings related to this topic will be further elaborated. Despite this, it should be noticed that the antioxidant additives showed a reducing effect on the NOx emissions from the engine without affecting the performance or the other characteristics of the emissions. By the articles reviewed related to compression ratio (CR), it was an almost unambiguously trend that by increasing the CR, the brake thermal efficiency (BTE) improved as well as reducing the hydrocarbon (HC), carbon monoxide (CO), and smoke emissions. However, the NOx emissions deteriorated with bio-diesel compared to diesel as fuel. The same behavior was obtained by increasing the injection pressure. The effect of injection timing showed that advancing the injection, and introducing the fuel earlier into the combustion chamber, led to a decrease in smoke, HC, and CO emissions, but with the side effect of increasing the NOx emissions. Also, the BTE showed a favorable behavior when advancing the IT. The opposite results were obtained by retarding the IT.

Another article investigating the effect of varying the operating parameters is the one from Mohan et al. [45]. They reviewed multiple articles related to fuel injection strategies for performance improvement and emissions reduction in CI engines. The parameters considered were varying IP, IT, injection shape, and split/multiple injections. When looking into pressure, it was an understanding, similar to what Ramalingam et al. [59] underpin, that increasing the IP leads to a higher BTE while lowering the CO, HC, and smoke emissions. The NOx emission worsened with the increase in pressure. This was argued to be a repercussion of increasing the injection pressure, leading to improved atomization and better air-fuel mixing. This again results in an earlier start of combustion, leading to higher temperatures during the combustion. These conditions facilitate the thermal NOx mechanism and increases the total NOx emissions because of the high premixed heat release rate. Another tendency was that the IT should be retarded with increased IP to meet the new operating conditions. This was stated to be an effect of early combustion caused by the increase in IP causing the fuel velocity into the chamber to increase, leading to a rapid mixing. Having ultra-high IP resulted in a reduction of soot emissions but increased NOx emissions. For IT, Mohan et al. concluded, in general, that advancing the IT leads to better performance but with an increase in NOx emissions and smoke. Retarding the fuel IT results in lower NOx and smoke

emissions with no or little deterioration in engine performance when considering thermal efficiency and fuel consumption. It is prominent that the optimal timing is dependent on the engine and the particular fuel used. So, optimization between performance and emissions is needed in each case. It was also concluded that pilot injection is beneficial for reducing combustion noise and NOx emissions, and post-injection could help with soot oxidation.

An article regarding the injection strategy for different fuel mixtures was carried out by Gumus et al. [17]. They performed an experimental investigation of the effects of fuel IP on the exhaust emission characteristics of a DICI engine. The fuel mixtures in this study consisted of biodiesel and diesel, with respectively 0%, 5%, 20%, 50%, and 100% biodiesel by volume as the fuel. The results showed that when the share of biodiesel in the fuel mix increased, so did the NOx, CO_2, and O_2 emissions. The brake-specific fuel consumption (BSFC) also increased, while the smoke opacity, CO, and unburned hydrocarbon (UHC) emissions decreased. One of the main reasons leading to an increase in NOx emissions with an increasing amount of biodiesel in the fuel can be traced to the increased peak temperature in the cylinder, hence making the thermal NOx essential. The increase in BSFC was traced to the lower LHV that biodiesel brings to the table. The effect of increasing the IP was, for blends with a higher percentage of biodiesel in the fuel mix, decreased the BSFC, while for a low percentage of biodiesel in the mix, the change in IP (both lower and higher) led to an increase of the BSFC compared to conventional operation. It was also found that an increase in IP led to a decrease in smoke opacity, UHC, and CO, while increasing the CO_2, O_2, and NOx emissions.

The IT aspects of the injection strategy were assessed by Abd Alla et al. [2]. They experimentally investigated the effect of IT on the performance of a dual-fuel engine. By conducting experiments on a single-cylinder CI engine, they found that advancing the IT of the pilot fuel could significantly improve the efficiency and high emissions at light loads. Their experiments, used diesel as pilot fuel, while methane or propane was used as the main fuel introduced in the intake manifold for mixing with the intake air. The thermal efficiency improved by advancing the IT, which was traced to the high pressure and temperature. The downside of the increased temperature was, also in this case, that it caused the NOx emissions to increase as the thermal NOx mechanism became more prominent. At medium to high loads for the dual-fuel operation, it was concluded that for their setup, advancing the pilot fuel IT was not effective for improving exhaust emissions, as this led to early knocking.

Another article investigating this aspect of engine optimizations through IT is from Mohammed et al. [44]. Here an experimental investigation on the effect of fuel IT at medium IP on the engine characteristics of an compressed natural gas (CNG) DI engine was carried out. The engine was fueled by a small amount of hydrogen in the CNG, more precisely the blends 0%, 3%, 5%, and 8% hydrogen-CNG at engine speeds varying from 2000 rpm to 4000 rpm. They found that at low engine speeds, the performance of the engine, brake torque (BT), brake power (BP), and break mean effective pressure (BMEP) occurred at the IT of 180 crank angles degrees (CAD) before top dead center (BTDC), followed by 300 CAD BTDC and 120 CAD BTDC. The results showed that the fastest heat release occurred at 180 CAD BTDC, which yielded the highest NOx emissions. The increase of hydrogen in the natural gas-based fuel led to an increase in the burn rate and enhanced the engine performance and combustion compared to pure CNG operation. At high speeds (4000 rpm), the IT of 300 CAD BTDC yielded the best engine performance, which implied the mixing of the fuel exhibits an IT dependency. This means that if an engine can work with different IT dependent on, i.e., load, the engine performance can increase. They also concluded that the addition of hydrogen enhanced the engine performance and its corresponding emissions.

Monyem et al. [46] also conducted a study evaluating the effect of injection and combustion timing. They did it on bio-diesel combustion and its associated exhaust emissions. The John Deere CI engine applied in this investigation was operated at three different IT under two different loads. The engine speed was set to 1400 rpm. The results showed a clear tendency that retarding the IT by 3 CAD, compared to advancing it by 3 CAD, led to a reduction in NOx emissions by 35% and 43% for the two different loads. For the CO and HC emissions, the retarded IT resulted in a 50% and 34% decrease compared to the advanced case. This retardation also increased the smoke number.

2.2 Ammonia and dual fuel operation

There have been conducted studies over a long period related to the appliance of ammonia in these CI engines. Han et al. [18] reviewed several articles to systematically address the utilization of ammonia as a fuel in combustion engines. They pointed out that studying the potential of ammonia usage as a fuel in engines has been on and off from as early as 1822, when an ammonia engine was invented to replace the steam engine [18]. Han et al. briefly discussed engines fueled with only ammonia and dual-fuel engines fueled both with ammonia and carbon-based or hydrogen fuels. The article underpinned some technical issues related to ammonia engines, which need further investigation to make the use of ammonia feasible. First, they pointed out the combustion characteristics of ammonia regarding the problems of low flame propagation speeds and high auto-ignition temperatures. These characteristics lead to instabilities in engine combustion and difficulties regarding cold starts. The most used method for handling this challenge is using dual-fuel or fuel blend technologies, such as diesel as pilot fuel. Another challenge pointed out with ammonia as fuel is the emissions related to ammonia combustion. In particular, NOx emissions are a major factor for pollution in ammonia engines. In addition to this, the low combustion temperature of ammonia can cause disadvantages related to complete fuel oxidation and resulting ammonia emissions or slip. Here it was stated that after-treatment technologies for ammonia engines are important for future research. Lastly, they pointed out the importance of accurate combustion models for engine combustion control strategies development. Here, SRM calculations can play a vital role and will be addressed later in this section.

One of the articles reviewed by Han et al. [18], which considers both ammonia and IT is one from Lee and Song [28]. They developed a combustion strategy for an internal combustion engine fueled with ammonia. In their study, simulations with various conditions with different ratios between the pilot injection and the main injection. They also looked at the timing for the start of injection (SOI). Their results showed that the total NO production was strongly dependent on the SOI variation compared to engine load. It showed that the lowest NO emissions were obtained when the SOI was close to the TDC and increased further away. For SOI earlier than approximately 10-15 CAD BTDC, the NO production started to decrease again. However, very early IT was not investigated. Since the lowest NO emissions were obtained near the TDC, an explanation of ammonia slip contributing to keep the NO low could be the case. However, the NO emissions were overall higher compared to conventional engines. Hence, also in this study, it was concluded that NO reduction methods were required. This article shows that the timing of injection and injection strategies could play a vital role in reducing NO.

One of the earlier works on ammonia usage in engines was a report that came out in 1967. The report was from a project performed by Gray et al. [15] for the Conventional Aviator and Engineering Corporation. The goal was to evaluate and develop additives to improve the performance of ammonia-fueled engines, both spark-ignited and compression-ignition engines. The motivation behind their studies was to find ways to utilize ammonia as a fuel for military operations where the supply of regular hydrocarbon fuels was low. Using spark- and compression-ignition cooperative fuel research (CFR) single-cylinder engines, the effects of the different additives and injection strategies on the engine performance were investigated. For the spark-ignition engines, the two gases, hydrogen and ozone, had the strongest effect on oxidation, whereas hydrogen showed to be the best additive. For the CFR single-cylinder CI engine, they found that acetylene was the best additive to sustain good engine performance at normal CR. Hydrogen as an additive performed well at higher than normal CR. By using dual-fuel, they managed to operate the engine with a CR of 15.2. The obtained CR is considerably less than the previous requirement for ammonia fuel-only engines where a CR of 35 was needed.

This means that other important factors related to optimizing fuel efficiency and emission reduction can be achieved through dual-fuel combustion and blending ratios. A study that has addressed this is the one from Nour et al. [52]. They investigated the impact of the blending ratio of an n-hexanol-diesel mixture on combustion, performance, and emission for a direct-injection compression-ignition (DICI) engine. Using different blending ratios varying from 10 to 50% of n-hexanol by volume, they looked at the effects during five different engine settings, 900 rpm at 10% engine load and 1500 rpm at 25%, 50%, 75%, and 100%. Their findings revealed that adding n-hexanol increased the ignition delay, improved premixed burn mode, and inhibited the diffusion burn mode. Similar

characteristics were seen in a study by Ryu et al. [62], which looked into ammonia and diesel mixtures. Ammonia and diesel mixtures are relevant to the present thesis and could help guide which blends are favorable for optimization. As for the case of Ramalingam et al. [59], adding a supplementary fuel to the diesel fuel decreased the BTE. In the study of Nour et al. [52], the regular diesel fuel had a 0.6% higher BTE than the n-hexanol-diesel blends. Arguably, it could be stated that this decrease is small. With the NOx emissions and smoke opacity reduced by 26% and 54% for a fifty-fifty volume fraction at 100% engine load, environmental benefits with small negative engine performance can be achieved with the dual-fuel operation. The long-term operation in the modes tested was not included in this study but should be considered, as the engine´s wear and tear could be affected.

Reiter and Kong [61] performed in 2010 an experimental investigation of the combustion and emission characteristics of a CI engine running on a dual-fuel approach with a fuel consisting of ammonia and diesel. The specific engine used in the experiments was a John Deere four-cylinder, turbocharged diesel engine with a compression ratio of 17 and a constant engine speed of 1000 rpm. The engine load throughout the experiments varied between 5 to 100%. The results showed that the NO emissions in general increased when ammonia was added to the fuel for the same engine output power. This was traced to the increased addition of fuel NOx. An interesting result was that for low ammonia concentrations in the fuel, up to around 20-30%, the actual NOx emissions were slightly reduced compared to diesel-only operation. This was explained by the fact that the temperature of the combustion and exhaust was reduced with the added ammonia, leading to a reduction in thermal NOx. Reiter and Kong further stated that the NO formation was not a problem as long as diesel accounted for more than 60% of the energy. It was also found that, as expected, CO_2 emissions decreased with the increase of ammonia. Also, the HC and CO emissions were higher with ammonia in the fuel. Further, the soot levels decreased significantly for high ammonia concentrations in the fuel. However, an increase in soot was observed for concentrations yielding a power contribution from the ammonia lower than 20%. The reason could be traced to the lower combustion temperature that ammonia brings, leading to poor oxidation. The results showed that as more diesel was replaced by ammonia, the cylinder pressure decreased, and the ignition delay increased. The longer ignition delay resulted in the fuel-air mixture having more time for mixing and led to more premixed combustion. The peak cylinder pressure decreased compared to diesel-only use. However, on the advantageous side, the expansion pressure appeared slightly higher, as the majority of the combustion occurred during the piston expansion. An important outtake from their article is that the favorable operating range concerning fuel efficiency required 40 to 60% of the energy to originate from the diesel fuel for their specific engine and the conditions investigated. If ammonia accounted for less than 40% of the fuel energy, the ammonia-air mixture in the engine approaches its flammability limit and could be too lean to achieve effective combustion. Based on this finding, one of the fuel-blends investigated in this thesis was within these limits. Reiter and Kong closed their article by stating that injection strategies and after-treatment procedures need to be further investigated to utilize ammonia as a viable alternative to fossil fuels.

Ryu et al. [62] investigated a DICI engine´s combustion and emission characteristics using ammonia and dimethyl ether (DME) mixtures. The engine used for the experiments was a Yanmar L70V single-cylinder DICI engine, operating with four strokes and a compression ratio of 20. To compensate for the cooling caused by the high latent heat of vaporization of ammonia, they heated the intake air to 90°C. The experiments were performed using three different fuel mixtures; pure DME, 60/40 DME/NH3 by weight, and 40/60 DME/NH3 by weight. Prior to injection, the ammonia was mixed with the DME in a fuel mixing tank. The engine was operated under low to medium loads at two different engine speeds, 1900 rpm and 2500 rpm. As the requirements for the IP and temperature get stricter when the ammonia concentration in the fuel is increased, the standardized pressure and temperature were kept quite high during all experiments, respectively 206 bar and 90°C. The results revealed that the engine performance decreased as the ammonia concentration in the fuel increased. It was also found that the IT needed to be advanced as the ammonia concentration increased in the mixture to yield the highest torque. This was also necessary to ensure stable combustion, as ammonia's high resistance to auto-ignition, described in Section 3.11, and the cooling effect caused by the high latent heat of vaporization led the ignition delay to increase. The noticeably advanced IT for the fuel with high content of ammonia gave homogeneous charge compression ignition (HCCI) combustion-like characteristics and low combus-

tion temperatures. Further, it was observed that increasing the engine load could lead to fewer variations in the cycle-to-cycle variations for ammonia-rich fuel. In contrast, a low engine load showed unstable conditions. This was argued to originate from the increased in-cylinder temperature caused by the higher load, reducing the energy loss from the fuel vaporization. The early injection also allowed more time for the fuel to evaporate and better mixing between air and fuel, leading to more rapid combustion. The resulting emissions from varying the fuel mixtures revealed that the soot emissions increased slightly with an increase of ammonia in the fuel. However, they were generally very low. The NOx emissions increased as well due to an increase in fuel NOx, as did the ammonia slip, which underlines the need for exhaust after-treatment. The same conclusion for after-treatment requirements to meet the regulation requirements was made by Reiter and Kong [61]. A previous study from some of the same authors [16] performed with the same engine as in [62] showed similar results with longer ignition delay and increased CO and HC emissions due to the decreased combustion temperature. Also in this case, the NOx emissions increased, traced to the fuel NOx mechanism, which became more prominent with the higher concentrations of ammonia in the ammonia-DME fuel mix. The study also concluded that increasing the IP can allow for more ammonia-rich mixtures and improve combustion and emission characteristics. Back to the later study by Ryu et al. [62], they found that to obtain successful combustion, the IT for 60/40 NH3/DME needed to be between 340 and 90 CAD BTDC, while for 40/60 NH3/DME 50 to 20 CAD, 20/80 NH3/DME between 35 and 5 CAD, and for pure DME 30 to 0 CAD BTDC.

2.3 N_2O

The above articles show that both NOx and soot emissions have been a hot topic for research. As mentioned in the introduction, the GHG N_2O has also been included in engine research in the later years. One article which has looked into both NOx and N_2O emissions in an engine is the one from Li et al. [32]. They experimentally investigated a CFR engine´s NOx, UHC, and N_2O emission characteristics. The engine was modified to operate in HCCI combustion mode. N-heptane was used as a fuel in the experiments. They changed the operating conditions such as intake air temperature and pressure, air to fuel ratio, compression ratio, and exhaust gas re-circulation, to both advancing (knocking) and retarding (incomplete combustion) the combustion. They found that the NOx emissions increased significantly for both knocking and incomplete combustion. The N_2O and UHC emissions deteriorated with retarded combustion. In general, the N_2O emissions were low, except when incomplete combustion was observed.

Recently a study conducted by Yosefi et al. [79] showed that the N_2O emissions deteriorated with ammonia addition. They investigated both experimentally and numerically the effect of different fuel blends and IT of an ammonia-diesel dual-fuel engine. The experimental test was carried out with a single-cylinder, heavy-duty CI engine modified to suit ammonia-diesel dual-fuel combustion. The numerical approach was later verified by comparing it to the experimental results. In their experimental and numerical tests, three different fuel compositions were investigated. These were based on NH_3 energy fraction in the ammonia-diesel fuel and were for the three cases 0%, 20%, and 40% energy fraction from ammonia. The ammonia was introduced with the air prior to the compression, while diesel was used as a pilot fuel injected directly into the combustion chamber 14.2 CAD BTDC. The results showed that increasing the ammonia energy fraction deteriorated the peak cylinder pressure. It also retarded the start of combustion, which was traced to the high auto-ignition temperature and low flame speed that ammonia brings. Contradictory to what one might think, and was the case, i.e., in the work by Reiter and Kong [61], increasing the ammonia fraction resulted in a decrease in NOx emissions. For the highest energy-fraction tested (40% NH3), the emission was reduced by 58.8%. A logical thought is that the ammonia addition to the fuel should greatly increase the fuel NOx mechanism, however, this study believed that the thermal De-NOx process was superior. Besides this, the GHG emissions deteriorated with increased ammonia. This was due to the increased N_2O emissions, which offset the favorable lower CO_2 emissions caused by less hydrocarbon content in the fuel. To further optimize the combustion, they investigated different IT (start of direct injection (SODI) = 14.2, 16, 18, 20, 24, 27 CAD BTDC) for the case where 40% of the energy was accounted for by ammonia. It was shown that the 40% case had its lowest GHG emissions when the start of injection was advanced to 24 CAD BTDC and was found to be 12% lower than the best diesel-fuel only case. The N_2O emissions decreased from

their peak at CADs just before TDC all the way to its most advanced IT. However, looking at efficiency, advancing the SODI further than 20 CAD BTDC led to a decrease in efficiency. From this investigation, valuable information on the N_2O and IT is obtained, both for the investigation that will be conducted in this present thesis and for the further improvement of the technology.

Niki [51] published in 2021 an article where he also investigated the ammonia and N_2O emissions from an ammonia-assisted CI engine. This study looked into different injection strategies to minimize the resulting emissions. He kept the engine speed and the ammonia energy contribution constant at 1500 rpm and 45% throughout the experiments while varying the diesel pilot IT every 5 degrees between 10 and 65 CAD BTDC. The reason for not advancing it past 65 CAD BTDC was that for 70 CAD BTDC and earlier, the engine load and speed became unstable. The results showed that the emission trends changed significantly between IT of 30 to 45 CAD BTDC. The N_2O and NH_3 emissions decreased drastically, while emissions from NOx, CO, and UHC increased. Above 50 CAD BTDC, the NOx and CO gradually decreased; however, UHC emissions continued to increase, and after 55 CAD BTDC, the N_2O and NH3 emissions were observed to increase.

2.4 ϕ-T maps

From these articles, it is clear that the IT can impact emissions greatly. In order to test and investigate a large range of IT, the use of numerical simulations are effective ways to obtain large quanta of results and can produce guidelines for further experimental works. One popular method is to produce ϕ-T maps where high emission regions are located. An example of such a map together with its use-fullness is presented in Figure 1. This figure was obtained from Akihama et al. [1] which investigated the effect of reducing the diesel combustion temperature on soot formation. Using a zero-dimensional calculation with the CHEMKIN II code and 3D-CFD simulations, they analyzed the smoke suppression mechanism in the smokeless rich combustion where the temperature was reduced by a higher exhaust gas recirculation (EGR) rate. It was found that the temperature of the smokeless combustion was reduced significantly with a higher EGR rate than conventional combustion. It was also found that the smokeless combustion avoided the soot formation regions on the ϕ-T map due to the significantly lower temperature compared to conventional operation. To create the ϕ-T map later used in the investigation of revealing the soot formation tendencies, zero-dimensional calculations was used. In their calculations, the formation of soot particles was obtained using a reaction model which describes fuel pyrolysis and oxidation up to C_6 alkanes, formation and growth of polycyclic aromatic hydrocarbons (PAH), and growth of the resulting particles from self coagulation and gas-surface reactions. Their method was inspired by a previous work conducted by Frenklach and Wang [20]. The chemical mechanism used to calculate the soot formation consisted of 292 chemical species and 2189 chemical reactions and was an extension of an earlier published mechanism [43]. The extension of their mechanism is well described in appendix B of their article. An earlier version of the GRI mechanism [67] from 1995 was combined with the mentioned mechanism to obtain the NOx emissions and formation levels. The conditions for the calculations were set to be constant pressure and temperature. To determine sufficient reaction time for creating the soot formation map, they investigated the effect of the reaction time on the 10% soot formation limit. It showed that after 1.0 ms, negligible or minimal changes in the behavior of this limit occur; hence they determined that, for the specific fuel used (n-hexane), a reaction time of at least 1.0 ms is required to avoid underestimation of the soot formation region. This was argued reasonably as it corresponds to a normal diesel combustion period at 2000 rpm (a normal rpm for small vehicles during regular operation). They also investigated the pressure dependency of the 10% sooting limit and found that 6 MPa is sufficient to avoid underestimation caused by pressure, as increasing pressure above this resulted in little change. By using a different fuel, cyclohexane, they found that the fuel dependency of the ϕ-T map is small, as changing the fuel type resulted in only a small change in the soot formation region and peak temperature. They concluded that the fuel type does not influence the ϕ-T map, as the soot yield is normalized by peak soot yield, and they suggested that the ϕ-T map had a universal application. This fuel-soot dependency showed different behavior later in a work by Kitamura et al. [27] and will also be up for discussion in this master thesis.

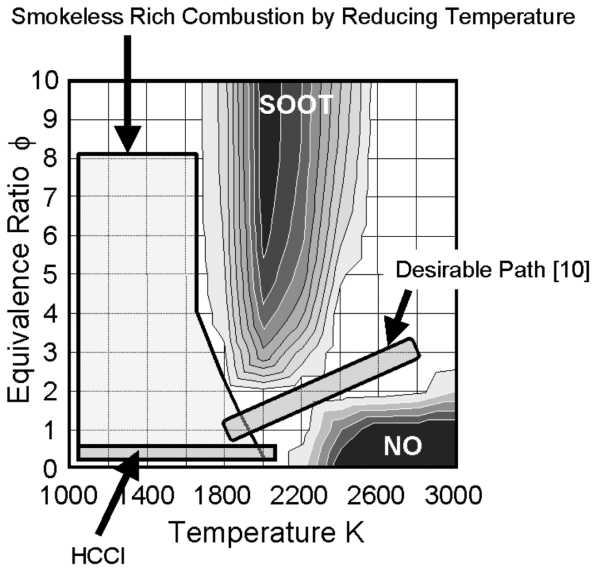

Figure 1: Example of a ϕ-T map, and its utility value. Adopted from [1].

As mentioned, Kitamura et al. [27] also investigated the ϕ-T maps and the dependency of soot formation for various fuels (n-heptane, benzene, toluene, and oxygenated fuels) under conditions similar to the conditions at an internal combustion engine's TDC. The conditions used in their simulations were ϕ from 0 to 7 and temperatures varying from 1300 K to 2500 K at a pressure of 6 MPa. The choice of this pressure was based on the work of Akihama et al. [1], which previously mentioned stated that to prevent under-prediction of soot formation, the pressure needed to be at least 6 MPa. Contrary to Akihama et al., Kitamura et al. used a reaction time of 2 ms in their calculations. This was done because of the wish to eliminate the effect of changing heat release, which depends on reaction time. An et al. [3] argued that using homogeneous gas-phase chemical kinetics for n-heptane and benzene, as used in [27] may not accurately predict specific engine conditions. However, the resulting ϕ-T map is widely used. The reaction model used in Kitamura et al. is based on the mechanism from Wang and Frenklach [75]. The earlier version of the GRI mechanism [67] was also allied to describe the small hydrocarbon reactions. The Wang and Frenklach mechanism was also extended with some reactions for fuel pyrolysis and oxidation for paraffinic hydrocarbons up to C_7 species, oxygenated hydrocarbons, and aromatic hydrocarbons. The GRI mechanism was used to obtain the NOx reactions and formations for the ϕ-T map. Contrary to Akihama et al., Kitamura et al. found that by comparing different fuels such as benzene, n-heptane, and DME, all the soot formation limits were strongly dependent on fuel type. The soot yield of the sooting ϕ-T regions becomes smaller in order of aromatic HC, aliphatic HC, and oxygenated HC. In general, the sooting trend was found to follow: Aromatics > alkynes > alkenes > alkanes. This implies that adding ammonia would change the emission regions in the maps, which will be addressed in Section 7.

So, the NOx and soot emissions have already been studied and implemented in ϕ-T maps; however, another strong greenhouse gas (GHG) has been left out. This GHG is N_2O, and, as previously mentioned has a warming potential around 300 times higher than CO_2. Hence, should be included in the ϕ-T maps. In recent years, the N_2O emissions in engines have received growing attention, mainly due to the increased N_2O emissions caused by NO after-treatment systems. Three articles [51, 79, 32] have been previously reviewed in this thesis, and they underpin why more research on this topic is needed in the nearest future. Therefore guidelines like the ones obtained from ϕ-T maps can be a helpful tool and should include N_2O to prevent making new equipment that fixes one problem but deteriorates another.

2.5 Modelling

To conduct experiments on several different injection strategies for a large variety of fuels demands a large amount of time and resources. To speed up the process of obtaining this knowledge, more time-effective methods can be used. One method which has gained some attention recently is SRM calculations. They have proven superior to regular CFD calculations when time is considered. With adequate emission and performance characteristics, they are a promising tool for first step movements in improving engine technologies. The working principles of a SRM will be outlined later in the thesis under Section 5.2.

One study investigating the validity of the appliance of an SRM in CI combustion is the one from Franken et al. [13]. They modeled a reactivity-controlled compression ignition (RCCI) combustion using SRM together with detailed chemistry. The goal was to check if the SRM-based modeling framework could predict the combustion process and emission formation during RCCI combustion mode in a heavy-duty engine. The engine was a 4-cylinder heavy-duty engine, where three cylinders kept running normally, while the last cylinder was isolated to run RCCI. The resulting single-cylinder research engine was operated under different speeds, loads, EGR, and gasoline fuel fractions. Respectively 10% load at 950 rpm, 50% load at 1500 rpm, and 86% load at 1800 rpm, with the gasoline fuel fraction varying between 10% and 92%. The model was computationally inexpensive compared to traditional 3D-CFD approaches. The obtained results revealed a good prediction of the combustion process, CO_2 and NOx emissions compared to the experimental engine. It was detected some deviations in the CO and HC emissions. The total soot emissions were not included in their research. All in all, they stated that the model was found to be capable of predicting the combustion phasing and the emission trends to some extent.

Other studies which have applied SRM in their investigations and obtained good agreement with experimental data with small deviations are Matrisciano et al. [38], Lewandowski et al. [30], and Mauraya and Akhil [39]. Matrisciano et al. [38] applied an SRM to model in-cylinder combustion in a heavy-duty CI engine and a passenger-car SI engine. Their simulations revealed that the SRM was capable of predicting mixing controlled and flame propagation driven combustion processes. The CO, CO_2, NO, and UHC emissions showed good agreement with experimental data. The obtained data was concluded well within uncertainty ranges caused by sensors inaccuracy, cycle-to-cycle variability, and so on. Lewandowski et al. [30] applied an SRM to numerically investigate the glycerol/diesel emulsion combustion in CI conditions. The SRM constructed exhibited, for the reference diesel fuel, well-reproduced emission characteristics, except NOx emissions which were slightly overestimated. The model missed the trend of increasing CO with the glycerol emulsion. Maurya and Akhil [39] used an SRM to perform numerical simulations on hydrogen HCCI combustion. The simulations were validated with experimental data and agreed well with experimental cylinder pressure and specific NOx emissions.

3 Theory and background knowledge

During a combustion process, a high amount of chemistry and physics-related processes occur. The influence of different factors and strategies such as IT originates and can be explained through basic chemistry and physics. So, to better understand why varying the operating parameters can affect the outcome of the combustion, a brief introduction to some of the most important background knowledge is presented in this chapter.

First, some basic chemistry is provided to get a basic understanding of equivalence ratio and fuel-air composition.

3.1 Chemistry

In most engine applications, the fuel gets burned or oxidized with air. Regular dry air is a composition of several species, amongst others oxygen (20.95% by volume), nitrogen (78.09%), argon (0.93%), and a trace of other gases such as methane, helium, and carbon dioxide [19]. In the present thesis simulations, the air is presumed to consist of mole fractions of 79% nitrogen and 21% oxygen. By applying this assumption, obtaining the stoichiometric conditions is more easily achieved. Stoichiometric combustion occurs when all the oxygen is consumed in the reaction, meaning no oxygen molecules nor any unburnt fuel are apparent in the products. For hydrocarbon fuels the amount of mole for each species, per mole of fuel is found from the following simplified formula:

$$C_xH_y + a(O_2 + 3.76N_2) = xCO_2 + (y/2)H_2O + 3.76aN_2. \tag{1}$$

Here, x and y represent the amount of carbon and hydrogen atoms in the fuel, while a is a function of x and y by the relation $a = x + y/4$. For n-heptane x and y are respectively 7 and 16 yielding the following relations for the stoichiometric combustion:

$$C_7H_{16} + 11(O_2 + 3.76N_2) = 7CO_2 + 8H_2O + 41.36N_2. \tag{2}$$

This means that 11 moles of air per mole of fuel (n-heptane) are required to consume all the oxygen in the combustion. This is, however, an idealization as in an actual combustion process, a significant amount of other species take part in the combustion, and several intermediate reactions are present. The products of the reactants will also contain other molecules such as NO, OH, NO_2, and CO. Regardless of this, stoichiometric combustion is an important quantity used in the combustion process for specifying several characteristics of the combustion such as the equivalence ratio and mixture fraction.

To find the equivalence ratio the air to fuel (A/F) needs to be known. This quantity is defined as the ratio between the mass flow rate of air, $\dot{m}_a$, and the mass flow rate of fuel, $\dot{m}_f$.

$$(A/F) = \frac{\dot{m}_a}{\dot{m}_f}. \tag{3}$$

For SI engines, the air to fuel ratio usually lies in the range of 12 to 18, while for CI engines (A/F) is between 18 and 70 [19]. The equivalence ratio indicates if the fuel-oxidizer mixture is rich ($\phi > 1$), lean ($\phi < 1$), or stoichiometric ($\phi = 1$). This could be an important factor for the combustion system's performance and represents the air to fuel ratio of the process compared to the stoichiometric case [71, 54]. It is defined as follows:

$$\phi = \frac{(A/F)_{stoic}}{(A/F)}, \tag{4}$$

where $(A/F)_{stoic}$ represents the stoichiometric air to fuel ratio.

Suppose one applies the assumption that the composition of the air is 21% oxygen and 79% nitrogen by volume. In that case, the stoichiometric air-fuel ratio can be found as [71]:

$$(A/F)_{stoic} = \left(\frac{m_{air}}{m_{fuel}}\right)_{stoic} = \frac{4.76a}{1}\frac{MW_{air}}{MW_{fuel}}. \tag{5}$$

For diffusion flames (explained in Section 3.3), the fuel and oxidizer streams are initially segregated, and another conserved scalar can come in handy. This scalar is called the mixture fraction. The definition of this scalar is the mass of material having its origin in the fuel stream divided by the mass of the mixture. In other words, it tells how the mass fraction between the fuel and oxidizer is compared to the products. For this scalar, we restrict the flow system to a single inlet stream of pure fuel and a single stream of pure oxidizers. These two then react to form a single product [71]. The mixture fraction, *f*, can be found from:

$$f = Y_F + \left(\frac{1}{\nu + 1}\right) Y_{Pr}, \tag{6}$$

where Y is the mass fraction of fuel (F) and products (Pr) in the mixture, and ν is the amount of oxidizer compared to fuel.

Both the equivalence ratio and the mixture fraction are factors that change locally when varying the IT. If the IT is late, there will be bigger differences in these factors between the different locations in the combustion chamber. If the IT is early, there will be a more homogeneous distribution in the chamber. This again will impact the propagation of the diffusion flame and the combustion.

3.2 Combustion

To understand the working principles and what is happening in an engine, a brief introduction to combustion and engine physics will be presented in the next paragraphs. This is done, as for the brief chemistry introduction, to make the understanding of why operating parameters can affect the engine output.

The next two paragraphs can be found in the previous work; the project thesis [54].

According to Webster´s Dictionary, combustion is defined as *"rapid oxidation generating heat, or both light and heat; also, slow oxidation accompanied by relatively little heat and no light"*. In perhaps more understanding words, Turns [71] summarized combustion as: *"combustion transforms energy stored in chemical bonds to heat that can be utilized in a variety of ways"*.

Today combustion systems are used to heat homes, power automotive and maritime transport systems, and generate power. Combustion occurs either in flame- or non-flame mode. In flame mode, a thin reaction zone of intense chemical reactions propagates through the unburned fuel and oxidizer mixture. It is probably the mode most people are familiar with when thinking about combustion. In the non-flame mode, rapid oxidation occurs in many locations simultaneously within the combustion chamber. When this occurs, the combustion takes place in the whole volume, and no flame located at a specific place is visible. For DICI engines, combustion takes place in flame mode.

3.3 Flames

Flames are classified according to several different characteristics, such as the mixing of the fuel, how the gas flows through the reaction zone, if it is steady or unsteady, and the initial phase of the reactants. If the fuel and oxidizer are closely or fully uniformly mixed, the flame is called a premixed flame. If that is not the case and the reactants must be mixed in the same region where the reaction occurs, the flame is referred to as a non-premixed or diffusion flame. The name comes from the fact that the mixing of the fuel and oxidants has to take place by a diffusion process. The reactants (fuel and oxidizer) are initially separated, and reaction occurs only at the interface between the fuel and oxidizer, where both mixing and reaction occur [71]. This is the case in CI engines. Furthermore, the behavior of the flame movement through the reaction zone can be split into laminar or turbulent. For laminar flow, the mixing and transport occur by molecular processes and can be identified by a low Reynolds number. Turbulent flows have a high Reynolds number, and the macroscopic relative motion of eddies or lumps of fluid drives the mixing and transport.

The initial phase of the reactants can be either gas, liquid, or solid. The flames inside ICE are

unsteady and turbulent (with small regions with laminar transport). For SI engines, the flame is also premixed, and the reactants are gaseous, while for CI engines, there is a diffusion flame and the reactants are initially in the liquid phase before they evaporates when they gets injected through the nozzle. This process is described more thoroughly in Section 3.6.

The CI flame being a diffusion flame is one of the reasons why IT impacts the combustion. Because the local conditions at each specific point are dependent on the IT, the diffusion flame propagates through the combustion chamber differently according to the degree of mixing at each location in the chamber. An early IT will produce, as earlier mentioned, a more homogeneously mixing through the chamber. At the same time, a late IT can lead to regions where the fuel-air mixture is not sufficiently mixed to allow ignition. Hence, the flame propagation will be different.

3.4 Internal combustion engines

Internal combustion engines (ICE) work with the principle of utilizing the chemical energy within the fuel to produce mechanical power. The energy from the fuel gets released by burning or oxidizing inside the engine, hence the name internal. The main two ICE types are spark-ignited (SI) engines and compression ignition (CI) engines [19].

The engines relevant for this thesis are called reciprocating engines. These engines produce power through a piston moving back and forth inside a cylinder. This results in power through a connecting rod and crank mechanism, which drives a shaft. This continuous rotation of the crank produces a cyclical piston motion. The crank makes the piston move up and down, shifting from the top dead center (TDC) to the top-bottom center (TBC). These two piston-placements are defined by when the piston is at its highest location and when it is at its lowest location. A presentation of this is given in Figure 2 as TC and BC, respectively. The minimum cylinder volume occurs when the piston is at TDC and is referred to as the clearance volume (denoted as V_c in Figure 2). The volume which occurs when the piston is at TBC is called the maximum or total volume. The difference between these two volumes is the displaced or swept volume (denoted as V_d in Figure 2) [19]. The swept volume directly affects the compression ratio of the engine.

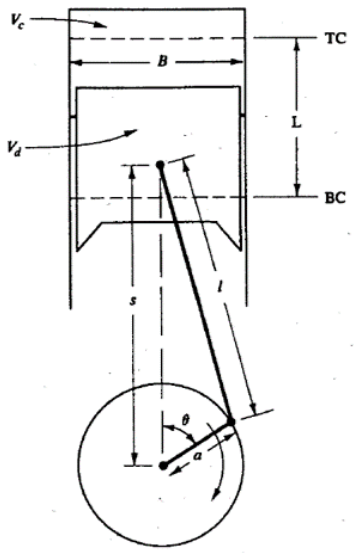

Figure 2: Illustration of one cylinder in a reciprocating engine. Adopted from [19].

3.5 Four-stroke engines

The most standard reciprocating engines operate with a four-stroke cycle. A four-stroke engine consists of several cylinders (from one to sixteen) and comes in many sizes and forms. Perhaps the most common in-vehicle applications are four cylinders in a V-formation. The name "four-stroke"

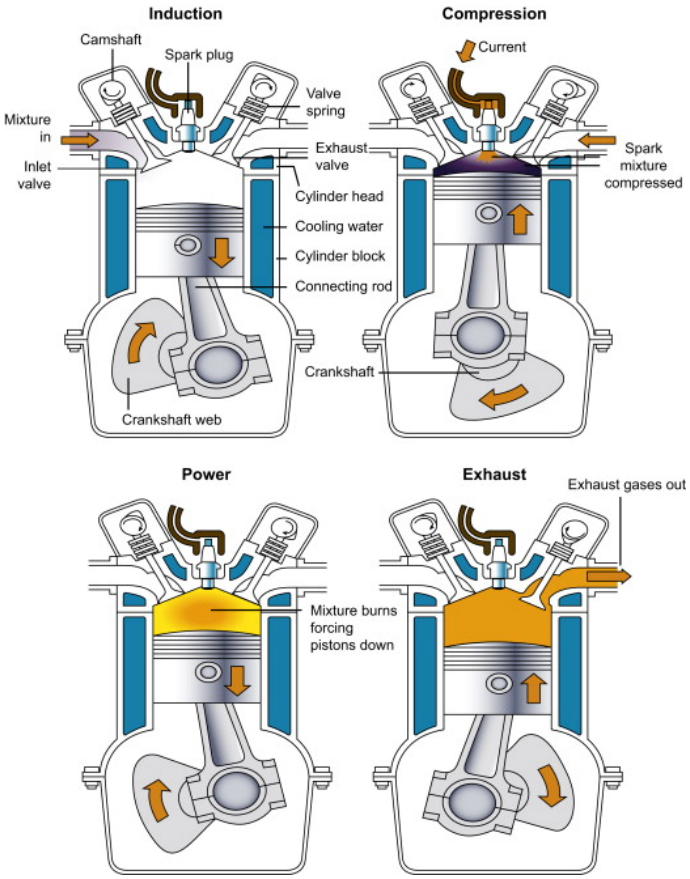

Figure 3: Illustration of construction and operation of a four-stroke SI engine adopted from [9].

comes from its operation where each cylinder has four strokes of its piston, meaning the crank will rotate two times before the whole process is complete. For SI engines, the four strokes consist of an intake or induction stroke, compression stroke, power stroke, and exhaust stroke. This process is represented in Figure 3, borrowed from [9]. This means that firing only occurs every second revolution of the crankshaft. In the first stroke, the intake or induction stroke, the piston moves down, allowing the fuel-air mixture through the intake valves. When the piston reaches TBC, these valves close, and the second stroke, the compression stroke, starts. Here the piston moves upwards, increasing the pressure inside the cylinder. When the piston reaches TDC, the power stroke gets started by a spark igniting the pressurized fuel-air mixture. At this stroke, the piston moves downwards, driven by the expansion of the ignited fuel-air mixture. This stroke produces around five times more work on the piston than what was needed on the piston during the compression stroke [19]. When the piston reaches its lowest position, the exhaust stroke starts. Here the exhaust valve opens, and the upward moving piston drives the exhaust from the combustion through the exhaust valves.

In a CI engine, the ignition inside the cylinder is not caused by a spark but by the heat produced inside the cylinder during the compression stroke. The first stroke in the four-stroke CI engine consists of sucking pure air into the cylinder by opening the inlet valve as the piston moves down. This is contradictory to the gasoline SI engine, where a mix of fuel and air gets injected throughout the intake stroke. At the bottom, the inlet valve closes, and the piston starts on its upwards moving motion compressing the air. The CR described in Section 3.9 is the ratio of the volume inside the cylinder from the start to the end of this stroke [66] and is an important measure of how much pressure the mixture will undergo during the compression stroke. In the compression stroke, only air gets compressed for the major parts of this stroke while the fuel gets injected into the chamber towards the end near TDC [70]. The third stroke, the power stroke, is the stroke where the power or the mechanical work that turns the crankshaft takes place. Here the increased pressure due to the fuel ignition near TDC during the compression stroke results in a force driving the piston

down. The exhaust stroke is the last stroke during one cycle. In this stroke, the exhaust from the combustion gets pushed through the exhaust valve by the upward moving piston. The whole process is presented in Figure 4.

There are some differences if the engine is operated with a duel-fuel approach. For such an operation, it is common to inject the less reactive fuel into the air intake manifold prior to the intake stroke. This leads to mixing between the fuel and air, and this mix gets sucked into the combustion chamber during the intake stroke. That means that not only the air will be compressed, but a mixture of air and fuel. This is possible as the pressure during the compression stroke does not exceed the requirements for auto-ignition of this mixture. The more reactive fuel, often referred to as a pilot fuel, gets injected during the compression stroke to initiate the combustion. This will be described more thoroughly in Sections 3.6 and 3.8

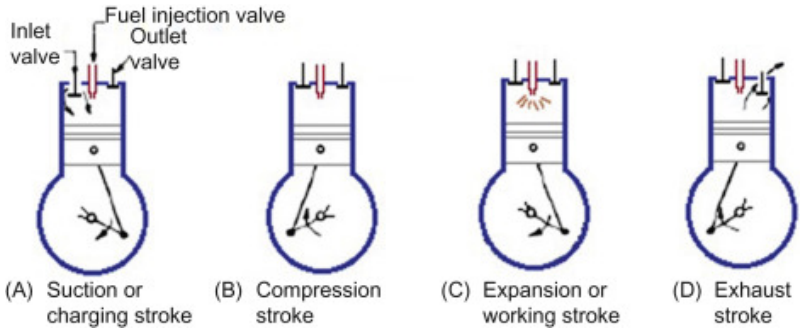

Figure 4: Illustration of construction and operation of a four-stroke CI engine adopted from [66].

3.6 Compression ignition engines

As mentioned earlier, the CI engine has a different approach than a SI engine. In these engines, fuel gets injected into the cylinder right before the combustion process starts, towards the end of the compression stroke. This means that only the air is introduced into the cylinder during the major parts of the intake stroke, unless it is a dual-fuel-operated engine. In this case, it is normal to have a less reactive fuel mixed with the air prior to the intake stroke. Under dual-fuel operation, it is also possible to only suck in the air during the intake stroke, while having two or more different IT during the compression stroke. Injecting the less reactive fuel early in the compression stroke, while the pilot fuel is injected normally towards the later part of this stroke. Nonetheless, the fuel in CI engines is introduced as a liquid that gets injected at high velocity by one or multiple jets through small orifices or nozzles in the injector. Through this process, the fuel atomize into small droplets and ends up in the combustion chamber. Here the fuel vaporizes and mixes with the air that has been pressurized and thereby heated up. Since the fuel gets injected towards the end of the compression stroke, the air has a temperature and pressure above the self-ignition temperature of the fuel-air mixture. Therefore, when the fuel has mixed sufficiently with the air, spontaneous ignition of the mixed fuel occurs after a delay period by a few crank angle degrees (CAD). This spontaneous ignition occurs firstly at the locations where the fuel has mixed well enough with the air, such that the mixture is above its auto-ignition conditions. This combustion causes the pressure within the combustion chamber/cylinder to increase further. The increased pressure results in a shorter delay for the unburned air-fuel mixture in the cylinder before it burns quickly. Varying the load is done by varying the amount of fuel injected, while the airflow for a given engine speed is usually fixed. The injection continues until the required, or desired amount of fuel has entered the combustion chamber. This means that injection of the fuel happens over a period of CAD, resulting in the mixing between the air and fuel being un-homogeneous [19]. The phenomena of un-homogenizes will be addressed later in this section. The conditions that the CI engine operate under depends on several factors and can be highly complex. The factors of importance for this thesis are; the fuel´s characteristics, the design of the engine combustion chamber and injections system, and the engine specific operating conditions.

As described in Section 3.3, the combustion process in a CI engine is unsteady, heterogeneous,

and three-dimensional. Compared to other engine types such as SI, the CI engines exhibit other operating results and requirements. Firstly, since the fuel injection is initiated just before the combustion starts, the risk of knocking, as in SI engines occur from spontaneous ignition of the premixed fuel and air, is negligible [19]. This means that a higher CR can be utilized in CI engines, improving fuel conversion efficiency. Secondly, the injection timing is used to control the combustion timing. This means that the time between the start of injection and the start of the combustion must be kept short. This is also an important factor, as if this period is too long, the maximum cylinder gas pressure can increase above the maximum limit that the engine can undergo. A way to control this is to set a specific requirement for the fuel´s cetane number (CN), described in Section 3.13, to be above a certain limit. Third, the engine can operate without a throttle, resulting in low pumping work requirements, and improved part-load mechanical efficiency. This is connected to the fact that the engine torque is controlled by varying the amount of fuel injected per cycle while the airflow remains almost constant. Forth, as the amount of fuel injected increases, the air utilization during the combustion can cause problems as it can lead to a formation of soot that cannot be burned up before it reaches the exhaust. This soot formation constrains the fuel to air ratio at maximum engine power to 20% leaner than stoichiometric conditions, resulting in lower values of maximum indicated mean effective pressure compared to, i.e., SI engines. Fifth, the CI engine gives a higher fuel conversion efficiency for a given expansion ratio compared to an SI engine. A repercussion of the fact that the diesel in CI engines operates with lean fuel to air ratios, the resulting effective heat capacity ratio ($\gamma = C_p/C_v$) over the expansion process becomes higher than in a SI engine. According to Haywood [19], one of the major challenges within a diesel combustion chamber is achieving sufficiently rapid mixing between the air and fuel to achieve complete combustion within a reasonable crank angle interval. For typical CI engines, Haywood writes that at about 20 CAD BTDC, the fuel injection into the cylinder starts.

CI engines are divided into two main categories based on the design of the combustion chamber. The first category is direct injection (DI) engines. These have a single open combustion chamber where the fuel gets injected directly. The second category is indirect injection (IDI) engines. Here the chamber is divided into one pre-combustion chamber and one main chamber. The pre-combustion chamber is attached to the main chamber through a nozzle or one or more orifices.

For DI engines, the moment and energy of the injected fuel results in a sufficient mixing and distribution of the fuel in the previously injected air inside the chamber. The fuel gets injected through a nozzle designed for each specific engine. The geometry of the piston within the combustion chamber can change concerning different mixing requirements and injection-nozzle specifications. The "bowl" located on the piston surface can have different geometries and, if necessary, contain regions to enhance the swirl inside the chamber. Haywood [19] made a representation of three common types of DICI engine combustion systems. This figure is borrowed and presented in Figure 5. The type provided in Figure 5 (a) is common for large engines, while Figure 5 (b) and (c) are typical for medium to small DI engines.

IDI engines or systems are used for smaller high-speed CI engines, as DI systems do not provide the required mixing of the air and fuel. This relates to the shorter mixing time resulting from a higher rpm. These IDI systems work by the following principle. The air in the combustion main chamber is forced into the auxiliary or pre-combustion chamber during the compression stroke. This leads to a vigorous flow inside the chamber and when the fuel gets injected into it, the combustion initiates. The pressure rise caused by the combustion forces the fluid back to the main chamber. Because of the jet´s high velocity into the combustion chamber, fuel atomizes and mixes with the air and combusts [19].

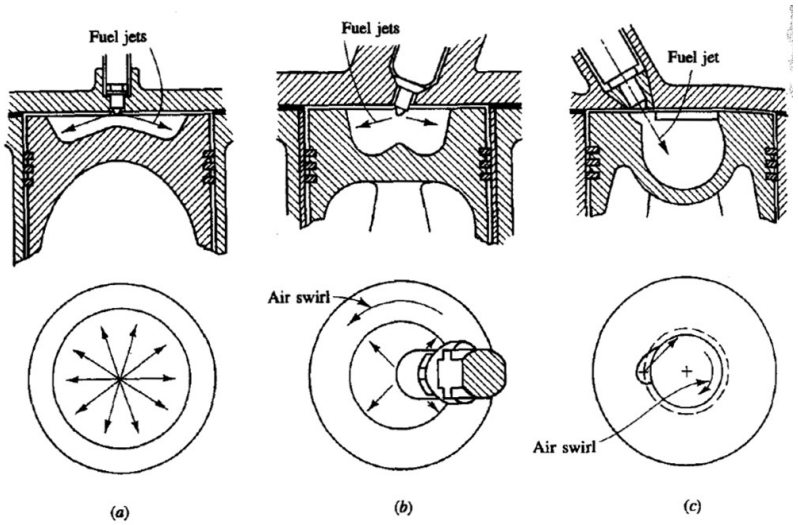

Figure 5: Illustration of common DICI engine combustion systems. (a) represents a quiescent chamber with multi-hole nozzle, (b) bowl-in-piston chamber with swirl and multi-hole nozzle, (c) bowl-in-piston chamber with swirl and single-hole nozzle. Adopted from [19].

3.7 Combustion process

Based on pressure measurements and photographs of diesel DICI combustion, different phases during the combustion process of a DICI engine have been defined. They are usually identified from a heat-release diagram, like the one presented in Figure 6. The first phase is called the ignition delay. This is the period between the fuel starts to get injected to the start of the combustion. The second region is defined as the premixed or rapid combustion phase. Here, combustion in the regions where the fuel has been sufficiently mixed with the air occurs rapidly and only within a few CAD. The third phase is called the mixing-controlled combustion phase. When the air and fuel, which have been premixed during the ignition delay, have been burned and consumed, the heat release rate is controlled by the rate of fuel injection and which rate the mixture becomes mixed and available for burning. In this phase, the burn rate is primarily restricted by the fuel-vapor-air mixing process. The last phase is referred to as the late combustion phase. Here the heat release rate is lower; however, we still have heat release due to, i.e., unburned fuel or if fuel energy is present in the soot. It is also possible that fuel-rich combustion products are present and can be released, or the cylinder charge is non-uniform, and mixing during this period promotes complete combustion [19].

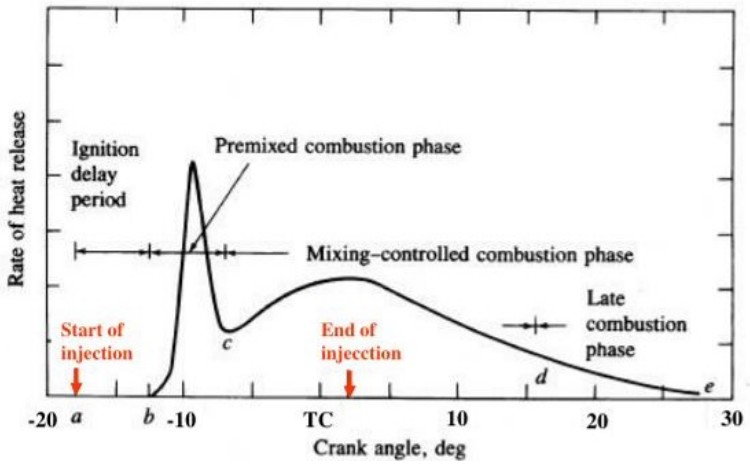

Figure 6: A typical DI engine heat-release-rate diagram with combustion phases identified. Adopted from [19].

3.8 Fuel injection

One of the important applications for the operation of a CI engine is the fuel injection system. As provided in the literature review, ref. Section 2, various parameters have been investigated through the years. These include IP, IT, and nozzle configurations. In this thesis, IT will be the important parameter of consideration when aiming to minimize pollution and emissions from the combustion process.

In a CI engine, the fuel gets injected into the combustion chamber or cylinder through a nozzle with a large pressure difference. This large pressure difference across the injector nozzle is necessary to ensure that the liquid fuel injected into the chamber has a sufficiently high velocity. The importance of this is related to the need for the liquid fuel to atomize into small droplets to enable rapid evaporation and to travel across the combustion chamber during the ignition delay [19]. The ignition delay will be described in Section 3.10. In addition to this, the fuel-injection system needs to inject the right amount of fuel for specific engine conditions. This includes the engine speed and load to each cylinder for each cycle and at the right time in the cycle with the appropriate rate and right spray configuration for the specific combustion chamber. It is also important to determine which CAD are favorable for the fuel injection to enable sufficient mixing before combustion.

There are different ways of introducing the fuels to the combustion chamber for a dual-fuelled engine. One of the more popular ways is to introduce the lower reactivity fuel to the air intake manifold, similar to a port fuel injection approach. This causes the fuel to get well mixed with the air during the intake and the compression stroke. The higher reactivity fuel, pilot fuel, gets directly injected towards the end of the compression stroke close to the TDC to initiate the combustion, as in a DI approach [49]. A representation of this approach is given in Figure 7. For these operations, the IT of the pilot fuel can impact the combustion. This is due to the IT dependency on the different mixing degrees before the piston-placement yields sufficiently high enough pressure and temperature to ignite the mixture. This approach will be used in the investigated in this work, and the results are presented in Section 7.7.

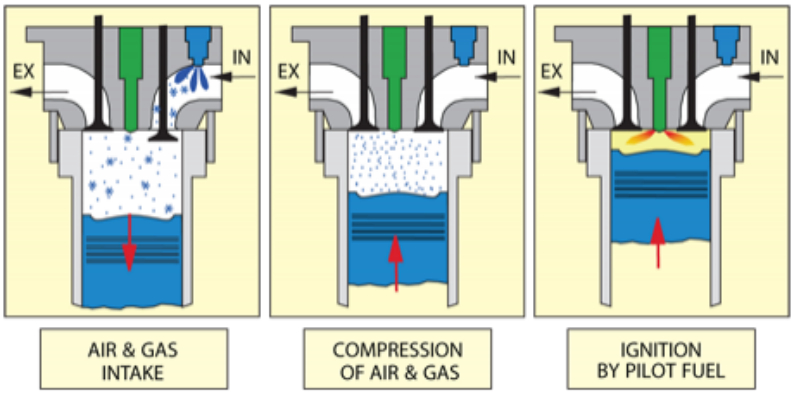

Figure 7: Representation of a dual-fuel CI engine approach. Adopted from [68].

Other approaches are linked to direct injection of both the high reactive and low reactive fuel. For these approaches, both fuels get directly injected into the combustion chamber, but at different IT. Perhaps the most common method within these approaches is to inject the low reactivity fuel early during the combustion stroke, while the high reactivity fuel gets injected later towards the TDC. This gives the less reactivity fuel more time to mix, however still less than by applying port injection for this fuel. Muniappan et al. [49] did a numerical investigation of this direct dual fuel injection in a CI engine. They also looked at another approach, injecting the high reactivity fuel first, followed by the low reactivity fuel. Both the method's resulting emissions and performance were varying with different IT. In this thesis however, only the injection strategy provided in the above section was investigated with obtainable results. Due to some uncertainties in the simulations direct injection of both fuels within the combustion chamber was not successfully computed.

3.9 Compression ratio

One important factor for the engine´s efficiency and operation is the compression ratio (CR). This is the ratio between the maximum volume to the minimum volume inside the cylinder. In other words, between the total volume and the clearance volume. For CI engines, the CR must be such that the temperature in the cylinder increases above the self-ignition temperature for the specific fuel. For regular diesel-fueled CI engines, the CR value is usually between 12 and 24. This CR requirement is less strict for SI engines because the need for self-ignition is redundant. This results in typical values for CR between 8 and 12 for SI engines [19].

3.10 Ignition delay

The ignition delay is an essential factor for determining the IT in a CI engine. For these engines, the ignition delay is defined as the time between the start of injection to the start of combustion, as can be seen in the heat release diagram in section 3.7. This could also be represented in crank angles. The start time of the combustion could be hard to measure, but usually, this time is determined from cylinder pressure data and, more precisely, taken from when the slope of the heat release rate changes. The measure is fuel dependent, and different fuel requires different IT. A low reactive fuel needs more time inside the combustion chamber to mix with the air, hence an earlier IT. A highly reactive fuel can ignite quicker and perhaps have less strict ignition limits. Hence, a later IT can be favorable.

3.11 Fuel characteristics and properties

This section will provide a summary of the characteristics and properties of ammonia, hydrogen, and diesel. This is provided as some properties for the different compounds or fuels can significantly impact the combustion characteristics and performance.

One of these important factors are related to fuels used for transportation, namely the specific gravity. This property is the ratio between fuel and water mass densities at the same temperature. In Table 1, it is chosen to include the fuel and energy densities of the fuel instead of the specific gravity. These, similar to the specific gravity, are good indicators of how much energy can be provided by the fuel on-site and how much fuel that needs to be provided. The energy density tells how much energy that can be utilized from 1 m^3 of fuel. Another important quantity for the combustion of the fuel is the auto-ignition temperature. This is defined as the lowest temperature required to achieve self-sustained combustion without any external drivers. If the fuel is heated to its specific value, with sufficient oxygen, it will ignite. This is one of the working principles of a CI engine as, during the compression stroke, the temperature will increase above the fuel's auto-ignition temperature. For safety considerations, the fuel flash point is an indicative factor. It tells the minimum temperature at which there will be sufficient vaporization of the liquid fuel to form a flammable mixture with air. For storing concerns of the fuel, this flashpoint indicates the maximum temperature the liquid fuel can be stored without the risk of fire. Another quantity regarding the vaporization of the fuel is the kinematic viscosity. If the kinematic viscosity is high, the fuel will be difficult to vaporize. Since most engine applications are based on the principle of vaporizing the fuel before ignition, this is an important measure. This viscosity varies with fuel and conditions, so a value for this is not included in the table. For qualities regarding the combustion and the performance, two factors linked to the heating value can be of interest. The heating value tells how much heat is released per unit volume or mass when it undergoes oxidation at normal pressure and temperature (0.1 MPa and 298 K). The higher heating value (HHV) is the heating value of the fuel when water is condensed. The second heating value, the lower heating value (LHV), is the amount of heat released by burning 1 kg of fuel when assuming the latent heat of vaporization in the reaction products is not recovered. Further, some measures tell how easily the fuel auto-ignites and the quality of the combustion. Two of these are the cetane number (CN), related to diesel fuels, and octane rating for gasoline fuels. The CN is described in detail in Section 3.13.

Properties	Units	Ammonia	Diesel*	Hydrogen (Liquid)	Hydrogen (Gas)
Storage method		Compressed liquid	Liquid	Compressed liquid	Compressed gas
Storage temperature	K	298	298	20	298
Storage pressure	kPa	1030	101.3	102	24821
Auto-ignition temperature	K	924	503	844	844
Flammability limits (gas in air)	Vol. %	16-25	0.6-7.5	4-75	4-75
Fuel density	Kgm^{-3}	602.8	838.8	71.1	17.5
Energy density	MJm^{-3}	11333	36403	8549	2101
Octane rating	RON	120	15-25	>130	>130
LHV	$MJkg^{-1}$	18.6	42.6	120.0	
HHV	$MJkg^{-1}$	22.5	45.6	142.0	
Flash point	K	405	325-369	20	
Normal boiling point	°C	-33.34	180-340	-252.8	
CN	-		40-55**		

Table 1: Main characteristics of ammonia, hydrogen, and diesel. Obtained from [11]. * Some fuels can consist of different compounds, so the value can be inaccurate, but should indicate approximate values. ** Normal modern highway diesel engines.

If one looks at the storage and fuel-energy-densities in Table 1, the challenges related to the utilization of hydrogen as a fuel are clear. Based on the energy densities, the need to store hydrogen as a liquid is prominent. The high pressure needed to store the fuel as a liquid can greatly impact the total fuel efficiency. Ammonia has a higher energy density than both liquid and gaseous hydrogen. This higher energy density, combined with the lower requirements for pressurizing and cooling, makes the storing costs of ammonia significantly lower than for hydrogen. Hence, it reveals the potential of storing hydrogen through this hydrogen carrier, ammonia. It is still noticeable that the energy density of ammonia is significantly lower than the energy density of regular diesel fuels.

One of the reasons why ammonia can stored easier than hydrogen is the normal boiling point. This property tells which temperature the fuel will go from a liquid to a gaseous phase at atmospheric pressure. From the fuels presented in Table 1, it is clear that the normal boiling point of ammonia is significantly higher than for hydrogen (-33°C vs. -258°C). This is why the pressure requirements for liquid storage are significantly stricter for hydrogen. If one looks at the normal boiling point of diesel, it is clear that they can be stored as a liquid in atmospheric pressure, as several hundred degrees is required to make the fuel gaseous. The auto-ignition temperature varies between the fuels. Ammonia has an auto-ignition temperature of 924 K, which is substantially higher than regular diesel (503 K). It is also high higher than hydrogen (848 K). This is one of the reasons why the ignition of this fuel is difficult and requires a secondary fuel or a very high CR if used as a fuel alone.

Compared to hydrogen, ammonia can easily be liquefied and stored, as it requires low pressure (1030 kPa) at ambient temperature. The flammability limit of ammonia in air is the following: the lower flammability limit of ammonia is around 16%, while the upper limit is around 25%. The exact number for these limits varies, and recent studies have shown that this range can be widened to around 15% to 28% [24]. Because of the relatively high concentration range for ammonia to be flammable, it is difficult to reach these concentrations outdoors as ammonia gas is lighter than air and would diffuse in the air. This, together with a relatively high flash point, make the fuel reasonably safe to store. However, it is important to take caution as it is a poisonous gas. Ammonia diffuses quite quickly in the air, so the risk is lower for outside storage than inside.

3.12 Surrogate fuels

Many fuels used in engine applications, i.e., aero-, maritime-, and road vehicles, have highly complex compositions and can consist of hundreds of different molecules, i.e., several different hydrocarbons. To perform computational simulations and investigations of the combustion of these fuels in engine applications, the compositions of the fuels need to be simplified to reduce the computational cost [33]. This has led to the development of chemical kinetic models for surrogate fuels, which have proven to be a useful tool. Surrogate fuels are blends of well-characterized pure components in specific proportions to give the same or similar physical properties and characteristics as the complex fuels under investigation. The properties and characteristics of the surrogate, such as thermal conductivity, density, specific heat capacity, viscosity, ignition delay, flame temperature, combustion velocity, and chemical reaction rate, must be similar to the fuel of interest to produce accurate results and to imitate the characteristics and behavior properly. This includes storage, heating, flow behavior, injection, ignition, combustion, and emissions [55]. Surrogate fuels are also useful in experimental applications, as they can provide a standardized fuel composition, enabling standardized experiments easy to reproduce. They can also be used to validate computational models. It can be a challenge to reproduce all the characteristics and behaviors of the target fuel. Hence, in many cases, specific characteristics and properties are chosen to match the target fuel for the specific purpose of the investigation. By doing this, the engine efficiency, emissions, and critical performance characteristics can be investigated under standardized conditions with good accuracy and reliability.

In this thesis, the diesel fuel is needed to be replaced by a surrogate fuel to be able to carry out the computational calculations. On the other hand, bio-diesel fuel can have a different approach. Pitz et al. [55] assessed in 2011 the current status of diesel fuel surrogate development. According to their advice, the best approach for kinetically modeling bio-diesel fuels is simply to develop kinetic models for each of the pure compounds in the fuel and combine them to produce a mechanism that imitates the target fuel accurately. Hence, no surrogate mechanism is required. This is because compared to, i.e., other diesel fuels, bio-diesel fuels typically have a composition of a small number of distinct ester compounds, and oxidation of all the compounds in the fuel can be computed directly.

For diesel fuels, different surrogate models and compositions have been studied. There have been several studies where different compositions of n-decane and 1-methylnaphthalene have been used and investigated as surrogate fuel for low-sulfur diesel with good results [29, 60, 55]. Another surrogate fuel used to represent diesel is n-heptane. Zhang et al. [80] conducted numerical simulations of diesel combustion based on a blend of n-heptane and toluene as a surrogate in a reduced mechanism. In their mechanism, the surrogate fuel distribution was 60% n-heptane and 40% toluene by mass. The mechanism was validated by combustion of diesel fuel in a constant volume vessel and later numerically and experimentally using a light-duty diesel engine and a marine diesel engine. The results showed that by using these two fuels in the reduced mechanism, the flame temperature distribution was reproduced well, and the combustion phase, NOx emissions, and pressure curves showed good agreement with experimental data. For the light-duty diesel engine, a tendency of the pressure curves to be slightly to high in short periods after the injection, and a peak a bit lower compared to experiments was observed. However, they concluded that the main characteristics were well reproduced numerically, and the maximum deviance was 3.5% from experimental values. For the NOx emissions, a slightly higher concentration in the computational results compared to experimental was obtained, but the trend in the decrease of NOx by injection delay was well evaluated.

3.13 Cetane number

An indicator used for diesel fuel combustion characteristics and ignition quality is the cetane number (CN). This is an indicator of the combustion speed and required compression needed for the ignition of diesel fuels. In other words, it is a measurement of the quality of diesel fuels. The higher the CN, the better the fuel burns within the engine´s combustion chamber. For gasoline fuels, a similar number is called the octane rating, however, the octane rating indicates how well the

fuel can resist pre-ignition due to compression. The CN for each fuel is determined by comparing the fuel to a specific blend of cetane and heptamethylnonane that give the same ignition delay. Cetane has a CN of 100, which means that this is the fuel with the shortest time between injection of the fuel into the combustion chamber to ignition. The isocetane heptamethylnonane represents the bottom of the specter with a CN of 15, meaning it has very low ignition quality [19]. Hence, comparing the fuel to a specific volume percentage of cetane and heptamethylnonane that yield the same ignition delay defines the CN number and is given by the following equation:

$$CN = \%n - cetane + 0.15 * \%heptamethylnonane. \tag{7}$$

According to Ronald et al. [9] and Haywood [19], the operating range of CN for regular diesel engines is between 40 and 55.

According to Dimitriou and Javaid [11], ammonia is highly resistant to auto-ignition. Hence it is dependent on the air-fuel mixture ignition source and the CN of a pilot fuel to allow smooth CI operation at normal CR. If ammonia is used as the only fuel, a CR of around 35 is needed to ensure auto-ignition. With a pilot fuel, operation around 15.2 and even 12 can be possible if one uses a high CN secondary fuel. The CN of ammonia was not found; however, having an octane number of around 130 [74] reveals the resistance to auto-ignite and thereby underpins the importance of what Dimitriou and Javaid [11] stated.

4 Emissions

Particulate matter (PM) and nitrogen oxides (NOx) are emissions regarded as sources of air pollution. There has for a long period been research on minimizing the PM emissions related to diesel engines, and several pollution regulations are set for these engines. This is due to the environmental impacts and the associations with health issues when exposed to atmospheres with a high pollution content. N_2O is regarded as the third-most-important GHG, a compound deteriorating the climate and environment. A detailed description of the emissions will be presented in the following sections.

4.1 Soot

In diesel engines, combustion-generated carbonaceous material, referred to as soot, has been a challenge for engine manufacturers for several years. Most of these particulate materials have their origin from incomplete combustion of hydrocarbons from the fuel and some from the lubrication oil in the engine. The particulate emissions from diesel combustion include compounds that could cause health and environmental hazards. Regarding the health issue, the soot particles are so small that they can easily enter the lungs or bloodstream and can lead to health issues such as premature death, heart attacks, strokes, acute bronchitis, and deteriorated asthma in children [53]. As soot particles have a high ability to absorb light and heat, they also contribute to global warming. They absorb heat in the atmosphere and darken the bright surfaces such as ice and snow.

Soot particles are mainly formed from the carbon in the fuel. The process starts with a fuel molecule containing 12 to 22 carbon atoms and a H/C ratio of around 2. The exact details of how soot formation takes place have been a headache for scientists over the years. Only a simple version of the process will be described in this paragraph. The formation process proceeds by condensing vaporized matter, usually by several polycyclic aromatic hydrocarbons (PAH). This complex process involves, amongst others, the production of benzene and acetylene originating from the fuel. Further, these compounds transform into phenyl, a single ring aromatic hydrocarbon. Through a fast polymerization process, the chain of aromatic rings grows. As the amount of aromatic rings grows, a nucleus soot particle is formed. The size of this particle is usually around a few nanometers, and it grows as additional condensation and coagulation occur. The resulting soot particles are spherically shaped and can, through coagulation, form chain-like structures [6]. It ends up as particles normally with a diameter of around a few hundred nm. These particles consist of spherules (20-30 nm in diameter) containing carbon atoms and a H/C ratio of around 0.1.

The composition of the PM is dependent on the conditions in the engine exhaust and the particulate collection system. At temperatures above 500 degrees, the particles are mainly clusters of many small spheres or spheres of carbon. At temperatures below 500 degrees, the particles are coated with absorbed and condensed high MW (molecular weight) organic compounds such as unburned, oxygenated, and polynuclear aromatic hydrocarbons.

Soot formation in a diesel combustion environment normally occurs at temperatures between 1000 and 2800 K, pressures from 50 to 100 atm, and with sufficient air to burn the fuel fully. Regular expressions used for describing the soot formation are soot volume fraction (volume of soot vs. total volume), F_v, number of soot particles per unit volume, N, and the size of the particles, d.

4.2 NOx emissions

The section is based on the earlier project report [54].

A heavily studied subject related to combustion processes is the chemical reactions of nitrogen compounds. The reason why this has been an interesting topic is the impact these species have on the environment and the atmosphere. Nitrogen oxide (NOx) are chemical compounds of nitrogen and oxygen formed from reactions during combustion at high temperatures. NOx is a collective

name for the molecules nitric oxide (NO) and nitrogen dioxide (NO_2). Usually, most of the NOx comes from NO, with smaller amounts of NO_2. In the atmosphere, NO gets continuously oxidized into NO_2, a precursor to acid rain and contributes to the generation of photo-chemical smog [14].

The formation of NOx during a combustion process is complex, and the chemical mechanism obeys hundreds of elementary chemical reactions. However, the conditions under the combustion could significantly impact the outcome. Based on the temperature range, stoichiometric ratio, and the nitrous species present in the combustion chamber, it is possible to distinguish the most dominant groups of chemical reactions. The biggest contributors or sources to NOx formation during the combustion process are the NOx that occurs from the reactions which involve the nitrogen in the air; thermal and prompt NOx, and the reactions that form because of the nitrogen content in the fuel, called fuel NOx.

NO is an important minor specie in combustion, as its contribution to air pollution is high [71]. For combustion with gaseous fuels with no or negligible amounts of nitrogen, nitric oxides are formed mainly by three chemical mechanisms using nitrogen from the air. These three are called the thermal or Zeldovich mechanism, the prompt or Fenimore mechanism, and the N_2O-intermediate mechanism.

Even though the fuel and oxidizer are kept the same, the total NOx can change significantly based on the combustion conditions. Several studies have shown that NOx emissions can be significantly reduced or increased by changing the conditions and injection strategies ([45, 17, 2, 46, 28, 61, 62]). This is why investigations of, for instance, the injection strategies are of importance. One of the major contributors dependent on the conditions is the thermal mechanism. This mechanism dominates the total NOx formation in high-temperature combustion over a quite wide range of equivalence ratios. The prompt mechanism contributes in rich combustion, while the N_2O-intermediate mechanism is of importance in lean, low-temperature combustion and when ammonia is apparent in the fuel [71, 78].

Iavarone et al. [21] have graphically displayed the major steps of determining which mechanism NO is formed from. The figure is presented in Figure 8 and is provided to give a simple introduction for understanding how the different mechanisms pathway to NO formation can be identified.

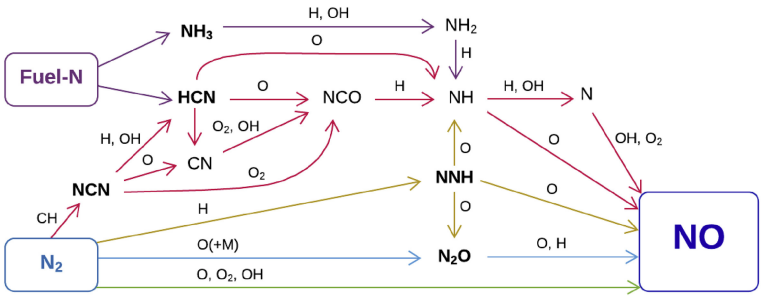

Figure 8: Simplified reaction path diagram illustrating the major steps in the formation of thermal NO (green), prompt NO (red), fuel NO (purple), N_2O(blue), and NNH (yellow). Adopted from [21].

4.2.1 Prompt mechanism

The prompt or often called Fenimore mechanism, is of great importance in rich combustion, where hydrocarbons are apparent in the fuel. For these conditions, nitric oxide formation rates from the prompt mechanism can exceed the contribution to direct oxidation of molecular oxygen by the thermal mechanism. The NO formation from this mechanism shares some of the same routes as the thermal mechanism, however it occurs earlier in the combustion process. It was named prompt NO by Fenimore in 1971 [12] because the NO formation was limited to regions near the flame zone. Here the hydrocarbon radicals react with molecular nitrogen to form amines or cyano compounds. These are then converted to intermediate compounds that finally form NO by oxidation. Before, it was believed that CH and N_2 reacted to form HCN and N, however it is now known to proceed

through the insertion of CH into the N_2 triple bond to give NCN + H [14]. For a fuel such as n-heptane, the process starts with reactions that evidently form CH, however if one ignores the process forming CH radicals for initialization of the mechanism, the prompt mechanism can be written as:

$$CH + N_2 \rightleftharpoons NCN + H,$$

$$NCN + H \rightleftharpoons HCN + N,$$

$$NCN + H \rightleftharpoons HNC + N,$$

where the first reaction is the primary path and the rate-limiting step. This is because this is the slowest reaction, hence limiting the whole process. For equivalence ratios higher than 1.2, the chemistry is highly complex, but for equivalence ratios less than around 1.2, the conversion of hydrogen cyanide, HCN, to form NO follows the following chain of sequence:

$$HCN + O \rightleftharpoons NCO + H,$$

$$NCO + H \rightleftharpoons NH + CO,$$

$$NH + H \rightleftharpoons N + H_2,$$

$$N + OH \rightleftharpoons NO + H.$$

In this thesis's work, it is expected that when the n-heptane fraction in the fuel is high, so is the contribution from the prompt NOx mechanism.

4.2.2 Thermal NOx

The thermal NOx or Zeldovich mechanism is a highly contributing mechanism for high temperature gas combustion. The mechanism is highly relevant in most combustion processes, and in the combustion of fuels which does not contain nitrogen compounds, oxidation of nitrogen (N_2) in the atmosphere could be a significant source of NOx formation [42]. The mechanism consists of two chain reactions. First, an oxygen atom reacts with the triple bond in the N_2 from the oxidizer or the nitrogen from the fuel, shown in the following reaction:

$$O + N_2 \rightleftharpoons NO + N.$$

Here, the released N atoms react quickly with oxygen to form NO.

$$N + O_2 \rightleftharpoons NO + O.$$

The mechanism can be extended by adding a third reaction

$$N + OH \rightleftharpoons NO + H.$$

By adding the third reaction, the set is often referred to as the extended Zeldovich mechanism. According to Turns [71], a rule-of-thumb is that the thermal mechanism is usually unimportant at temperatures below 1800 K. Wünning and Wünning [77], however, argued that the mechanism becomes of importance when $T > 1600$ K.

The reactions described above contain the radicals O and OH, which also attributes for fuel-related NOx emissions. It is also clear that the extended reaction also is included in the prompt NOx pathway. This emphasizes the complexity of determining the sources of emissions. However, because of the timescale of the oxidation process in the fuel, NO is formed rather slowly by the thermal mechanism and is considered to be formed in the post-flame gases. By following this suggestion, the thermal NOx can be decoupled from the fuel NOx mechanism.

4.2.3 N_2O - intermediate mechanism

The N_2O-intermediate mechanism can substantially contribute to NOx formation in lean ($\phi < 0.8$), low-temperature combustion processes. This mechanism is formed by the three steps:

$$O + N_2 + M \rightleftharpoons N_2O + M,$$

$$H + N_2O \rightleftharpoons NO + NH,$$

$$O + N_2O \rightleftharpoons 2\,NO.$$

M represents a third body species. Under conditions where lean premixed combustion is the case, this mechanism can be important in NOx control strategies.

If ammonia is apparent in the fuel, the formation of N_2O is one of the main concerns. This will be addressed in the results, under Section 7.3.

4.2.4 Fuel NOx

Some fuels contain nitrogen in their molecule structure, which applies to ammonia, NH_3. This is usually called the fuel NOx mechanism, and in the combustion of these fuels, the fuel-bounded nitrogen can be a great source of NO and NO_2 and constitutes the dominant source for nitrogen oxides. In this mechanism the nitrogen gets quickly converted to hydrogen cyanide, HCN, or ammonia, NH_3. After this conversation, the molecules follow the prompt-NO mechanism described in Section 4.2.1.

4.2.5 Thermal De-NOx Mechanism

In some applications, ammonia is injected into the exhaust gasses of stationary combustors. The reason for doing this is to initiate a series of reactions that convert NO to molecular nitrogen, N_2 [42]. This process is called Thermal De-NOx and displays some interesting features. To ensure effectually reduction of NO through this process, molecular oxygen must be present in sufficient quantities when adding ammonia. Increasing the ammonia concentration to where it is comparable to the oxygen concentration prevents the process under certain conditions. An illustration of the most important reaction paths in the process is presented in Figure 9.

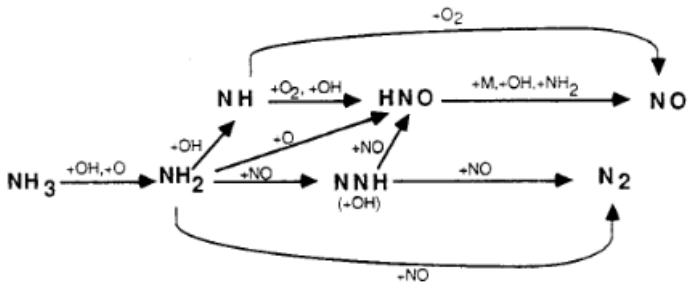

Figure 9: Reaction path diagram for the Thermal De-NOx mechanism. Adopted from [42].

This mechanism could come of great importance when ammonia is apparent in the fuel blends. Moreover, an investigation of the different mechanisms for the cases where the fuel has a fraction of ammonia will be carried out in Section 7.2. It has also been discussed if ammonia slip could help lower the NOx emissions through this mechanism.

4.3 N_2O

Nitrous oxide (N_2O) is regarded as the third-most-important and influential, long-lived greenhouse gas, behind carbon dioxide (CO_2) and methane (CH_4) [50]. N_2O is considered to have around 300 times larger impact on the climate than CO_2, however its amount is still substantially lower in the atmosphere than CO_2. Its lifetime in the atmosphere/troposphere is found to be around a decade, around 109 years depending on the life time estimation model used [57]. N_2O is a relatively inert chemical molecule, but is considered a strong infrared absorber. This result in a heat trapping capabilities in the atmosphere, around 310 times stronger than CO_2 [32].

Another negative impact N_2O has, is that in the stratosphere, the N_2O consume ozone (O_3) to form NO, hence enhance ozone depletion.

Studies have shown that the formation of N_2O in ammonia combustion is due to the two main reaction pathways presented below, and occurs usually at temperatures below 1400 K in the presence of NO and NO_2 [79].

$$NH + NO \rightleftharpoons N_2O + H,$$

$$NH_2 + NO_2 \rightleftharpoons N_2O + H_2O.$$

5 Numerical computations

Since the combustion processes follows the laws of thermodynamics, all simulations conducted with the software LOGEresearch [35] needs to solve the balance equations for mass, energy, and momentum, which all are based on the Navier-Stokes equation for reactive flow.

The balance of mass equation can be expressed as the sum of the total mass flux in and out of the control volume:

$$\frac{\partial m}{\partial t} = \sum_{l}^{N_{in}} \dot{m}_l - \sum_{k}^{N_{out}} \dot{m}_k \tag{8}$$

Here, m is the mass, and l and k represent the inlets and outlets flow. The balance equation for species mass fraction is defined as:

$$\frac{\partial Y_t}{\partial t} = \sum_{l}^{N_{in}} \frac{\dot{m}_l}{m}(Y_{i,l} - Y_i) + \frac{\omega_i W_i}{\rho}, \tag{9}$$

where Y_i is the mass-fraction of species i, ω_i the species net reaction rate, W_i the specie molecular mass, and ρ is the density.

The energy balance equation can be expressed in terms of different parameters, i.e., specific internal energy or specific enthalpy. Suppose specific enthalpy is chosen as the parameter at constant pressure. In that case, the change in energy can be expressed by a term representing the change in enthalpy of the gas entering the control volume and the gas inside it, the heat released by chemical reactions, and two terms that represent the heat exchange with the walls through convection and radiation [36]:

$$\rho c_p \frac{dT}{dt} = \sum_{l}^{N_{in}} \frac{\dot{m}_l}{V} \sum_{i}^{N_s} Y_{i,l}(h_{i,l} - h_i) - \sum_{i}^{N_s} \omega_i H_i + \frac{h_c A}{V}(T - T_W) + \sigma\epsilon\frac{A}{V}(T^4 - T_W^4) \tag{10}$$

The energy balance equation (10), includes the specific heat at constant pressure, c_p, the Stefan-Boltzmann constant, σ, ϵ the emissivity, T_W the wall temperature, and H_i the enthalpy defined as $H_i = W_i h_i$, where h_i is the specific enthalpy. A and V represent the surface area and volume of the control volume.

5.1 Constant pressure reactor

In the present work, a constant pressure reactor (CPR) was used to compute the simulations needed to create the ϕ-T map. The CPR represents a gas that is allowed to expand freely. This results in constant pressure throughout the combustion and is used to replicate, i.e., a tube closed at one end and a movable piston at the other end, similar to an engine cylinder. Because of the characteristics of a CPR, the balance equations (8), (9), and (10) simplifies. First, since the CPR is assumed to be a closed system, no inflow or outflow is considered. This simplifies the mass conservation and species mass fraction equations to become:

$$\frac{\partial m}{\partial t} = 0, \tag{11}$$

and

$$\frac{\partial Y_i}{\partial t} = \frac{\omega_i W_i}{\rho}. \tag{12}$$

Since the specific enthalpy is equal in the whole system, $h_{i,l} = h_i$, the energy conservation equation can be expressed in terms of specific enthalpy as follows:

$$\rho c_p \frac{dT}{dt} = \sigma\epsilon\frac{A}{V}(T^4 - T_W^4) - \sum_{i}^{N_s} \omega_i H_i, \tag{13}$$

where only the heat exchange with the wall through radiation, and the heat released by chemical reactions are left on the right-hand side of the equation.

5.2 Stochastic reactor model

For the simulations computed to replicate the engine operation, a stochastic reactor model (SRM) was applied. SRMs have in later years received an increased interest for engine investigations regarding different fuels. The reason for this attracted interest is the relatively low computational cost compared to the more commonly used CFD. In addition, achieving acceptable accuracy for engine emissions and combustion outputs [13]. As mentioned in Section 2, several studies have applied this reactor type in their investigations already, providing promising results.

Contrary to CFD simulations, which solves transport equations in all spatial dimensions, the SRM calculations describe the state variables and the mixing process based on a probability density function (PDF). This approach lowers the computational cost significantly as it creates a 0D domain- whose mass is discretized in particles. The stochastic particles are a collection of flow elements such as solid particles, gas particles, and turbulent exchange of heat and mass in practical systems. Every particle contains information of the solid phase, pore gas, and bulk gas interaction, and they can mix between each other changing mass properties and heat. Also, it accounts for the interactions regarding heat exchange with the cylinder walls.

In the SRM the PDF gets discretised by mass into particles. The number of particles can be determined in each case. Lesser particles, means that the locality of the particles gets poorer described. As each particle has a set of local quantities that describes chemical compounds, or species mass fractions, and temperatures as random variables. These random variables are denoted by $\phi_1, ..., \phi_{S+1}$. $\psi_1, ..., \psi_{S+1}$ denotes the sample space realization of the S number of variables considered. These discretisations can represents a mass density function, that can be written as: $F_\phi(\psi_1, ..., \psi_{S+1}, t)$. At inlet valve closing, usually where the inlet conditions are set, a specific composition, mass, and temperature are set for each particle, whereas the further behavior of the particles are determined by these conditions as well as some other external interactions. Hence, the partial differential equation describing the change of properties for the particles (the MDF) takes into account the piston movement (Pm), mixing between the particles (M), the heat and composition behavior from chemical reactions (Cr), and heat transfer in the chamber to, i.e, the walls (Ht):

$$\frac{\partial F_\phi}{\partial t} = \frac{\partial F_\phi}{\partial t}|_{Pm} + \frac{\partial F_\phi}{\partial t}|_{M} + \frac{\partial F_\phi}{\partial t}|_{Cr} + \frac{\partial F_\phi}{\partial t}|_{Ht}. \tag{14}$$

A simple representation of the basics and understandings of an SRM is provided in Figure 10.

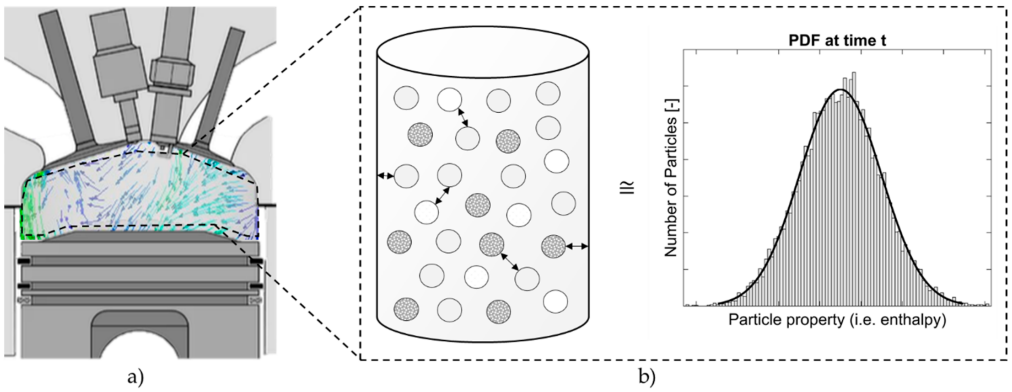

Figure 10: Representation of the basics behind a SRM concept. a) engine system with fuel particles. b) 0-D particles in a SRM somputational space with an visualization of an PDF. Adopted from [38].

6 Method

In the present thesis, an investigation of favorable injection strategies was carried out. The approach consisted of first creating ϕ-T maps with regions highlighting high concentrations of NOx-, N_2O-, and soot emissions for five different fuel mixtures. Secondly, detailed 0D SRM simulations were used to obtain the behavior of particles within the combustion cylinder. The simulations were carried out using the numerical softwares called LOGEsoft [35] and LOGEengine [34]. The software has similar capabilities as the often used CHEMKIN and CANTERA, where complex chemical processes can be simulated and calculated.

The chemical mechanism applied in the simulations was developed by Seidel et al. [64]. This mechanism is well validated for n-heptane and ammonia blends. An extensive elaboration and verification of this mechanism are presented in the project thesis [54] and the paper from Seidel et al. [64]. Nonetheless, the mechanism consists of 402 species and 4750 reactions and is modified based on a previous mechanism provided by Shrestha et al. [65].

6.1 CPR simulations

The first step of the investigation required the creation of ϕ-T maps, revealing how the NOx-, N_2O-, and soot- emissions are expected to behave during engine operation. These maps were obtained by applying a constant pressure reactor (CPR) in LOGEresearch [35]. The physics and kinetics of the simulations using such reactors are presented in Section 5.1.

For the results to be reliable and valuable, the settings of the CPR simulation needed to be specified. To prevent underestimations of the emissions, the conditions were based on the previous studies by Kitamura et al. [27] and Akihama et al. [1]. Akihama et al. examined, amongst others, the effect of pressure and reaction time on the soot formation limits when creating a sooting ϕ-T map for regular diesel operation. They stated that for hydrocarbon fuels, such as n-heptane, a pressure of 6 MPa and a reaction time (final time) of 1 ms were sufficient to avoid the effect of changing heat release and prevent under-prediction of the emissions. Kitamura et al. [27], investigated amongst others n-heptane, similar to the present work. They also tested the condition-dependency for the maps. The results showed that a reaction time of 2 ms and a pressure of 6 MPa were sufficient to achieve usable results. As the setup in the present thesis was compared to the obtained NOx map presented by Kitamura et al., it was in this thesis chosen a reaction time of 2 ms and a pressure of 6 MPa. Another benefit of using this reaction time is that it represents a reasonable time for regular light-duty diesel engine operation. These engines usually operate around 2000 rpm, meaning that a 2 ms reaction time is equivalent to 24 degrees; a normal number of CAD allowed for a combustion sequence. For marine diesel engines, the cruising operation is down to around an rpm of 700 [56], which for 2 ms corresponds to 8.4 CAD. An investigation of the effect of changing this reaction time to 10 ms was also carried out. For an operation with an engine speed of 700, a reaction time of 10 ms is equivalent to 42 crank angle degrees. This investigation is briefly discussed in Section 7.5. The conditions for the CPR simulations are listed in Table 2.

Parameter	Unit	Value
Reactor model	-	Constant pressure reactor
Chemical Mechanism	-	Seidel et al. [64]
Pressure	kPa	6000
Inlet temperature	K	700-3000
Equivalence ratio ϕ	-	0.1-7 ($\Delta\phi = 0.25$)
Final time	ms	2

Table 2: Conditions for simulations.

Furthermore, to capture the main conditions experienced in a DICI engine, it was essential to

ensure outlet temperatures between 1000 K and 3000 K and equivalence ratios between 0.1 and 7. This was achieved by varying the inlet temperature between 700 K, below the self-ignition temperature, and 3000 K. To achieve enough outlet temperatures prone to interpolation between each data point, different increments of the inlet temperature were needed. In regions far prior to ignition, the temperature increment for the inlet temperature was set to 75 K. Closer to the ignition zone, the temperature increments varied between 5 K, 1 K, 0.1 K, and 0.01 K. The equivalence ratio had an increment of 0.25, starting from 0.1. These were thought to produce sufficient data points to ensure reliable results.

The output data points based on equivalence ratio and outlet temperature exhibited behaviors displayed in Figure 11 for ammonia (Figure 11a) and n-heptane (Figure 11b). In Figure 11b, it is evident that simulations and calculations cover large areas of the maps. For $\phi = 0.6 - 2.1$, there are regions during the ignition phase (shown later in Figure 12) where, due to combustion, the outlet temperatures do not have data points over a vast temperature difference. This large area without data points is a repercussion of the steep temperature increase caused by the combustion. A representation of this problem will be given in Section 6.3. Between the data points, the values were linearly interpolated using the in-build MATLAB [37] function interp1. Hence, the resulting N_2O and NOx could be unreliable, in regions where the data points appear scattered. Further, a decrease in temperature was observed for cases with high equivalence ratios and temperatures. This can be seen for high equivalence ratios in Figure 11b, as the inlet temperatures for all the data points go up to 3000 K. An explanation for this is not found in this work, but this is usually a region outside of interest.

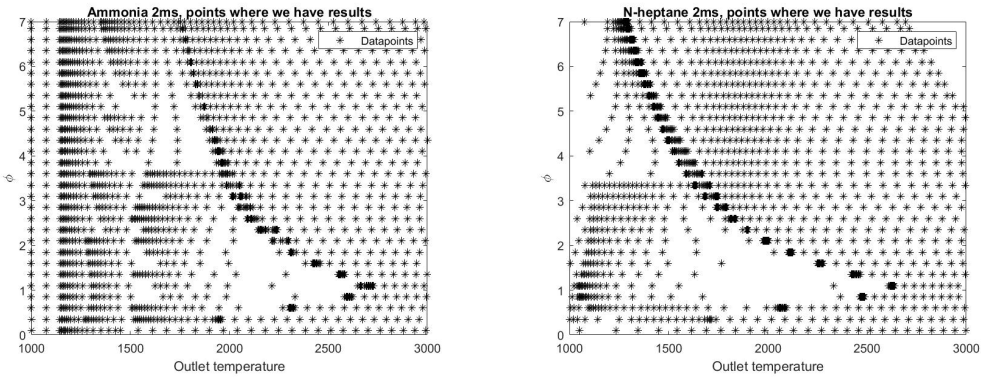

(a) Ammonia (b) n-heptane

Figure 11: Data points for ammonia and n-heptane with a reaction time of 2 ms.

To validate the set-up of the ϕ-T map-producing reactor, and ensuring simulations actually provides the right and wanted results, a comparison against the n-heptane map produced by Kitamura et al. [27] was conducted. The results showed a good coherence despite the fact that they were produced with different chemical mechanisms, different software, and almost 20 years apart. The results of this verification of the computational setup are provided in Section 7.1.

6.2 Cases

When the verification was carried through, maps for fuel blends of both n-heptane and ammonia were created. It was chosen to include five different fuel blends for two different reaction times and three different dilution levels in the investigation. The different cases are presented in Table 3. In that table the ammonia energy fraction were defined based on the lower heating value of ammonia and diesel (LHV_{NH3} and LHV_{diesel}), and the mass fraction Y_{NH3} and Y_{diesel} of the two fuels. The relation is provided in Eq. (15) where E_{NH3} is defined as the energy fraction by ammonia.

$$E_{NH3} = \frac{Y_{NH3} LHV_{NH3}}{Y_{NH3} LHV_{NH3} + Y_{diesel} LHV_{diesel}}. \tag{15}$$

Case number	Fuelblend (based on energy)	Massfraction	Reaction time [ms]	Oxidizer (molefraction)
1	0 % Ammonia 100 % N-heptane	0 % Ammonia 100 % N-heptane	2 ms	21 % O2 79 % N2
2	20 % Ammonia 80 % N-heptane	37.9483 % Ammonia 62.0517 % N-heptane	2 ms	21 % O2 79 % N2
3	50 % Ammonia 50 % N-heptane	70.9828 % Ammonia 29.0172 % N-heptane	2 ms	21 % O2 79 % N2
4	80 % Ammonia 20 % N-heptane	90.7278 % Ammonia 9.2822 % N-heptane	2 ms	21 % O2 79 % N2
5	100 % Ammonia 0 % N-heptane	100 % Ammonia 0 % N-heptane	2 ms	21 % O2 79 % N2
6	50 % Ammonia 50 % N-heptane	70.9828 % Ammonia 29.0172 % N-heptane	10 ms	21 % O2 79 % N2
7	50 % Ammonia 50 % N-heptane	70.9828 % Ammonia 29.0172 % N-heptane	2 ms	15 % O2 85 % N2
8	50 % Ammonia 50 % N-heptane	70.9828 % Ammonia 29.0172 % N-heptane	2 ms	10 % O2 90 % N2

Table 3: Summary of the eight different cases investigated.

Using the lower heating values of 18.6 MJ/kg and 45.5 MJ/kg, for ammonia and diesel, respectively, the fuel mass fractions presented in Table 3 were obtained. In the further mentioning, case 1 to 5 is referred to as the base cases. Case 6 was used to investigate the effect of increasing the reaction time, while cases 7 and 8 were used to study dilution effects. As shown in Table 3, the two different dilution levels were 15 and 10 % oxygen, while the reaction time in case 6 was set to 10 ms.

6.3 Output data

The output results from the simulations were obtained at the final time of 2 ms. Here the NOx emissions were based on the mole fraction of NO and NO_2 in the output files. The N_2O was also obtained in mole fraction, later multiplied by a million to obtain parts per million (ppm). To investigate how the N_2O behaves with outlet temperature, the outlet temperature was recorded for each simulation and data sampling location. The output data for soot formation was soot yield, hereby, soot mass fraction.

As the results provided in Section 7 reveal, a significant amount of reactions occur during the ignition period. The ignition period is, in this thesis, defined as the range of inlet temperatures for a given equivalence ratio that covers the temperatures right before ignition of the fuel, where T_{out} is approximately equal to T_{in}, to the point when the outlet temperature has reached its stabilized temperature after ignition. To be able to distinguish results during the ignition phase and the rest of the map, a stabilized outlet temperature condition is presented and provided as a line for the given equivalence ratios in the ϕ-T ratio maps. The stabilized outlet temperature was found by finding the maximum temperature difference between inlet and outlet temperature for each equivalence ratio. The basis for choosing this definition is that the outlet temperature is approximately equal to the inlet temperature until ignition occurs for each equivalence ratio. If the inlet temperature is increased further, the outlet temperature will increase rapidly before its increase again stabilizes. This phenomenon is presented in Figure 12. After the temperature has reached its stabilized increase, increasing the inlet temperature even further, causes the temperature difference between inlet and outlet temperature to be lower than this obtain peak increased temperature. This is exhibited in Figure 13.

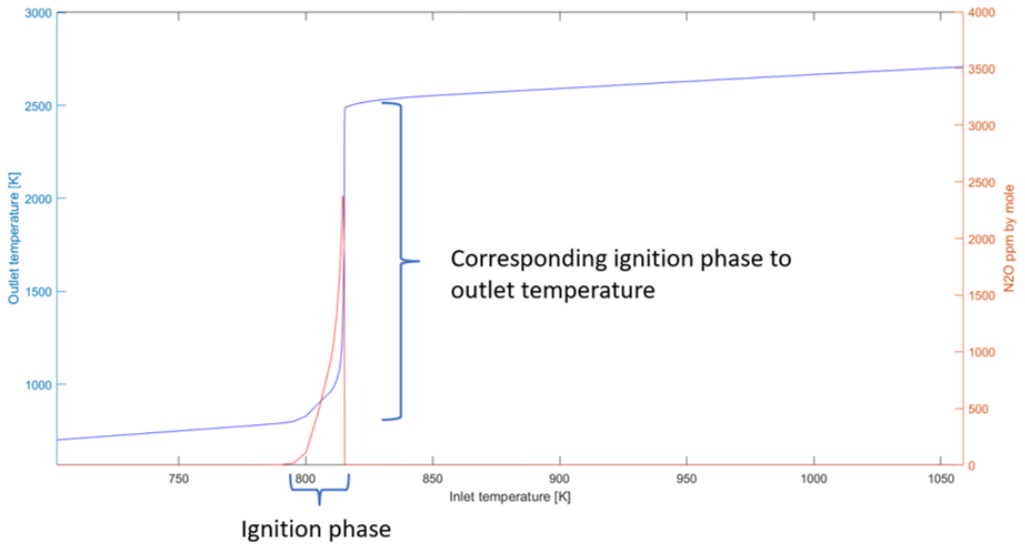

Figure 12: Ignition phase highlighted during the CPR simulations of case 3 at an equivalence ratio of 1.1.

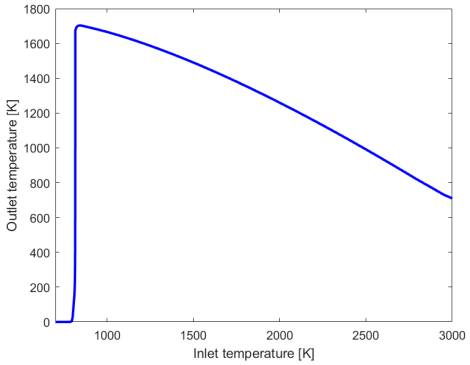

Figure 13: Temperature difference between inlet and outlet temperatures (ΔT) during the CPR simulations of case 3 at an equivalence ratio of 1.1.

6.4 Soot modelling

In combustion including hydrocarbons, the soot formation is a product of many local chemical and physical processes. In this thesis, the modeling of the soot formation was conducted using LOGEresearch's [35] soot modeling tool. This soot model is a detailed kinetic model based on the approach of Mauss [40]. A simplified version of the model is presented in Figure 14 and will be described in detail in this section.

In the model, two processes leading to soot formation are involved and of importance. These are referred to as the source of particle inception, hereunder condensation and coagulation, and the chemical process. The latter describes the reaction occurring on the soot particle's surface, which contributes to surface growth, fragmentation and oxidation. The software solves a set of chemical based moment equations that results in a reasonable prediction of the amount of soot formation by employing a particle size distribution function (PSDF). This means that the total soot mass is assumed to be distributed on a large size scale. To do this, LOGEresearch needs to find the formation of PAHs, particle inception, surface growth, fragmentation, condensation, coagulation, and oxidation by O_2 and OH.

So, first, to investigate the PAH formation rate, an assumption is made to enable the opportunity to find the rate of particle inception and condensation of soot. The assumption is that the PAHs are at a steady-state with the soot. Thereby, based on the concentration of acephentanthrylene

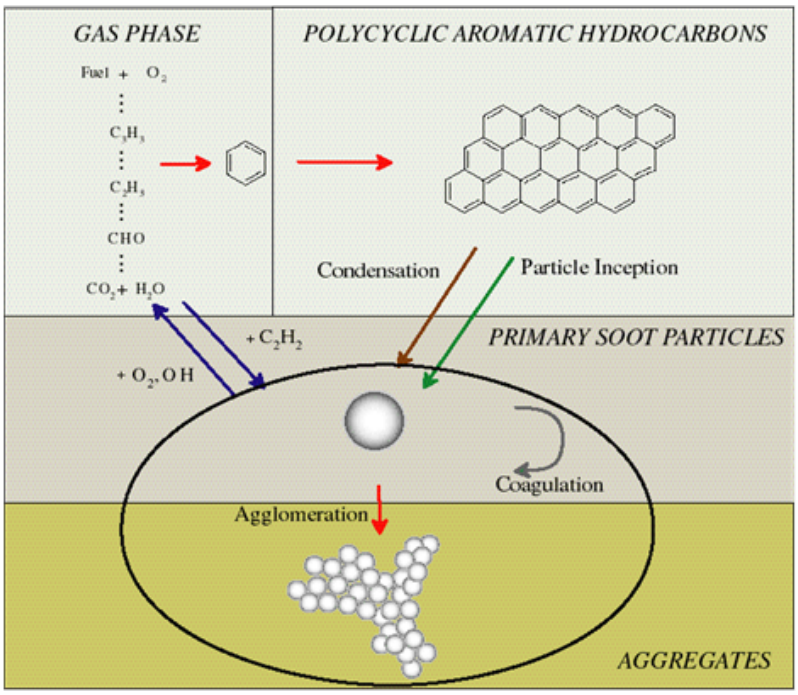

Figure 14: Overall display of the detailed kinetic soot model applied in LOGEresearch. Adopted from [36].

molecules ([A_3R_5m]), an PAH, the reaction rate coefficient for the reaction of acetylene with the A_3R_5m molecules, K_{51}, and lastly, the Avogadro's constant, N_A, the formation rate of PAH can be calculated by the following manner:

$$rPAH = [A_3R_5m]K_{51}N_A10^6. \tag{16}$$

The investigation of the soot surface chemistry is done via modeling a mechanism referred to as Hydrogen-Abstraction-Carbon-Addition-Ring-Closure (HACARC) within the soot model. This mechanism captures the reactions of smaller gas-phase species with solid soot particles and is applied to capture the change of mass of the particles as they either get attached to or removed from the surface of the soot particle. This mechanism is a representation of heterogeneous surface growth and oxidation.

To describe the PSDF, a set of PDEs (partial differential equations) needs to be solved. To model this, the method of moments is used. This method uses a statistical approach and works with the principle that all the mathematical functions are described by their statistical moments. For the soot PSDF, the moments are prescribed in the following way:

$$M_r = \sum_{i=1}^{\infty} i^r N_i, \tag{17}$$

where N_i is the number density of soot particles in the size class i. M_r is the r moment. The first two moments, M_0 and M_1, represent two often used physical properties of soot formation. Namely, M_0 is related to the overall particle number density, in other words, the total number of soot particles without considering the size. M_1 is related to the mean mass or volume of the particles. To find M_1, an expression based on N_i getting multiplied with its size is used. In LOGEresearch [35] the moments are solved by the following equations:

$$M_0 = \sum_{i=1}^{\infty} N_i = N, \tag{18}$$

$$M_1 = \sum_{i=1}^{\infty} iN_i = \gamma_s \frac{\rho}{m_1} = f_v \frac{\rho_s}{m_1}. \tag{19}$$

In these equations, γ_s is the soot mass fraction, ρ the density, ρ_s the density of soot, m_1 the mass difference between two adjacent soot size classes, and f_v is the soot volume fraction. Furthermore, the third and fourth moments are used to find information about the variance and skewness of the PSDF.

In order to run this soot model, the chemical mechanism needs to include a set of soot precursors. The soot precursors have shown to be a good indicator for soot formation and is hence used as a predictor of soot. As stated previously, one of the indicators for soot is the amount of PAH. From other known soot models, such as presented in Kitamura et al. [27], it is evident that on the way to soot coagulation and formation, the process goes through PAH. This is based on the fact that PAHs grow mainly through acetylene (C_2H_2) addition from aromatic rings. This can result in solid soot nuclei by the PAH molecules interacting and bonding with hydrogen. The applided chemical mechanism by Seidel et al. [64] contains the neccesary species required to perfom the soot analysis.

The output from the soot model used in this thesis is the resulting soot mass fraction, Y_{soot}.

6.5 SRM

During the calibration of the SRM, an available LOGE chemical mechanism was applied. This mechanism contains 56 species and 206 reactions. After the calibration was conducted, the mechanism was changed to the same mechanism used to produce the ϕ-T maps. This mechanism from Seidel et al. [64] consists of 402 species and 4750 reactions, more than six times as many species and 23 times as many reactions, requiring a significantly longer CPU time. By applying this enhanced mechanism, a new simpler calibration was need as including more species in the system made some small changes to the combustion process. This secondary calibration will be presented in Section 6.6.

The SRM calculations in this thesis are based on the tutorial case in the LOGEengine software [72] called *DI-Tutorial*. Here a DICI engine experiment fuelled with n-heptane operating at 2000 rpm and a single shot injection were modeled and applied as a reference case for the calibration of the SRM. As the reference case originates from an experiment, the engine geometry and settings are known and presented in Table 4.

Parameter	**Value**
Engine speed [rpm]	2000
Bore [m]	80.0E-3
Stroke [m]	96.0E-3
Connecting rod length [m]	140.0E-3
Compression ratio [-]	16.5
Swirl ratio [-]	0.0
Inlet Valve Closing [CAD ATDC]	-140.0
Exhaust Valve Opening [CAD ATDC]	130.0

Table 4: Engine settings

The gas compositions for the experimental case are also known. Hence, these settings could be directly set as shown in Table 5.

6.6 Calibration of the SRM

As the gas and engine setup is known and set, the next step was calibrating the model. The first analysis needed to replicate the experimental case was the thermodynamic analysis. This targets the pressure trace of an experiment from closing the inlet valve until the end of the compression phase. The analysis was set to end at 2 CAD BTDC, which for this model is 1 CAD before the SOI.

Parameter	Value
Fuel flow rate [$kgs^{-1}cylinder^{-1}$]	3.2E-4
C:H:O count [-]	7:16:0
Surrogate fuel analysis	Compression ignition
Equivalence ratio [-]	0.625
EGR amount [%]	33.0
EGR flag	Relative to mole fraction of EGR and oxidizer
Specific Humidity @ IVC [$g(kg\ air)^{-1}$]	0.0
EGR composition calculation type	Calculate EGR via equivalence ratio

Table 5: Settings for gas compositions.

In this analysis, the pressure offset and EGR amount varied between −15000 Pa and 15000 Pa, and 31% and 35%. The heat transfer model used, was the Woschni model [76], with its constants equal to; Woschni C1 = 2.28, Woschni C2 = 0.0035, and Woschni Swirl ratio = 0. The resulting optimized parameters from the thermodynamic analysis are presented in Appendix A.

To calibrate the rest of the SRM, the combustion analysis package in LOGEengine [34] was applied. This generic algorithm is used to analyze some parameters effect on the combustion process. It uses an algorithm to tune the model to fit the reference combustion process. The target parameter set for calibration is user-specified, and for the calibration done in this thesis, it is set to target the pressure trace from a reference case. This was done by implementing a specific error restriction for pressure at nine different CAD locations, and the pressure deviation limits were set to be below 5%. The parameters whose effect were analyzed were the start of vaporization (SOV), k-epsilon mixing time factor, k-epsilon mixing time injection factor, and k-epsilon VVA mixing time L2 factor. The parameter span for the different factors is presented in Table 6. The rest of the parameters were kept constant and presented in Table 7.

Parameter	Lower limit	Upper limit
SOV [CAD BTDC]	1	-2
k-epsilon mixing time factor [-]	1	15
k-epsilon mixing time injection factor [-]	0.005	0.1
k-epsilon VVA mixing time L2 factor [-]	1	3

Table 6: Combustion analysis parameter span.

The combustion analysis gave the rest of the operation settings for the model to replicate the reference case to its best ability. The case that provided the most accurate results had the operating parameters, with the optimized values as following; SOV = 0.376998 CAD BTDC, k-epsilon mixing time factor = 7.61862, k-epsilon mixing time injection factor = 0.0377661, and k-epsilon VVA mixing time L2 factor = 2.15205. The total error was at 15.58%, while none of the pressure recording locations surpassed the tolerance limit of 5%. The complete report from the analysis is provided as Appendix A.

When the calibration was done the number of particles was increased to 1000, and the chemical mechanism was replaced by the one from Seidel et al. [64]. As the change of chemical mechanism produced slightly different results, a manually calibration were carried out using the new mechanism. Based on the results from the first calibration, changes in the SOV and mixing time injector factor were made. This led to new values of 0.0475 for the mixing time injector factor, and -1.00 for the SOV. The rest of the parameters were kept constant as provided in Appendix B. The pressure trace for the reference experimental case, the calibration with the old mechanism, and the new calibration with the Seidel et al. [64] mechanism is presented in Figure 15.

Parameter	Value
Number of particles [-]	200
Timestep size [CAD]	0.5
Number of consecutive cycles [-]	10
IVC [CAD ATDC]	-140
EVO [CAD ATDC]	130
Mixing Model	Hybrid Curl/EMST (DI)
Stochastic variation	Check
Stochastic Vaporization	Check
Use crevice model	Unchecked
Mixing time model	k-ϵ for compression ignition
Intake valve diameter [m]	0.028
Maximum intake valve lift [m]	0.009
Mean fuel injection pressure [Pa]	2E+08
Mean liquid fuel density [kgm^{-3}]	850
Angular momentum [kgm^{2}s^{-1}]	1E-07
Exhaust valve diameter [m]	0.025
Friction factor [-]	1.5
Length scale factor L1 [-]	7
Length scale factor L2 [-]	3
Axial flow factor [-]	0.2
Init TKE [m^{2}s^{-2}]	18.49

Table 7: Set-up for the SRM.

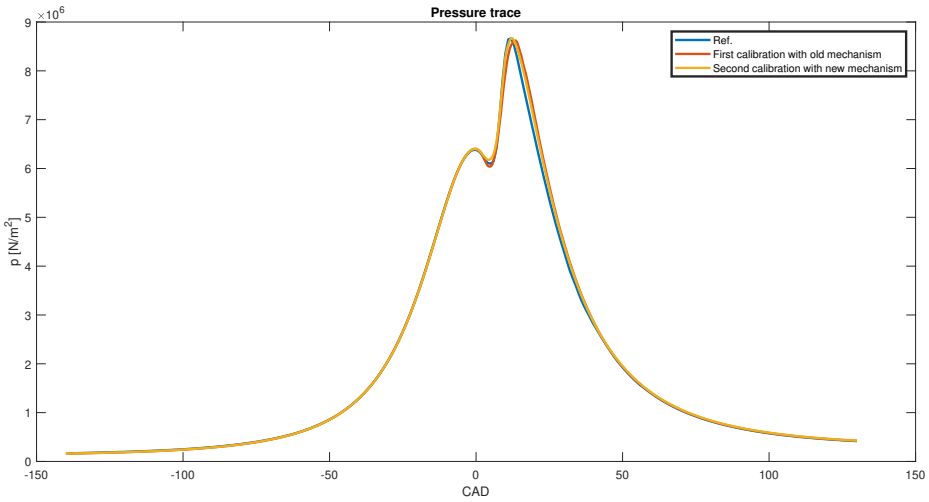

Figure 15: Pressure trace of calibrated SRM and the reference case (ref. [72]).

6.7 Simulations with the SRM

The simulations with the SRM and new mechanism were performed on resources from the NTNU IDUN computing cluster. The outputs from the simulations, were set to produce scatter plots of temperature and equivalence ratio. These were later post-processed in Matlab [37] to produce ϕ-T maps with scatters of particles. The following simulations were conducted; Case 1 with 1000 particles, then three different injection timings for case 2, 3, and 4. For these simulations, the injection of n-heptane was held as the original case, while the ammonia injection varied from -20, -40, -60 CAD BTDC. Lastly port injection of ammonia was simulated for cases 2-4. Here the ammonia was introduced through the gas composition. The amount of n-heptane and ammonia is

each of the cases was set based on achieving similar energy in all cases. This was done by changing the mass of fuel based on the new LHV.

7 Results

In the following sections, an extensive presentation of the obtained results using the method described in Section 6 will be provided, alongside a discussion on how to interpret the results. The simulations conducted with the CPR were set up according to Section 6.1, and the simulated cases are presented in Table 3. In this thesis simulations were conducted to locate NOx-, N_2O-, and soot emissions for the five base cases. The result section will provide results looking into the high NOx emission regions to elaborate on driving kinetics and observed trends. This will also be presented for N_2O and soot regions. Later, all these regions will be combined and presented in one map before SRM calculation results will be presented alongside a discussion on favorable injection strategies.

To validate the set up, as well as having a basis for comparison, one case has been chosen to be pure n-heptane. This is due to available research and to exhibit the behavior of regular diesel operating conditions. Previous maps from Kitamura et al. [27] will be used for verification and are referred to as the reference study. Furthermore, dual fuel operation were investigated for the fuel blends of ammonia and n-heptane. The fuel blends were based on energy fraction from the two fuels yielding 20/80, 50/50, and 80/20 respectively for ammonia/n-heptane. Lastly, a case of pure ammonia was tested, yielding a total of five different fuels. The latter cases have, at the moment this thesis was written, few experimental or previously numerical comparison opportunities. Therefore, a novel investigation that later needs verification.

As the interpretation of the results depends on where in the combustion process the results are obtained, it is in most of the results provided a line differing the fully combusted region from the rest. This is especially highlighted in the N_2O formation investigation. The details around this region are presented in the method section (Section 6.3).

7.1 Verification of the numerical setup

As previously mentioned, to validate the numerical setup, a comparison against the results obtained by Kitamura et al. [27] (reference study) was performed. Figure 16a and 16b show the comparison of both soot and NO emissions. NO is a reliable indicator for the total NOx emissions, as usually the NOx emissions consists of larger portions of NO, and small contributions from NO_2. In the figures, the thesis obtained results are marked with red contour lines upon the map gathered from the reference study.

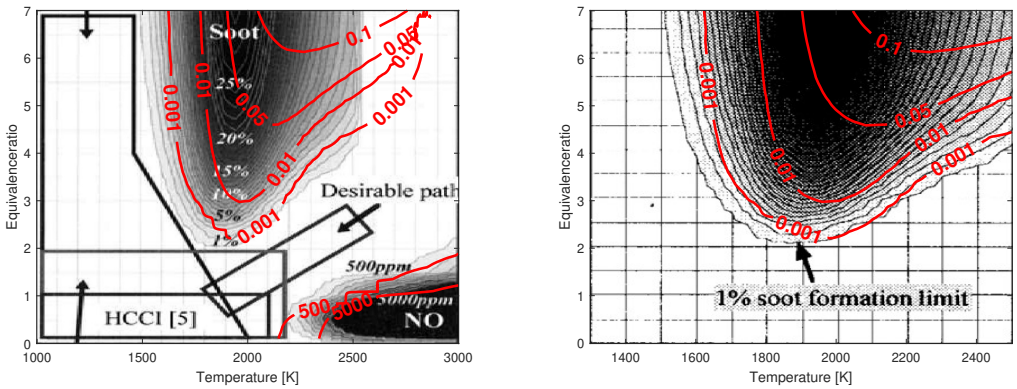

(a) NOx and Soot emission comparison.

(b) Soot emission comparison.

Figure 16: Comparison between the results obtained in this thesis and by Kitamura et al. [27]. The red lines represent 500 ppm and 5000 ppm limit and soot yield limit for 0.1% 1 %, 5%, and 10%.

As Figure 16a reveals, the obtained NO emissions correlate satisfactorily with the reference study [27]. The trends for the 500 and 5000 ppm lines exhibit similar behavior as in the reference study.

However, it is essential to consider that, in their study, the equivalence ratio goes down to 0, while in the present thesis, only the interval between 0.1 and 7.0 was investigated. This results in the half-circle shape obtained in the reference study not being present in the map of the present thesis. Equivalence ratios close to zero might be challenging to estimate either way and may not be relevant for practical applications, as combustion around these conditions is unfavorable. However, inside the combustion chamber, some particles can experience such conditions, and if investigated, it is expected to produce similar trends as in the reference case at lower equivalence ratios. This is because getting combustion in this region becomes more difficult, resulting in low or non NO in the exhaust. The line presenting the 5000 ppm limit is arguably very similar to the reference map, especially for equivalence ratios above 0.5. On the other hand, the 500 ppm limit contour deviates slightly from the reference case. Perhaps the most crucial goal of this thesis is to reveal the trends when changing the fuel composition, and when comparing the 500 ppm limit to the reference line, it is safe to state that the trends for the NO emissions are reproduced well and can be regarded as verified for its purpose. Despite this, it is important to keep in mind that the resulting NOx emissions can appear underestimated if one assumes that the reference study's NO emission results are obtained accurate. It could be argued that their results could be inaccurate or out of date. One argument backing this is that their NO regions were obtained with an early version of the chemical mechanism GRI-mech [67]. This mechanism has been renewed several times since 2002 when the paper of Kitamura et al. [27] was published. According to the publisher of the mechanism [67], the newer version has improved, updated, and expanded the kinetics and target data, as well as added new NO formation and reburn targets. Another important consideration is the equivalence ratio increment used in the reference study of $\Delta\phi = 0.5$, while in this present thesis, a $\Delta\phi$ of 0.25 was applied. The more significant increment for the equivalence ratio could result in higher emissions between the measuring points due to interpolation. However, this requires further investigation using the same chemical mechanism and software. With regards to software, the software used in the two investigations is also different. However, from the project thesis [54], it was found that similar results could be obtained with both SENKIN (as was used in the reference study [27]) and LOGEresearch [35].

When it comes to the soot formation prediction, it is evident from Figure 16b that there is clear deviance in the results from this thesis and the results obtained in the reference study [27]. The first to notice is the magnitude. The 1% soot formation limit differs approximately by an order of magnitude, with the lowest results obtained in this thesis. Further, the difference grows as the region with higher sooting levels quickly shrinks in the present thesis. It can be seen from Figure 16b that the trend for the 1% sooting limit (marked with 0.01 in the thesis-obtained results) is relatively similar to the reference limits for 10% and lower. The same goes for the 0.1% limit (marked with 0.001), which is quite similar to the reference 1% limit. This could imply a magnitude error, and it can be argued that if one wishes to investigate the trend of the soot formation for different blends, the 0.001 limit is a reasonable indicator. However, the value of the sooting limit is questionable. Hence, the soot formation obtained in the further investigation can, based on these results, appear significantly under-predicted compared to the actual emissions. For further comparisons made between the different cases in this thesis, the 0.001 sooting limit is chosen to indicate the potential of soot formation. This is done based on its similarities to the 1% sooting limit from the reference case, and the argument of good trend producing results.

Another reason for deviation in the soot yield can be traced to the soot model, and the chemical mechanism applied. In the reference study [27], a chemical mechanism based on the mechanism from Wang and Frenclach [75] was applied. This mechanism has been applied for several different soot formation studies and has provided results correlating well with experiments. The mechanism was also extended to, for instance, include paraffinic hydrocarbons up to C7 species. The Seidel et al. [64] mechanism was applied in this thesis also including species up to C7. The detailed soot model LOGEresearch applies, is based on the PhD thesis by Mauss [40]. These approaches regarding the soot model and the chemical mechanisms are not identical, meaning deviations between the results could originate from these differences. More detailed investigation of these differences are outside the scope of this thesis.

For conditions where the equivalence ratio is above 4.5 and temperatures above 2500 K, a sudden straight line is presented in the reference map results. An explanation for this trend can be traced to the inlet temperature conditions. They investigated inlet temperatures between 1300 and 2500

K. In the present thesis it was investigated inlet temperature conditions between 700 and 3000 K. The results revealed that for high equivalence ratios and temperatures the outlet temperature decreased. This phenomenon can be seen in Figure 11, which presents the data points for the results. The figure shows that for equivalence ratios above 5.0 and temperatures between 2700 to 3000 K, there are regions without data points, even though the inlet temperature was set to 3000 K. Based on this observation, it is reasonable to believe that the reference study did not obtain results for these conditions and excluded them from their results. The trends can be expected to behave as in the present thesis results. However, the importance of this high temperature and equivalence region is, based on previous studies, out of the area of importance as one rarely experiences particles within the combustion chamber with these conditions.

To summarize, the soot and NOx investigation in the present thesis aims to see the trends when mixing ammonia with the diesel fuel. For this purpose, the numerical setup can be regarded as sufficient. All in all, the numerical setup is regarded as verified, and the further results obtained with the same setup were determined as acceptable.

7.2 NOx emissions

The obtained NOx emissions for cases 1 to 5, given the conditions listed in Table 2, are presented in Figure 17. Here, the NOx levels apparent at 2 ms are presented with a color bar equal for each case. The limit for this color bar is set such that ppm levels between 500 and 20000 are shown with varying shading. Levels above 20000 ppm are all black. The thick red line differs the fully combusted region from the rest, while the thin red line in each figure marks the 10000 ppm-level.

The results presented in Figure 17 show that the majority of high NOx ppm levels are located at high temperatures and low equivalence ratios. This is true for all the five base cases, implying a weak fuel dependency. Especially noticeable is that all of the recordings above 10000 ppm are located in this region, a region between 2200 - 3000 K and $\phi \leq 1.1$. Low ppm levels exhibit a quite different behavior.

For the case of pure n-heptane, the only region visible within these color bar limits is located in the region with high temperature and low equivalence ratios. Hence, it is reasonable to assume that the primary mechanism contributing to the formation of NOx is the thermal NOx mechanism. A further discussion on this will be provided later in this section. For the four cases involving ammonia in the fuel, the high ppm region is still located at high temperatures and low equivalence ratio. However, the region with lower ppm levels exhibits different behavior. This region extends into the ignition phase, where its highest concentrations are located at equivalence ratios below 2 and then decrease in value towards higher equivalence ratios within this region. Also noticeable is that the low ppm level region is most prominent for case 2 and decreases in influence towards higher ammonia concentration cases. However, it is clear that the behavior and shape of this region is similar in all cases containing ammonia.

When the conditions leave the ignition phase region and enter the region where the outlet-temperatures have stabilized again, the NOx emissions exhibit similar behavior as the pure n-heptane case, with emissions above 500 ppm located at high temperatures and low equivalence-ratios and no regions exceeding 500 ppm elsewhere.

If, at first, considering the high ppm region, defined as ppm levels above 10000 (marked with a red line in Figure 17), it is clear that the fuel dependency is relatively low. To underpin this, Figure 18 is crated to show the 10000 ppm limit for all the cases plotted against each other. The figure clearly shows that the region containing levels surpassing 10000 ppm is located below an equivalence ratio of 1.1 and exhibits similar behavior for all the fuel blends. It is a small tendency that the ppm limit stretches towards lower temperatures as the ammonia content increases in the fuel, but above 2600 K, the behavior for this limit, given the verification uncertainties discussed in the verification section (7.1), is equal for each case.

In the high ppm region the majority of the NOx is accounted for by NO. By investigating the main NO formation pathways within this region, the origins of the NOx emissions can therby be explained. Hence, a flow analysis of the conditions yielding $\phi = 0.6$ and $T_{out} \approx 2800 - 2900$ K, well

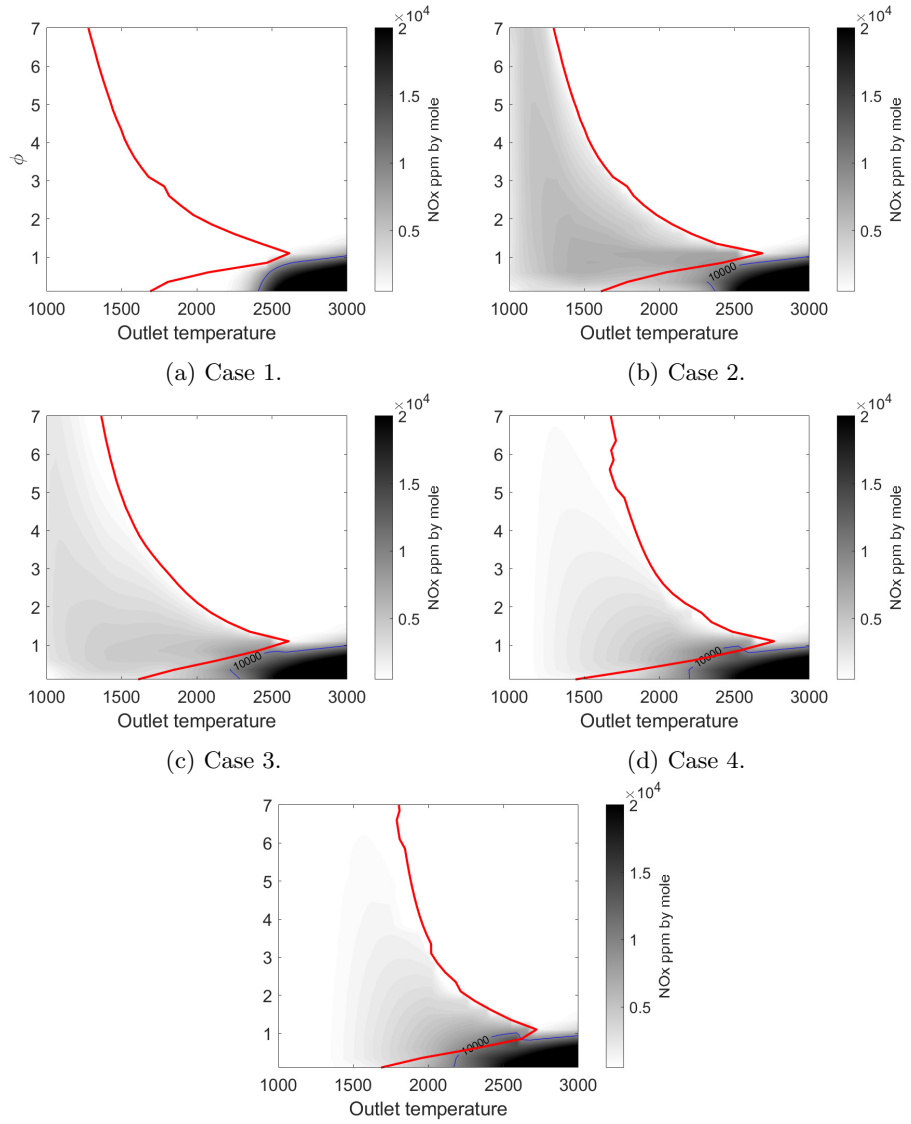

(a) Case 1.

(b) Case 2.

(c) Case 3.

(d) Case 4.

(e) Case 5.

Figure 17: NOx emissions represented on ϕ-T maps for the five base cases. The 10000 ppm limit is presented with a blue contour-line. NOx values above 500 ppm are visible. The red line represents the end of the ignition phase.

inside the 10000 ppm region, was carried out. The five most significant net formation pathways of the cases are presented in Figure 19. For all the five base cases, the five most contributing formation pathways were equal, and is presented in that figure. The magnitude similarities implies that the fuel dependency for the NO formation within this region is small or negligible.

The main formation pathway of NO for all the cases is $\mathrm{NO} + \mathrm{O}(+\mathrm{M}_{17}) \rightleftharpoons \mathrm{NO}_2(+\mathrm{M}_{17})$. Three of the other four pathways are related to HNO consumption either by reacting with OH, H, or O_2. The last pathway is the only one that can directly relate to the thermal NO mechanism, as it is the pathway: $\mathrm{N} + \mathrm{O}_2 \rightleftharpoons \mathrm{NO} + \mathrm{O}$, described in Section 4.2.2. Based on the conditions (high temperatures) and the low fuel dependency in this region, it is assumed that the high NOx levels are a repercussion of the thermal NOx mechanism.

One outtake from the figure is that the pathway $\mathrm{NO} + \mathrm{O}\,(+\mathrm{M}_{17}) \rightleftharpoons \mathrm{NO}_2\,(+\mathrm{M}_{17})$ has its highest value for case 2, which also has the most visible NOx appearance within the ignition phase. Towards the higher ammonia content cases, this formation pathway decreases slightly, and so does the visibility of the ignition phase regions emission. This could be a connection, however,

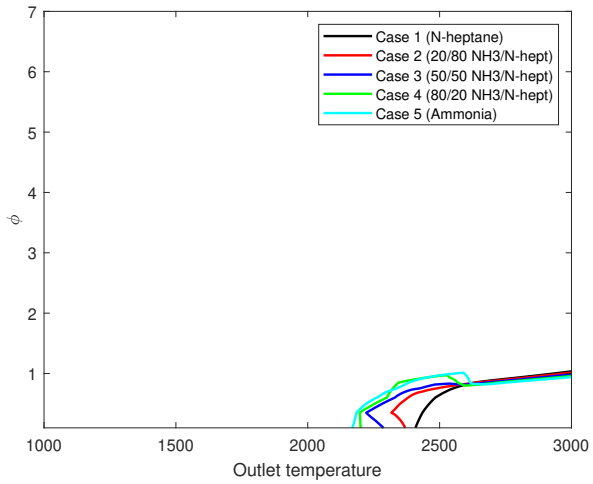

Figure 18: The 10000 ppm NOx limit for all the five base cases

as the data points become denser with higher concentration of ammonia, the uncertainties due to interpolation can contribute in lower emissions.

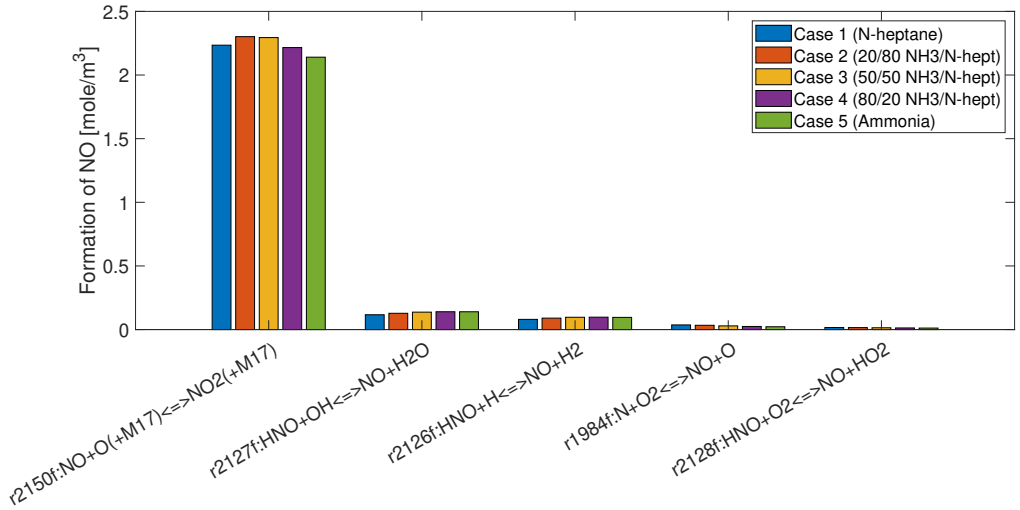

Figure 19: Five largest formation and consuming pathways for NO under the conditions of T_{in} = 1825 K, $p = 6$ MPa, reaction time = 2 ms, $\phi = 0.6$, and Tout $\approx 2800 - 2900K$.

For the lower ppm levels, the fuel dependency is more prominent where most of the emissions are located in the ignition phase. As mentioned, as ammonia gets introduced to the fuel, this region exhibits great changes. For case 1, this region is non-existing for NOx levels surpassing 500 ppm. However, the emissions are clear for case 2, which yields the highest levels in this region. As more ammonia is introduced into the fuel, the lower the NOx levels in this region becomes, and the region is shrinking towards the high emission region ($\geq$10000 ppm).

In the ignition phase region, the main formation pathways are related to the formation through HNO. The three pathways including this specie is as follows; $HNO + O_2 \rightleftharpoons NO + HO_2$, $NO + H(+M_{18}) \rightleftharpoons HNO(+M_{18})$, and $HNO + NH_2 \rightleftharpoons NH_3 + NO$. For case 2, the case with the most defined region has, in addition to these pathways including HNO, the most contribution pathway: $NO_2 + H \rightleftharpoons NO + OH$. Pathways including HNO, are linked to the oxidation of NH_3 and are expected to appear as ammonia gets introduced into the fuel [42]. First, NH_3 oxidizes to amidogen (NH_2). Then this amidogen gets oxidized to NO through HNO by a reaction sequence,

including the reactions listed earlier in this section. This oxidation of ammonia increases as more ammonia is introduced to the fuel and leads to an increased NO formation. However, when this happens, the net NO formation decreases. This is mainly due to the increasing impact of the thermal De-NOx mechanism, where NO gets consumed through interactions with NNH and NH_2 via the pathways presented in Figure 9. The ϕ-T map, including NOx emissions and the five most contributing and consuming pathways for NO formation, for cases 2 to 5, are provided in Appendix C.

In addition to the mentioned pathways, one can by looking at the formation pie charts for cases 2 and 4, presented in Figure 20, address the source for NO formation, as well as the fuel dependency. These two cases represent two quite different fuel compositions, containing energy contribution from ammonia of 20 and 80%, respectively. Here it is clear that the formation through HNO, thereby through NH_3 oxidation, which implies fuel NOx contributes to a higher percentage, 67% compared to 53%, as the ammonia content increases. This is expected as more fuel bounded nitrogen appears in the fuel. The HONO contribution decreases from 30% to 14% simultaneously, indicating that the prompt NOx decreases with the reduced amount of hydrocarbons in the fuel. Also, as mentioned in the previous section, the thermal De-NOx mechanism's impact is evident. In case 4, 48% NO consumption ends up as NNH, while for case 2, this number is 18%. As seen in Figure 9, it occurs in this mechanism amongst others through the interaction between NO and NH_2. What also backs up the argument of the thermal De-NOx mechanism's increasing impact with increased ammonia concentration in the fuel, is the increased share of NO consumed to N_2 from 18% in case 2 to 31% in case 4.

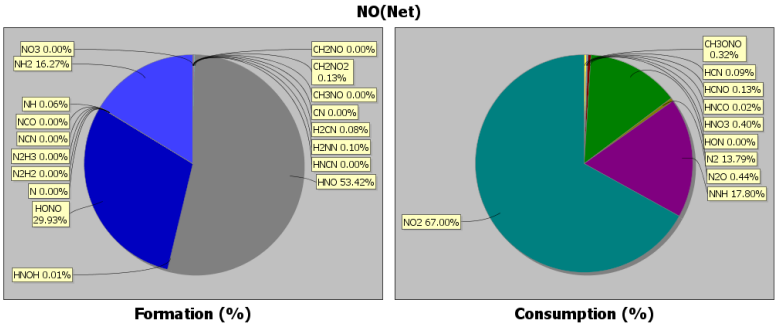

(a) Case 2.

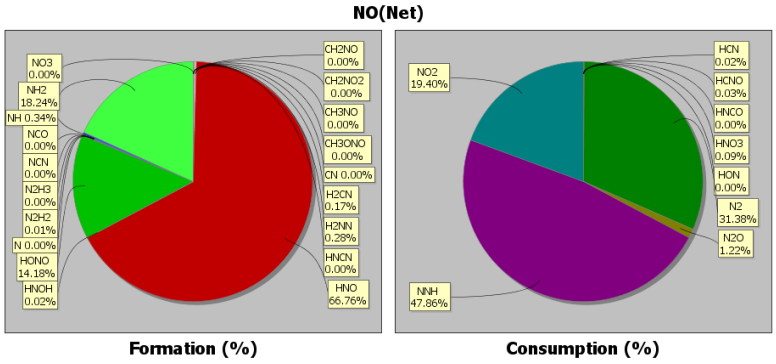

(b) Case 4.

Figure 20: Pie charts showing which molecules forms and consumes NO. The charts are for case 2 at $Tout = 1400$ K and $\phi = 2.1$, and case 4 at $Tout = 1523$ K and $\phi = 2.1$.

So, to summarize the NOx investigation briefly, the results shows that the fuel dependency is low for high temperatures, as most of the NOx obtained in this region originates from the thermal NOx mechanism. For the lower temperature regions, especially during the ignition phase, they exhibit a stronger dependency on the fuel composition, as for different blends the prompt NOx, fuel NOx, and thermal De-NOx mechanism are the determining origins for NOx in varying degrees.

7.3 N_2O concentrations

In the following section, the results of the N_2O analysis will be presented. As a significant amount of the N_2O is apparent in the ignition phase region, described earlier in Section 6.3, there will be two different interpretations of the results. One where all the data points will be considered, and one where only the results in the post ignition phase will be considered. This is provided as the different favorable injection strategies are highly dependent on which results that actually replicate the actual combustion during operation.

7.3.1 All conditions considered

Figure 21 shows the resulting N_2O emissions over the whole range of outlet conditions, from temperatures between $1000 - 3000$ K and ϕ between 0.1 and 7.0. The red line present in the figure distinguishes the incomplete combustion region and the complete combustion region. The figure contains all base cases, with a fixed color bar visualizing ppm levels from 0 to 3000. It is clear that with this scale, there are no N_2O emissions visible for case 1, with a pure n-heptane fuel. This is in accordance with previous research, as diesel operation have obtained N_2O levels in the range of single digits or low two digits ppm emissions [32]. Further, Figure 21 shows that when ammonia is introduced into the fuel, an island of N_2O gets visible. This island is located in the ignition phase region, described in Section 6.3. The relation between N_2O and temperature will be elaborated later in this section. Moreover, the results shows that the "N_2O-island" shifts to higher temperatures as more ammonia is apparent in the fuel. This is related to the high auto ignition temperature of ammonia. Also, the color on the maps becomes stronger, meaning that the N_2O levels increases. For case 2, the peak N_2O levels lie in the range of around 1000-1500 ppm, while for the case of pure ammonia as fuel, case 5, the peak levels exceed 3000 ppm.

The clear region with high N_2O levels is, as stated, in the ignition phase region. To understand the behavior of the N_2O together with temperature, Figure 22 was created. This figure shows how the N_2O emissions are connected to the outlet temperature of the combustion. It is clear that the majority of N_2O concentrations are located in a small region from where the outlet temperature increases from being equal to the inlet temperature to its post-combustion temperature. Namely, during the ignition phase. The N_2O peak seems to cover only a small region in this figure, while in the maps presented in Figure 21 covers a large area. When the condition changes from insufficient to ignite the mixture to combusted conditions, a rapid increase in the temperature occurs. The ϕ-T maps in Figure 21 have the outlet temperature on the x-axis, so the relatively small region in Figure 22 where ignition occurs, around 30 K, gives a large region on the maps, over a temperature range of around 1500 K. The same behavior is true for all the cases, as shown in Figure 23. This figure also shows how rapid the change from no combustion to combustion occurs. It reveals that the ignition region increases as more ammonia are apparent in the fuel. In other words, there is a larger range of inlet temperatures that gives outlet conditions equal to this incomplete combustion zone. It is also evident that as the ammonia content in the fuel increase, the temperature increase ($T_{out} - T_{in}$) gets lower. This lower temperature increase results in a narrower area of the "N_2O-island" on the ϕ-T maps. An explanation for this can be linked to, amongst others, the lower reactivity of the ammonia, presented in Section 3.11, also causing the temperature increase due to ignition to occur slower. This is not clear from Figure 21, but as Figure 23 shows, the temperature where N_2O starts to increase is below 1000 K for cases with below 80% energy from ammonia. Hence, the island stretches out of the mapped area between 1000 and 3000 K. Nonetheless, despite the narrower island, the peak N_2O level increases with the ammonia concentration in the fuel, from single digits ppm levels for case 1 to almost 3500 ppm for case 5. After combustion has taken place, the behavior of the N_2O emissions exhibits very few differences between the different cases. Here, the N_2O concentrations drop quickly down to less than single digits ppm levels before it slowly increases towards high temperatures reaching around 10 ppm for low equivalence ratios and outlet temperatures around 3000 K.

The increasing visibility of the high concentration region reveals how the potential for N_2O formation increases as more ammonia is apparent in the fuel. This underpins that optimizing injection strategies becomes crucial when the utilization of ammonia as fuel is investigated.

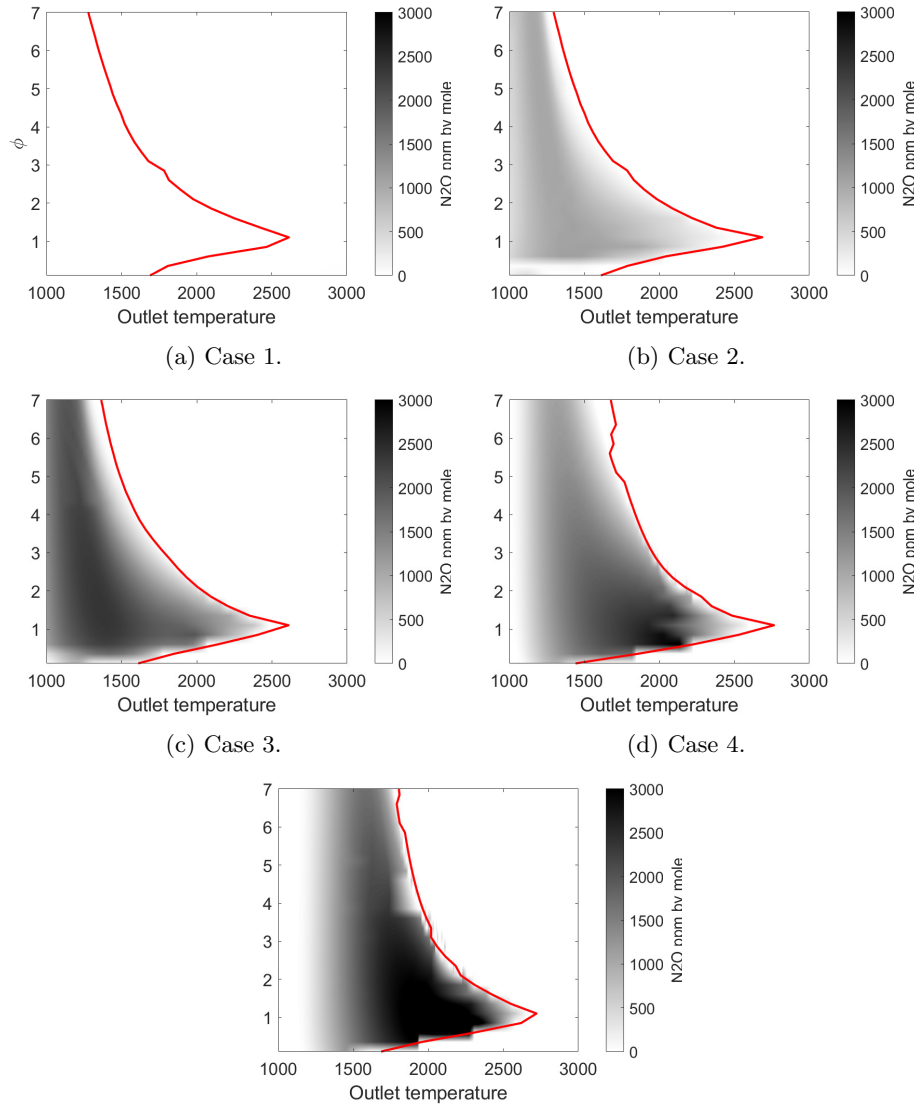

(a) Case 1.

(b) Case 2.

(c) Case 3.

(d) Case 4.

(e) Case 5.

Figure 21: ϕ-T maps including N_2O concentrations for the five base cases. The red line represents the end of the ignition phase.

Li et al. [32] stated that for their n-heptane fuel study, the N_2O emissions were low, except when incomplete combustion was observed. This statement backs up the interpretation of the results considering all conditions in the investigation. Even if the color-bar limits set in Figure 21 make the relatively low N_2O concentration for case 1 invisible, it can be seen in Figure 23 that, an increase in N_2O emissions was observed in the ignition phase, despite being much lower than for the other cases. It also shows that low levels are observed for complete combustion conditions. Even if the results for cases with ammonia in the fuel are not validated, this can be an indicator that the trends with high N_2O emissions in this region are representable and such conditions must be avoided. Also, avoiding these regions gets more critical the more ammonia the fuel contains.

The progress of the ignition process is also an important factor when obtaining data points in the ignition zone. If the gradient of the temperature increase is steep, like in the case of pure n-heptane (Figure 23), the data points in this region are spread out, and regions with a temperature difference between each point could surpass 100 K. The datapoint illustration for n-heptane in Figure 11 reveals how the reaction speed can influence the accuracy of the results. As linear interpolation is used between each point for its given equivalence ratio, this could lead to uncertainties. In this thesis, the data points are seen as sufficient in all cases as most of the regions in the ϕ-T maps

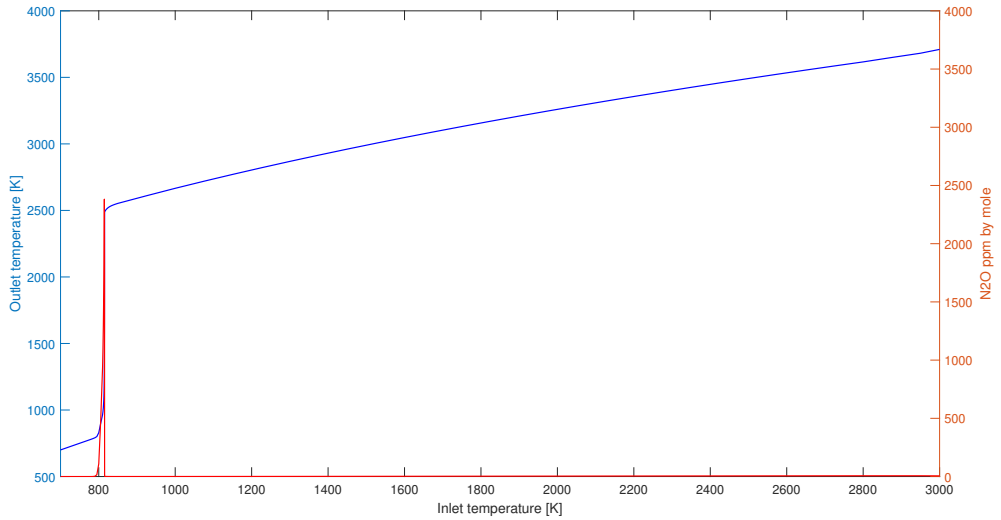

Figure 22: Plot of the behaviour of the outlet temperature and N_2O emissions based on inlet temperature. The figure exhibits the behaviour of the conditions of $\phi = 1.1$ for case 3.

were covered.

To address the origins of, and understand why, the emissions appear high during the "N_2O-island" region, a flow analysis was performed for case 3. Here three different locations on the map were used, all for the equivalence ratio of 1.1. The three different conditions were chosen such that one is located early in the ignition phase, at the lower temperatures of the island ($T_{out} = 1221$ K). The other location is towards the ignition phase's end ($T_{out} = 1914$ K), while the last is after the temperature has stabilized itself ($T_{out} = 2610$ K). The results from this analysis are presented in Figure 24. The results show that for low temperatures, early in the ignition phase, the primary N_2O formation can be traced to the consumption of NH_2 through the pathway $NH_2 + NO_2 \rightleftharpoons N_2O + H_2O$. Towards the end of the ignition phase, represented by the second location, the N_2O gets formed mainly by the consumption of NH, through $NH + NO \rightleftharpoons N_2O + H$, and some from the NH_2 pathway as in the first location. For the last location, the relatively low N_2O emissions, 0.3741 ppm, traces mainly to the pathway $NH + NO \rightleftharpoons N_2O + H$ and the consumption of NH. These two main formation pathways prominent in all the three locations, are expected and in good accordance with previous studies, as mentioned in Section 4.3. Because the consuming reactions for N_2O have not started in a major way during the ignition phase, the total N_2O levels appear high in this region. Towards the end of the ignition phase, the NH concentration has grown, as seen later in the section, and the central contributing reaction pathway $NH + NO \rightleftharpoons N_2O + H$. Here the consuming reactions are more active, so even though the NH contributing reaction pathway is significantly higher than the NH_2 pathway at lower temperatures, the total N_2O levels differ just slightly. After the ignition phase, the $NH + NO \rightleftharpoons N_2O + H$ pathway is the major contributor until the NO levels increase, making $2\,NO \rightleftharpoons N_2O + O$ the main contributor of N_2O formation. It is also clear that for the last location, the N_2O consumption is active and the N_2O gets consumed to form N_2 by $N_2O + H \rightleftharpoons N_2 + OH$, $N_2O + M \rightleftharpoons N_2 + O + M$, and $CO + N_2O \rightleftharpoons N_2 + CO_2$. Hence, keeping the total emissions low.

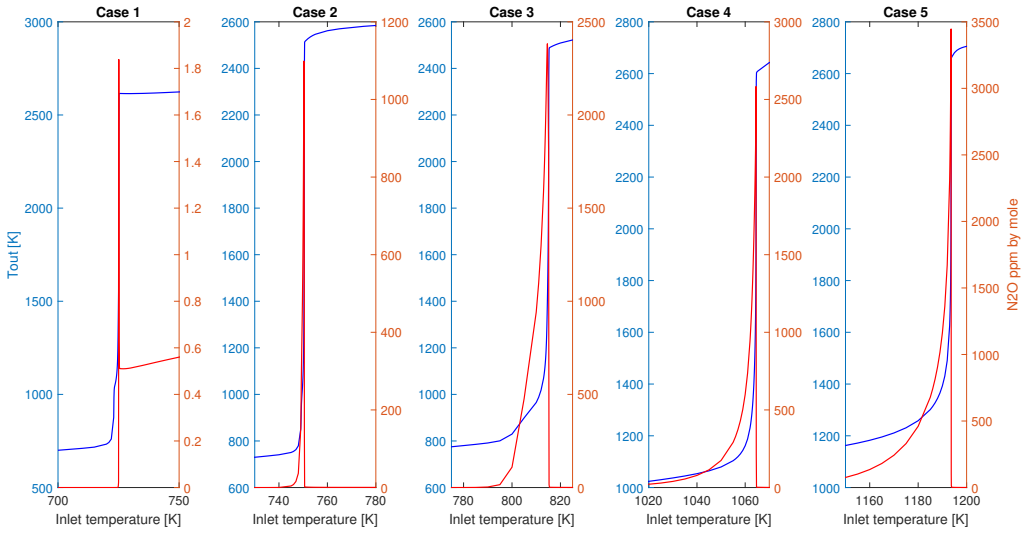

Figure 23: Temperature and N_2O concentrations in the ignition zone for the 5 different base cases. $\phi = 1.1$, p = 6 MPa.

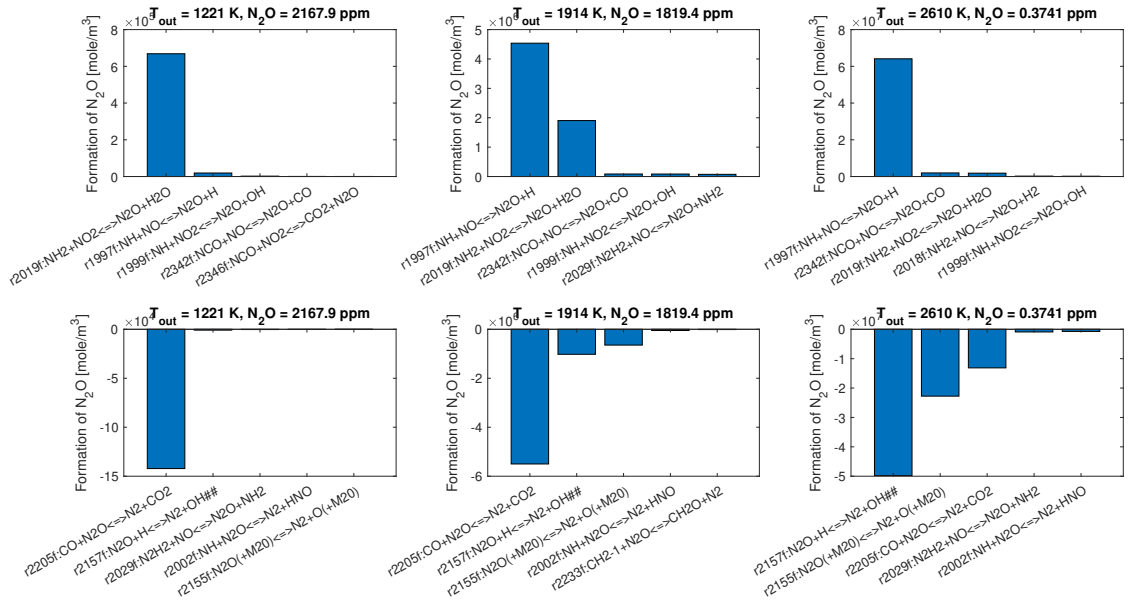

Figure 24: Flow analysis for three different inlet conditions for case 3. The top row shows the five most contributing formation pathways for N_2O, while the bottom row shows the five most consuming pathways.

Prigent and De Soete [58] stated that N_2O formation results from the reaction between NO and combustion intermediates, including NH and NCO. They also stated that N_2O, which originates from these processes, gets rapidly consumed by post-flame reactions, lowering the N_2O emissions substantially. As these pathways are highly contributing to N_2O formation in the ignition phase region, it could imply that the potential for lower emission levels in the exhaust could occur. The reaction mainly causing this reduction in post flame is: $N_2O + H \rightleftharpoons N_2 + OH$. As Figure 24 reveals, this mechanism contributes to consumption of N_2O with and increasing amount towards higher temperature. Hence, the exhaust results could deviate from these moment investigated results as previously mentioned.

Introducing the NH and NH_2 concentrations on the ϕ-T map could help understanding the reason why there are two different main formation pathways for the different regions. These maps can also be used as indicators for which pathways are important for leading to N_2O formation for different conditions. The two species concentrations for case 3 are presented in Figure 25. It is clear that NH has most of its concentration located towards the red combustion line for equivalence ratios between 0.6 and 3.1. In contrast, the NH_2 concentrations have higher levels and span over a broader region. NH_2 shows higher levels towards lower temperatures as well, explaining why it is the main formation pathway for conditions early in the ignition phase. These two molecules are related to ammonia combustion, and the formation through these species can imply why the need to consider N_2O formation increases as ammonia is introduced into the fuels.

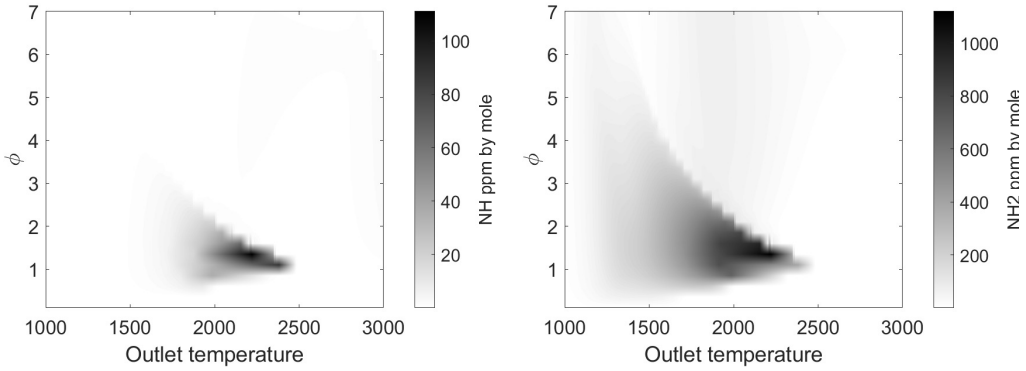

(a) NH concentration.

(b) NH_2 concentration.

Figure 25: ϕ-T map for case 3 showing the NH and NH_2 concentrations.

However, the one thing which is certain by investigating all the results, together with Li et al.'s [32] findings, is the importance of fully combusting the fuel. The particles within the combustion chamber will then be out of this high concentration region, and the N_2O emissions are substantially lower immediately after the ignition phase. This is also clear from Figure 23, which shows single digits or even below 1 ppm levels right after the peak values. So, the following sub-section will now address the emissions after the end of the ignition phase.

7.3.2 Post ignition phase results

The N_2O emissions for outlet conditions after the ignition phase are presented in Figure 26. Here the results left of the red line are removed. The figure shows that all the base cases yield similar results. In the figure, the color bar is set to distinguish N_2O ppm levels from 0 to 15, in other words, relatively low levels. In addition to similar behavior, it is also clear that all cases yield low ppm levels. If one plots the contour line at 5 ppm for each case, Figure 27 can be produced. This show that the fuel dependency on N_2O emissions in this region is very low.

It is important to emphasize that the results obtained in these simulations are the conditions that occur 2 ms after the fuel is injected or introduced to the inlet conditions. Hence, what happens in the expansion stroke and the exhaust is not addressed. The produced emissions may undergo a series of reactions before it reaches the atmosphere. However, the emissions are still such as provided after 2 ms, and if these are limited, less of the exhaust emissions can end up as N_2O. So, if one avoids particles within the ignition phase in the combustion chamber, the resulting N_2O is expected to appear low. This is reasonable as an engine would not be set to an operation that yielded unburned parts of the fuel. However, such conditions can occur during operation.

This means that during typical diesel engine conditions, the N_2O levels are low and usually single digits numbers. These conditions make the N_2O behave as the NOx levels. Investigating which chemical reaction is responsible for the N_2O formation make it understandable why the N_2O and NOx regions are located at similar places on the maps. This is because most N_2O originates from the consumption of NO through the reaction $2\,NO \rightleftharpoons N_2O + O$.

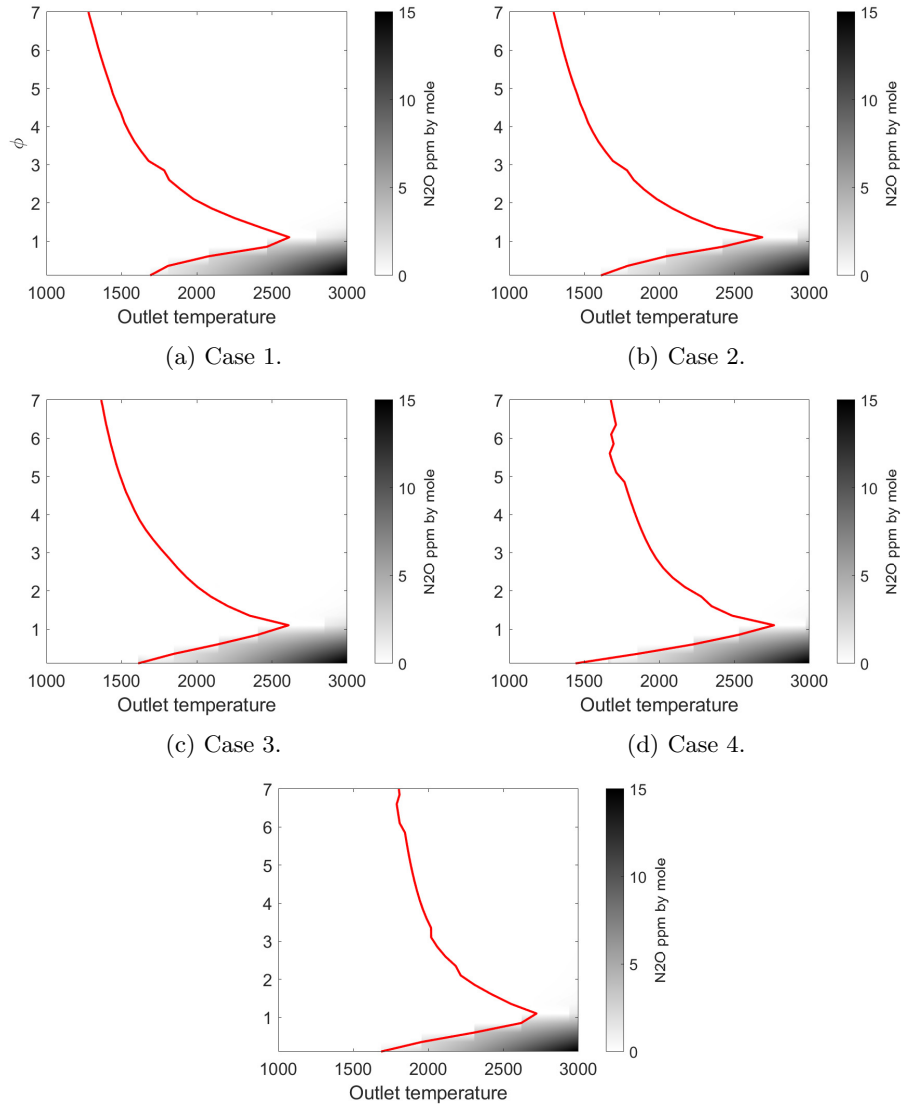

(a) Case 1.

(b) Case 2.

(c) Case 3.

(d) Case 4.

(e) Case 5.

Figure 26: ϕ-T map for the five base cases revealing N_2O emissions for stabilized outlet temperatures. The red line represents the end of the ignition phase.

Looking at different injection strategies, there are different answers for favorable conditions depending on which results one includes. Ryu et al. [62] showed that the advancement of the injection timing produced HCCI combustion-like characteristics. If one looks at the results in Figure 17, this could be beneficial for reducing high emissions from thermal NOx as well a soot, which will be shown in Section 7.4. However, it could cause N_2O-pollution if the ignition phase region is included. If one assumes that the results after the stabilized temperature line are correct, then similar injection strategies that reduce thermal NOx will work for N_2O reduction. Different injection strategies will be further discussed in Section 7.6.

The challenge of interpreting which results are correct is a discussion that previous studies have been exempt from. The reason is that in these studies, the ϕ-T maps included soot and NOx emissions. These emissions, for hydrocarbon fuels, are only apparent in high concentrations well clear of the ignition phase region. This means that the simulation outputs have stabilized for these conditions and is not expected to change after 2 ms. For the N_2O, this is quite different. High concentrations of N_2O are observed right in the zone where the combustion system ignites. As is obvious from Figure 22, the N_2O concentration increases when the temperature-gradient increases and reaches its peak value in the incomplete burning zone. When the temperature stabilizes at

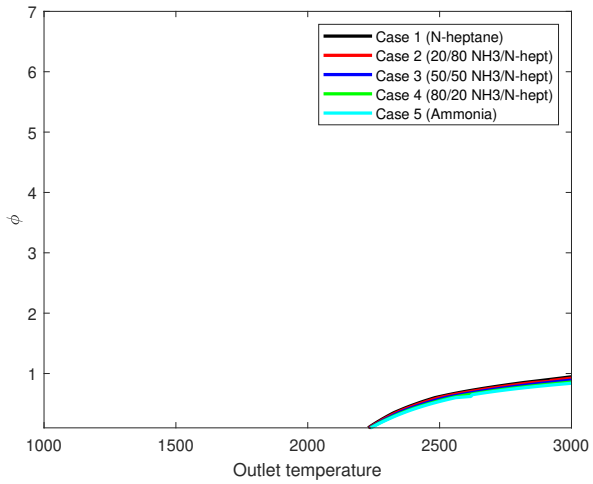

Figure 27: The 5 ppm N_2O limit for all five base cases for results after the ignition phase.

a "post-combustion" level, the N_2O concentration drops significantly to yield single digits ppm values. This behavior can question the validity of presenting N_2O in this way, including the ignition phase. As mentioned, it could be expected that during the expansion and exhaust stroke, the compounds could react, and the experienced N_2O emissions could deviate from the results.

7.4 Soot formation

As pointed out in Section 7.1, the resulting soot formation produced with the applied method (ref. Section 6.4) combined with the use of the mechanism by Seidel et al. [64] is questionable, and an under-prediction of the emissions could be the reality. Despite this, the trends for soot formation should be well represented and could contribute to a better understanding of the combustion in a dual-fueled reactor.

The results presented in Figure 28 show the soot yield for the four first base cases (cases 1, 2, 3, and 4). The color bar is set differently for each case as the resulting emissions are highly fuel dependent. Similar to all the cases, the red lines present the 0.001, 0.01, and 0.1 sooting yield limits, respectively 0.1%, 1%, and 10 %. For the two cases with the highest ammonia content, the emissions are below this 0.001 soot yield limit over the whole range of conditions. The choice of including the 0.001 limit contour line is for its correspondence with the 1% sooting limit from the reference case. To highlight how this limit changes with different fuel blends, Figure 29 is created. In that figure, the contour of the 0.001 soot yield limit for cases 1, 2, and 3 are plotted on a ϕ-T map. Case 4 and 5 are neglected from this comparison, as the soot yield does not reach this limit within the temperatures between 1000 and 3000 K and equivalence ratios between 0.1 and 7.0. This comparison shows that as the ammonia concentration increases, the region embraced by the 0.001 limits becomes narrower and shifts to higher equivalence ratios. For case 3, an equivalence ratio of 5 is needed to reach the 0.001 soot yield limit, while for case 1, this limit is reachable for equivalence ratios of 2.

By inspecting the results presented in Figure 28 and Figure 29, it is clear that the soot formation is highly dependent on the amount of hydrocarbons in the fuel. This is reasonable as soot formation results from the hydrocarbons in the fuel reacting to form aromatic rings. For case 1, where the fuel consists of just pure n-heptane, the soot formation potential is vital to consider. As the ammonia content increases, the need to consider soot gets less and less critical, and for cases 3 to 5, this is of little concern. However, with ammonia, the potential for ammonia slip increases. This is not discussed in detail in this thesis. However, the potential for ammonia slip increase with increased concentration in the mixture, is presented in Figure 30. In this figure, the NH_3 concentration is plotted on the ϕ-T maps. As the peak values for NH_3 concentrations change as the amount of ammonia in the fuel changes, the color bar limits are different for all the cases. However, it is

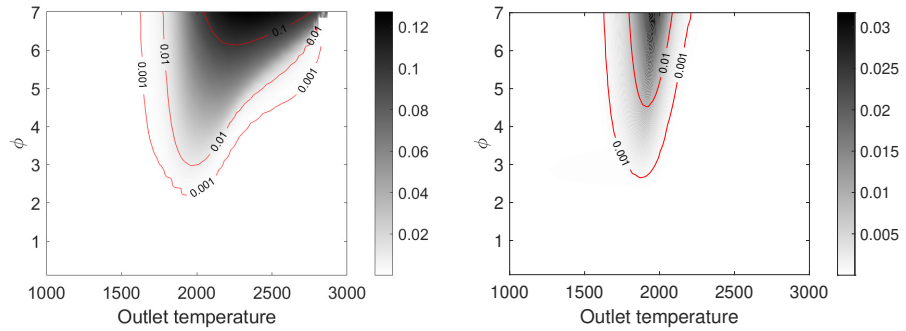

(a) Case 1. (b) Case 2.

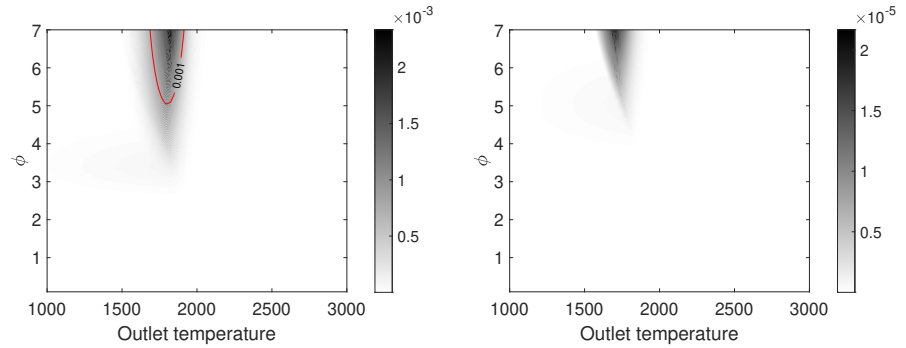

(c) Case 3. (d) Case 4.

Figure 28: ϕ-T map with soot yield for the base cases 1 to 4. The red lines represents the 0.001 and 0.01 soot yield limits.

observed that in the high equivalence condition regions, the ammonia concentrations have a higher slip potential as the ammonia content increases. This reveals why the search for favorable injection strategies is a complex question, where many different aspects need to be considered. When the combined ϕ-T maps are presented in Section 7.6, the NH_3 concentrations are not included and will not be a factor of consideration in the present thesis investigation of injection timing. However, it is vital to keep in mind that favorable conditions for some emissions could deteriorate others. So, as a result, it is the optimizations to reach the lowest combined emissions which is of importance.

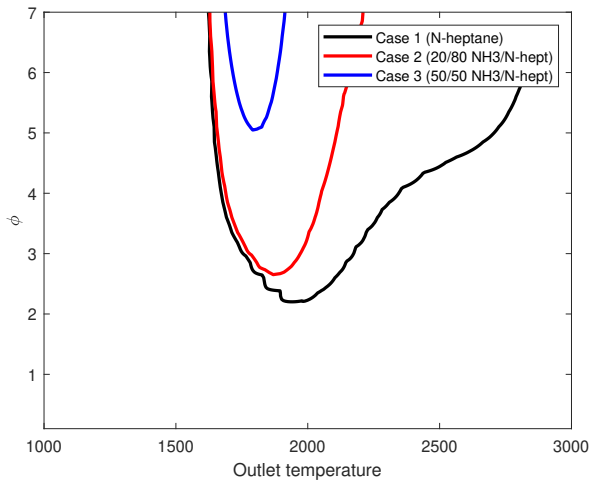

Figure 29: 0.001 soot formation limit for cases 1, 2, and 3.

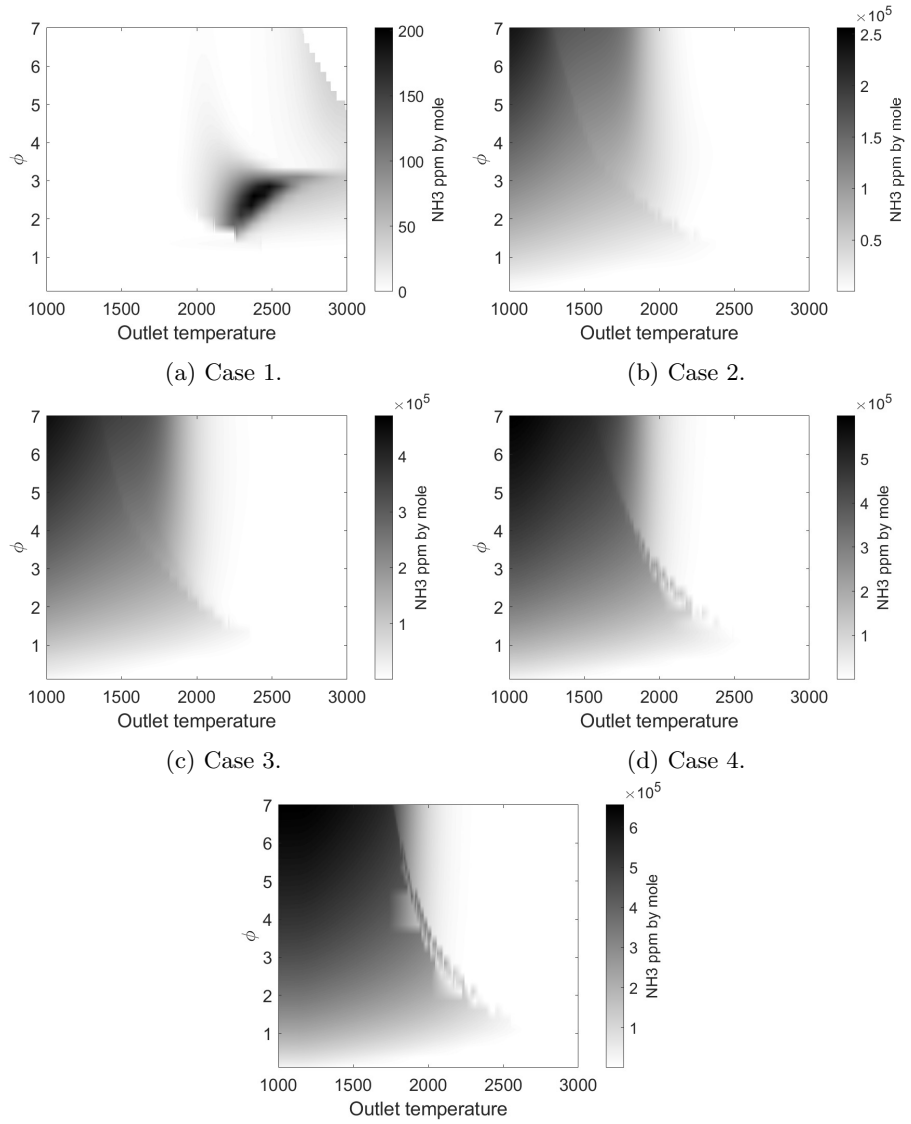

(a) Case 1.

(b) Case 2.

(c) Case 3.

(d) Case 4.

(e) Case 5.

Figure 30: ϕ-T map showing NH_3 concentrations for the five base cases. Be aware of the changing colorbar values.

7.5 Dilution and reaction time effects

In this section, the effects of changing the dilution and reaction time will be addressed. This is provided as the local conditions within the combustion chamber can deviate from each other during a combustion process. It was tested two different dilution levels in addition to the already obtained air as an oxidizer. These two levels were 15 and 10% oxygen in the oxidizer, while the rest was nitrogen. The effects of changing the reaction time was done by increasing the reaction time from 2 to 10 ms. This was done for case 3, and the resulting N_2O emissions will be provided in this section, while the NOx emissions effects are attached in Appendix D. The soot emissions behavior with changed reaction time and dilution was not investigated in this thesis. First, the effect of dilution is addressed and presented in Figures 31 and 32.

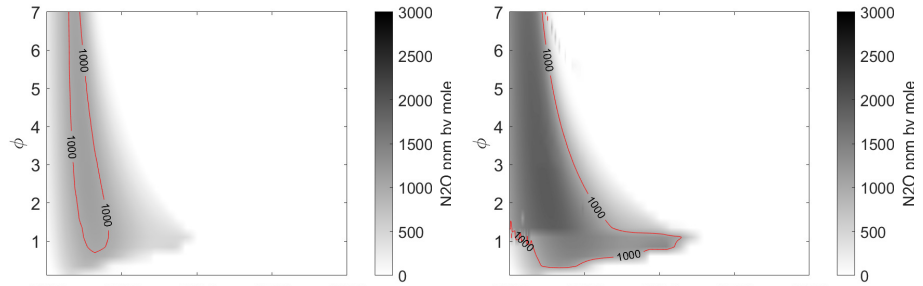

(a) $O_2 = 10\%$, $N_2 = 90\%$.

(b) $O_2 = 15\%$, $N_2 = 85\%$.

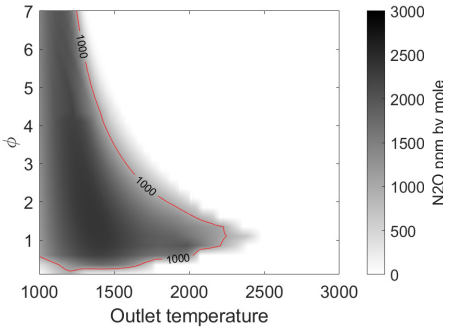

(c) Air ($O_2 = 21\%$, $N_2 = 79\%$).

Figure 31: ϕ-T map for case 3 showing the effect of dilution on N_2O emissions.

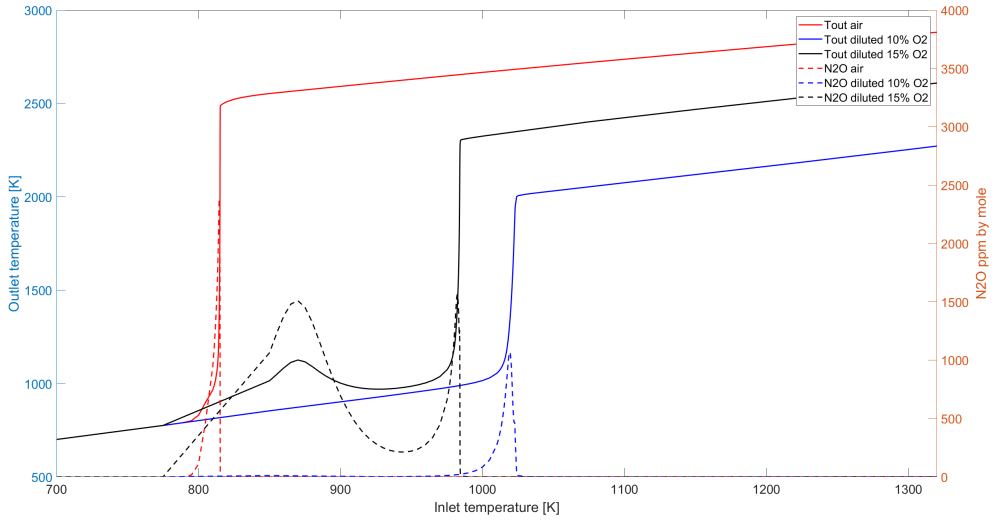

Figure 32: Temperature and N_2O dependency of changing the dilution levels.

Figure 31 shows the effect of changing the dilution levels regarding the N_2O emissions, while Figure 32 shows how the temperature and N_2O are dependent on the dilution levels. For the case of 15% oxygen, there seems to be a pre-combustion at low temperatures. This is not further addressed in this thesis, and only the last temperature increase is considered. The takeouts from the figure are that, as the dilution levels increase, the temperature increase during the ignition phase gets lower and so do the N_2O peak levels. The temperature increase for $\phi = 1.1$ is above 1700 K for the regular air operation, and the N_2O levels reach almost 2500 ppm. By diluting the oxidizer to 15%, the temperature increase is at around 1300 K, and the N_2O peak levels are around 1500 ppm. For the case of 10% oxygen in the oxidizer, the temperature increase is around 1000 K, and the peak

N_2O levels are now slightly above 1000 ppm. The reduced temperature increase during ignition results in a narrower "N_2O-island", as the peak N_2O concentrations are located in the ignition phase region. It is also clear from both Figures 31 and 32 that the visibility of the "N_2O-island" and hence the emission levels decrease significantly. When air is used as an oxidizer, the peak N_2O levels reach almost 2500 ppm, while for dilution yielding 10% oxygen in the oxidizer, the peak levels are just above 1100 ppm. This shows that dilution strategies can provide lower N_2O emissions; however, this is not investigated further in this thesis. It is however noteworthy that this can justify the use of low-temperature combustion technologies as, under these conditions, particles will appear in the "N_2O-island" region. However, because these particles may experience local dilution levels, they can in fact be outside of the high N_2O region. This is cause for further investigation in the future.

As addressing the N_2O is the main purpose in this thesis, only these results are discussed. For the NOx emissions, the results showed that the shape of the NOx region were similar to air operation, however the levels were decreased slightly. The resulting ϕ-T maps for the dilution investigation is presented in Appendix D.

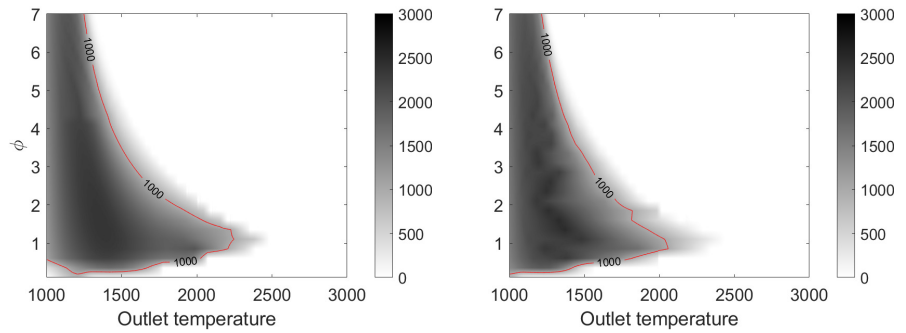

(a) Reaction time = 2 ms. (b) Reaction time = 10 ms.

Figure 33: ϕ-T map for case 3 showing the effect of reaction time on N_2O emissions.

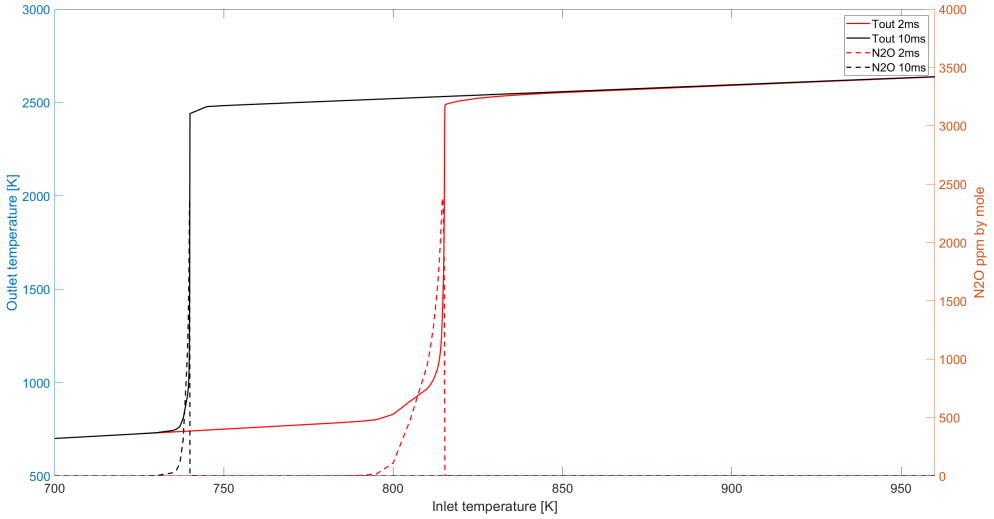

Figure 34: Temperature and N_2O dependency of changing the reaction time for case 3 at an equivalence ratio of 1.1.

Regarding the reaction time, an investigation of the effects of increasing the reaction time is presented in Figures 33 and 34. From the results, it is clear that both reaction times yield similar behavior and emission levels. The effect of increasing the reaction time from 2 to 10 ms is that the

mixture gets more time to react, yielding combustion to occur at lower temperatures. This causes the whole "N_2O-island" to shift slightly to lower temperatures. Despite this shift, the behavior and appearance of the emissions are fairly similar. Both have similar peak emission levels, and both have their emissions located in the ignition phase regions. Still, this thesis does not address what happens when the temperature and conditions change in the exhaust. Based on these results, it was deemed sufficient to include only the 2 ms results in the investigation. This is also a realistic time for agriculture and smaller vehicles. A longer reaction time would be unrealistic compared to what is actually happening in such a diesel engine, as these vehicles often operate around 2000 rpm. For the NOx emissions the similar behavior was experienced. No significant changes in the levels nor the placement of the emission region. It is fair to assume that changing the reaction time past 2 ms, will not change the results. Hence, 2 ms is sufficient to avoid under-prediction of the results.

7.6 ϕ-T maps

In this section, the resulting ϕ-T maps from Sections 7.2, 7.3, and 7.4 will be combined together and presented for all the five base cases in Figure 35. Here the limits for visibility for each of the three emissions are set as the following. For NOx, the concentrations above 10000 ppm are visible and shaded to show the difference up to 20000 ppm. Levels above 20000 ppm is black. For the soot, the lower limit is set to 0.001, while the distinguishable upper limit is 0.01. Soot yield above 0.01 is black. Lastly, the limits for N_2O are set to show the colormap between 1000 and 3000 ppm. Levels above these appear with a dark green color and are only visible for case 5. In addition, contour lines are set to mark the 10000 ppm limit for NOx, 0.001 and 0.01 limits for soot, and 1000 and 2000 ppm limits for N_2O. Similar to the previous results, a red line is apparent to distinguish the conditions after the ignition phases from the rest. It is worth mentioning that the N_2O emission in these maps are chosen to be for the whole investigated region. A more thorough discussion on N_2O emissions can be found in Section 7.3.

From the five different maps presented in Figure 35, it is clear that the fuel dependency is prominent and reveals the importance of treating each fuel independently. The exception for change is the thermal NOx or the high ppm level region for NOx. This region is quite stationary for all the cases, located at high temperatures and low equivalence ratios. There are some small changes in this region as well, as the ammonia concentration in the fuel increases. However, these changes are small compared to what is experienced for the other two emissions. If lower NOx levels were included, the maps would be different. This is described further in Section 7.2. The soot yield region is only apparent in cases 1, 2, and 3. For cases 4 and 5, the potential for soot is below the set limit in this thesis and in general very low (Section 7.4). This emphasizes that soot is a concern and needs to be addressed, especially in cases 1 and 2, as the region stretches to relatively low equivalence ratios and low temperatures. For case 3, the soot region is located in the upper middle part of the map, with only the 0.001 limit visible. This implies that a quite uncommon engine operation is required to reach this region and to obtain a substantial amount of soot. When the fuel is contained with a 50/50 energy contribution from ammonia and n-heptane, there are other emissions which are of greater concern. For these cases, the N_2O region becomes of significance, and the ammonia slip, as briefly mentioned in Section 7.4. However, ammonia slip is not investigated in this thesis. The NOx region is for all cases quite similar to case 1, meaning that concerning NOx, the same favorable injection strategies would be equal for all cases. For case 1, caution must be taken, as the soot region covers a large portion of the ϕ-T map. Kitamura et al. [27] presented a similar map, including some desirable pathways and injection strategies to surpass these regions. These included the combustion strategies such as HCCI, low-temperature rich combustion, and MK (Modulated Kinetics) combustion. For HCCI, most of the particles within the combustion chamber are homogeneously mixed with air. The injection timing needs to be advanced significantly relative to regular operation to achieve this kind of combustion, since the fuel needs to have sufficient enough time to mix with the air prior to ignition. By operating with HCCI, a large portion of the particles are located at low equivalence ratios and over different temperatures. This means that many particles will land on the "N_2O-island", that could turn out, based on this behavior, as undesirable. However, such operation has proven earlier to produce good emission results. Hence, an experimental investigation will need to be carried out before repelling

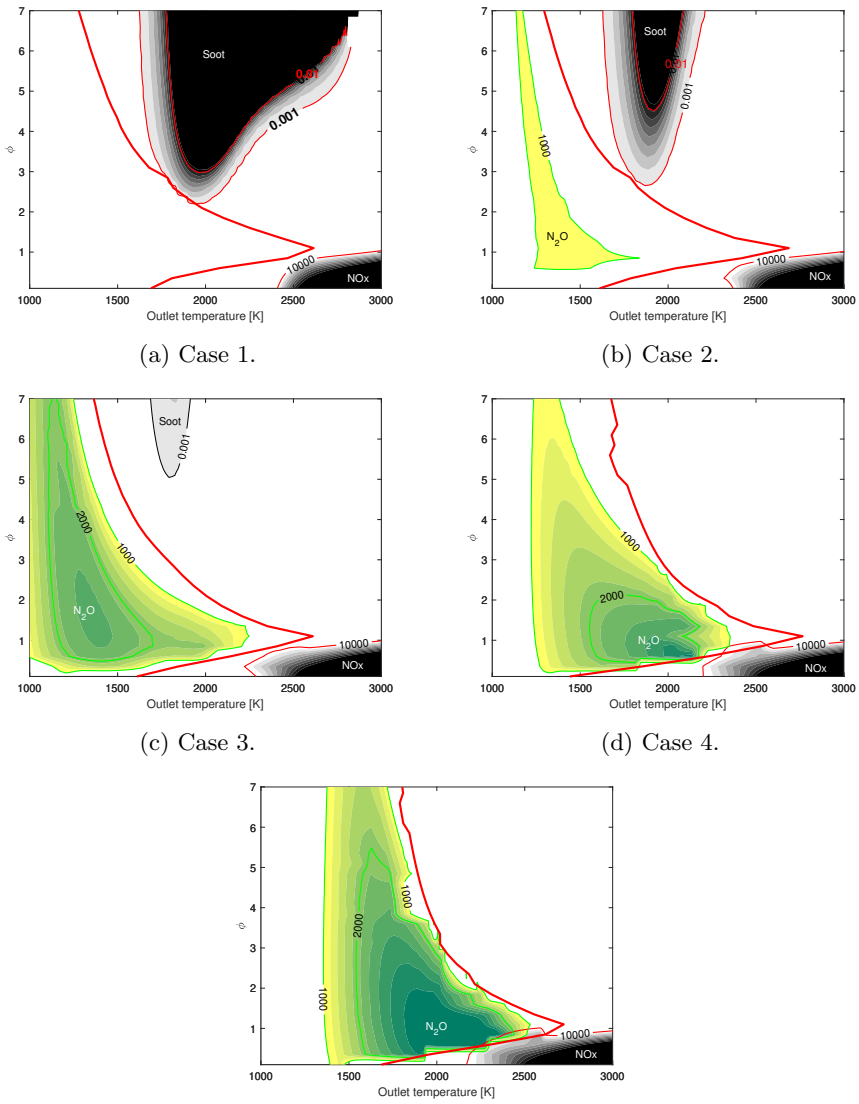

(a) Case 1.

(b) Case 2.

(c) Case 3.

(d) Case 4.

(e) Case 5.

Figure 35: ϕ-T map for five different cases. The red line represents the end of the ignition phase.

the strategy. MK is also a low-temperature premixed combustion that has shown to yield low NOx and soot emissions [26]. As HCCI, the MK could also potentially end up in the "N_2O-island" region.

Regarding the N_2O emissions, the premixed low-temperature combustion strategies meet a challenge. For the four cases containing ammonia in the fuel (2, 3, 4, and 5), the N_2O emission region is located right where these types of combustion strategies are located. Suppose, as mentioned before, one neglects the results prior to stabilized conditions, then all strategies which prevent NOx would also prevent high N_2O emissions. However, interpreting the results with severe high N_2O emissions occurring during the ignition phase shows that in order to achieve low N_2O emissions, it is important to achieve fully combusted conditions. As mentioned in Section 2, Ryu et al. [62] found that a specific IT was needed to ensure successful injection using DME and ammonia fuel blends. For cases with high ammonia content, too late IT can lead to incomplete combustion, while for cases with lower ammonia concentration, a certain range led to successful combustion, meaning that both too advanced and too retarded injection was unwanted. Again, this underpins why dual fuel operation can be complex and the importance of treating different fuel blends separately is crucial. Also, Li et al. [32] found that not achieving successfully or fully combustion could significantly deteriorate the emissions, not just N_2O, but NOx and UHC as well. So, either way

which results are interpreted as accurate, the need to fully combust the fuel is prominent.

Using CFD simulations, Dempsey et al. [10] looked at the effects of in-cylinder fuel stratification and low-temperature combustion, and produced scatter plots, based on the stochastic particles, for the different injection strategies. They tested conventional diesel combustion, partial-, moderate-, and heavy- fuel stratification. For the partial fuel stratification (PFS), most of the fuel is premixed with an injection in the range of 300-120 CAD BTDC. The moderate fuel stratification (MFS) has multiple direct injections during the compression stroke and gives partially premixed conditions. In this mode, usually, the fuel gets injected in portions between 120-40 CAD BTDC. For heavy fuel stratification (HFS), no fuel is premixed, and injection occurs near TDC, usually 40 to 0 CAD BTDC. Their scatterplots showed that conventional diesel combustion yielded particles within the soot and NOx formation regions. HFS yielded particles within the NOx region, while no particles were obtained above an equivalence ratio of around 1.6, meaning well clear of the soot formation region. MFS gave a more homogenously distributed distribution with particles located at different temperatures between equivalence ratios of 0.2 to 1.1 and just slightly into the NOx region. The most homogeneous operation, PFS, yielded all particles in the equivalence ratio range from 0.3 to 0.6 and for temperatures between 600 and 1850 K. They were well clear of both the NOx and the soot region. So, by applying low-temperature combustion strategies, they managed to reduce the potential of producing soot and NOx significantly. However, based on this thesis results, a challenge with these low combustion strategies regarding the N_2O can be clear. As the particles get located at an equivalence ratio of around 0.3 to 1.0, and the temperatures range from 600 to 2100 K, there are severe amount of particles located in the N_2O formation region. Hence, the potential for producing N_2O increases as these low-temperature strategies gets applied. However, low-temperature combustion strategies work with the principle of achieving sufficiently premixed conditions between the fuel and oxidizer in a globally diluted environment. By ensuring this, the combustion takes place at lower temperatures. Here the diluted approach is important to consider. The particles within the combustion chamber can experience different dilution conditions, which could result in the ϕ-T maps being misleading. This thesis produces the ϕ-T maps for fuel and air mixtures, meaning that no dilution is applied, and the oxidizer consists of 21% oxygen. In low-temperature combustion, the oxygen concentrations can go lower than this. Section 7.5 addresses the changes of the ϕ-T map as dilution yielding 15 and 10% oxygen in the oxidizer. This investigation makes it clear that if particles experience local conditions different from the global conditions, the resulting emissions can be affected. This is basis for further work, as not to erroneously reject injection strategies based solely on global conditions.

In general, the results show that there is a leeway for low emissions at lower temperatures over the whole specter of equivalence ratios for cases with low ammonia concentration. Due to the soot formation potential, caution needs to be taken for medium to high temperatures at high equivalence ratios. For cases with high ammonia concentration, cases 3 to 5, the leeway for low-temperature combustion is cleaned out. For these cases, the soot formation potential eases off and does not play a concern for regular combustion strategies. This opens up an opportunity with low emissions at higher temperatures and higher equivalence ratios, which can be utilized. For case 3, there is still a possibility between the NOx and "N_2O-island" that could yield lower emissions. However, in case 4 and 5, the two island meets, leaving little or no free spaces for the particles to avoid these high emission regions of either type.

7.7 SRM results

Now, as the ϕ-T maps are presented and discussed, the SRM results can be included in the discussion regarding different IT favorable. This thesis work planned to have dual direct injections, where different IT for the less reactive fuel, ammonia, would be investigated while keeping the n-heptane IT constant at 1 CAD BTDC. The results of these simulations showed an unexpected behavior, traced to some uncertainties regarding the mixing time models' approach to the dual-fuel operation. The obtained mixing profile for injections at two different IT was similar to only having one injection, which gives cause for implying that there are some uncertainties regarding the mixing model.

As the time restrictions for this thesis work did not allow any further investigation towards de-

veloping an SRM capable of correctly calculating this dual-fuel approach, this must be included in the further work section. Despite this minor setback, it was decided to include two different approaches prone to comparison. This was for case number 2, one approach injecting both of the fuels simultaneously, at 1 CAD BTDC, and one approach where the ammonia gets introduced through port injection. The results of this comparison are presented in Figures 36 and 37. Here the obtained scatter data is retrieved at 24 CAD after start of injection, which was at 1 CAD BTDC. For an engine running at 2000 rpm, this corresponds to 2 ms. One important aspect to consider is that in the case of port injection of ammonia, ammonia is included in the oxidizer when obtaining the equivalence ratio. This results in little difference between the two strategies when presented as Figure 36. By changing this interpretation of the oxidizer and fuel, such that ammonia is included in the fuel and not the oxidizer, the resulting scatter data is assumed to have been located in a narrower region at lower equivalence ratios. This is because the ammonia has gotten sufficient time to mix with the air during the intake and compression stroke. The narrower region indicates that several particles would appear inside the "N_2O-island" region, increasing the emissions. The emissions compared in Figure 37 back up this assumption. As in the case of port injection, the N_2O emissions are significantly higher than when the fuels get injected simultaneously. Also, if this assumption holds, it is a viable argument for the decreased soot emissions with port injection, indicated with unburned hydrocarbons in Figure 37. Since, the scattered points for port injection would be gathered around a lower equivalence ratio compared to regular operation.

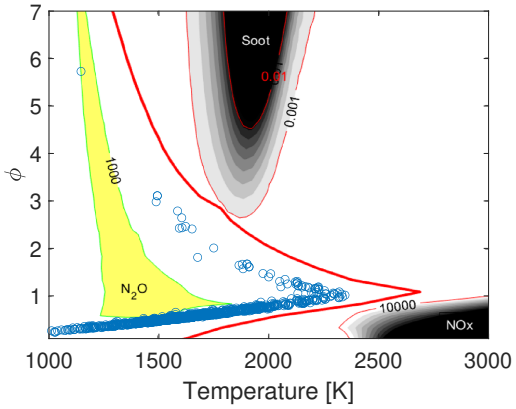

(a) Direct injection.

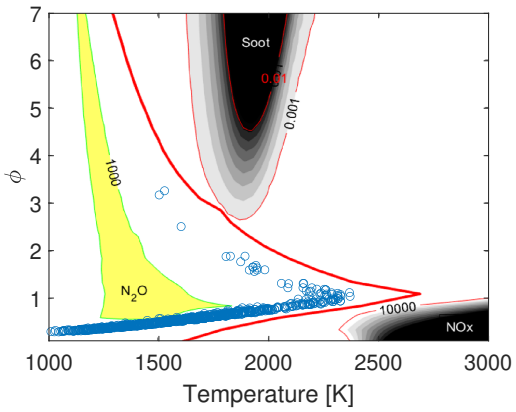

(b) Port injection.

Figure 36: ϕ-T maps with scatter plots of particles at 24 CAD after start of injection for case 2. (a) shows direct injection of both fuels at 1 CAD BTDC. (b) figure shows port injection of ammonia while n-heptane is injected at 1 CAD BTDC.

For cases 3 and 4, the results revealed that combustion was unsuccessfully for port injection. When injecting the fuels simultaneously right before TDC, combustion occurred. However, especially for case 4, a significant amount of ammonia was apparent in the emissions, indicating a large portion of unburned fuel. These observations from the SRM simulations reveal that as ammonia is apparent

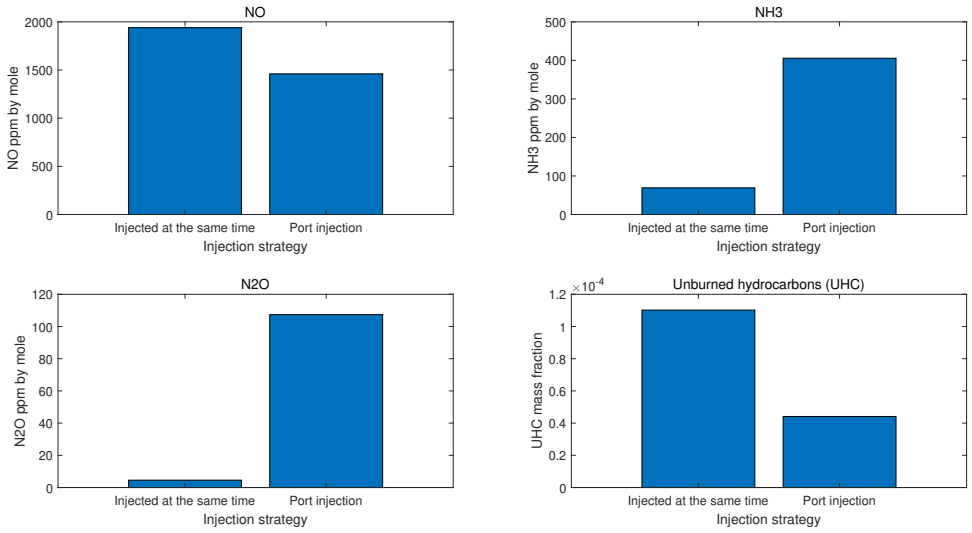

Figure 37: Outlet mole fractions of NO, NH_3, and N_2O and mass fraction of unburned hydrocarbons. The blue circles represent each of the stochastic particles.

in the fuel, the requirements for ignition become stricter. For this tutorial case engine with a CR of 16.5, the pressure, and thereby the temperature, does not reach the required value for combustion for port injection. This is somewhat following what previously is found in the literature, where a CR of above 30 was needed for ammonia operation only. However, as Gray et al. [15] found, if a more reactive fuel such as hydrogen is used as a pilot fuel this requirement could drop. N-heptane does perhaps not contribute to a low enough self-ignition temperature. Hence, when most of the fuel consist of ammonia, the mixture will not be sufficiently reactive to be ignited by the used CR. A further investigation with higher CR should be conducted in a further work. However, to validate such an investigation, experimental data is needed.

Ryu et al. [62], also found that to achieve successful combustion in a dual-fueled operated engine with a DME and ammonia-based fuel, there were requirements for the IT for different blends of the fuel. To achieve successful combustion with a 60/40 NH3/DME weight ratio, the IT needed to be between 340 and 90 CAD BTDC. For a 40/60 weight ratio, the IT needed to be between 50 to 20 CAD BTDC. When the unexpected problem regarding the mixing profile gets addressed and verified, similar studies as done by Ryu et al. should be conducted together with the resulting scatterplots on the ϕ-T map.

8 Conclusion

In this thesis, a thorough investigation of a dual fueled direct injection compression ignition engine was carried out. Five different blending ratios of the fuel were investigated with compositions of ammonia and n-heptane (0/100, 20/80, 50/50, 80/20, 100/0 based on energy accounted for by ammonia/n-heptane). The aim of the study was to create guidelines for injection strategies in the form of injection timing (IT) favorable for minimizing emissions. Through the use of the numerical software LOGEsoft [35] and a constant pressure reactor model, ϕ-T maps were created. On the maps, high concentrations of NOx, N_2O and soot were highlighted. Lastly, stochastic reactor modeling (SRM) was applied to investigate favorable IT with the goal of avoiding high emission regions. It is important to emphasise that the ϕ-T maps were verified for the case of pure n-heptane. Hence, the results including ammonia in the fuel needs to be further validated to be stated correctly. It is however, argued that the trends, which was the main investigation purpose, are presented in a good manner, and its behavior can be a great guidance for further studies.

The results showed that the ϕ-T maps exhibited a fuel dependency, especially with respect to N_2O and soot. Regarding the NOx concentration regions, it was clear that the region of high NOx ($\geq$ 10000 ppm) had small effects of changing the fuel blends. This was traced mainly to the contribution by thermal NOx, and little changes accounted for by fuel bounded NOx. For lower concentrations ($\leq$ 500 ppm), the dependency on fuel bounded nitrogen was to some extent stronger. This low concentration region appeared clearly as ammonia was introduced in the fuel. The region reached into the ignition phase region, where its most significant concentrations were obtained for case 2 (20/80 ammonia/n-heptane). As the ammonia concentration in the fuel increased, this low NOx concentration region shrunk and became less significant. This effect was thought to be a repercussion of the increasing impact of the thermal De-NOx mechanism. However, despite the appearance of this lower-NOx-concentration region at lower temperatures, similar injection strategies as for hydrocarbon fuels, appear favorable for all the five fuel compositions investigated.

Regarding the soot emissions, the fuel dependency was strongly exhibited. From its most influential appearance for case 1, pure n-heptane as fuel, its influence quickly eased off, and for cases 4 (80/20 ammonia/n-heptane) and 5 (pure ammonia), became of little or no concern, exhibiting no regions with a soot yield of 0.001 or higher. As the ammonia concentration increased in the fuel, the soot region became narrower and only appeared for higher equivalence ratios. For most operations the soot region is only of importance for cases with below 50 % energy accounted for by ammonia in the fuel. However, it is important to emphasise that with increased ammonia concentration, the possibility for ammonia slip increases and should be considered. This was only briefly discussed in Section 7.4, and further work should include such an investigation.

For the N_2O emissions, there are two different approaches to interpret the results. As a significant region with substantially high N_2O emissions ($\geq$ 1000 ppm) was apparent during the ignition phase region for cases including ammonia in the fuel. After fully combustion was assured, low levels were obtained experienced. It was in this thesis provided two different interpretations regarding N_2O. One with all conditions included, and one including results only after the ignition phase had ended. If first considering the second approach, low levels of N_2O were obtained. Levels above 5 ppm, were only obtained for high temperatures and low equivalence ratios, in the same region as thermal NOx contributes to a significant amount of NOx. Avoiding high N_2O levels interpreting this approach, requires similar strategies as for avoiding the NOx region. This was the case for all the five fuel blends. For the first approach, including all conditions, an increasing region with high N_2O levels became apparent, as the ammonia content in the fuel increased. This reveal the need of considering injection strategies when ammonia is utilized as a fuel. The region, referred to as the "N_2O-island" increases in both value and span as more ammonia were apparent in the fuel. The region makes the use of homogeneously mixed injection strategies questionable, as local conditions within the combustion chamber can end up inside this region. The outcome from this investigation is that caution regarding N_2O as ammonia is apparent in the fuel is important, likewise achieving fully combustion. If combustion is assured successfully, then low N_2O emissions can be expected. The uncertainties regarding the ϕ-T maps to account for local dilution levels request for more investigation both experimentally and numerically for the topic of N_2O and ammonia based fuels.

The SRM simulations revealed the need for improving the mixing time modelling for the dual

fuel injection operation. Therefore, for the purpose of the present work limited number of cases were considered to indicate differences in homogeneous and stratified ammonia combustion. Consequently, two conditions were created, emulating port injection and direct injection of both fuels simultaneously. The results have indicated a tendency of increased N_2O emissions and ammonia slip when homogeneous mixing in the chamber occurs, but higher unburned hydrocarbons and slightly higher NO emissions with direct injection. Yet, due to the preliminary character of the SRM results, these conclusions require further verification. They underpin the need for future investigation of the mixture formation process during dual fuel operation concerning N_2O and ammonia fuels.

9 Further work

Further work on this topic should include calibration of the stochastic reactor model against a dual-fuel operated engine, in order to verify more closely the results of this thesis. A study investigating the ignition phase kinetics should also be carried out. This to further understand the origins of the obtained "N_2O-island". An investigation of the local conditions behavior of low-temperature combustion strategies, could yield answers to N_2O emissions, and perhaps why other methods of obtaining such ϕ-T maps should be studied. It is clear that such maps could substantially reduce the time and resources related to experimental testing, and thereby speed up the technology development towards utilizing ammonia in engine applications.

Another important development towards a less pollutant transport sector, is substituting the high reactivity fuel for a less climate deteriorating fuel. As time fell short during the present investigation regarding bio-diesel and ammonia application of a DICI engine, this topic will be further investigated at a later stage, however the method and basics of this investigation is provided in this thesis. Also, reactivity controlled combustion strategies could be an interesting implementation.

10 Acknowledgements

I would like to thank Michał T. Lewandowski and Terese Løvås for their great guidance and inspiration throughout the project. I would also like to them for good help in reviewing the master's thesis.

I would like to thank Michal Pasternack for help and tips for the use of LOGEsoft.

LOGE AB is acknowledged for providing the license for LOGEsoft.

NTNU is acknowledged for providing the computing cluster IDUN.

Bibliography

[1] Kazuhiro Akihama et al. 'Mechanism of the smokeless rich diesel combustion by reducing temperature'. eng. In: *SAE technical paper series* (2001). ISSN: 0148-7191.

[2] G. H. Abd Alla et al. 'Effect of injection timing on the performance of a dual fuel engine'. In: *Energy Conversion and Management* 43 (2002), pp. 269–277. DOI: https://doi.org/10.1016/S0196-8904(00)00168-0.

[3] Yanzhao An et al. 'Numerical simulation of combustion and soot under partially premixed combustion of low-octane gasoline'. eng. In: *Fuel (Guildford)* 211 (2018), pp. 420–431. ISSN: 0016-2361.

[4] Maher Al-Baghdadi. 'An Overview of Hydrogen as an Alternative Fuel'. In: 6 (June 2020), pp. 1–22. DOI: 10.32545/encyclopedia202006.0003.v1.

[5] A Bhave et al. 'Analysis of a natural gas fuelled homogeneous charge compression ignition engine with exhaust gas recirculation using a stochastic reactor model'. In: *International Journal of Engine Research* 5.1 (2004), pp. 93–104. DOI: 10.1243/146808704772914273. eprint: https://doi.org/10.1243/146808704772914273. URL: https://doi.org/10.1243/146808704772914273.

[6] P. Chylek, S.G. Jennings and R. Pinnick. 'SOOT'. In: *Encyclopedia of Atmospheric Sciences*. Ed. by James R. Holton. Oxford: Academic Press, 2003, pp. 2093–2099. ISBN: 978-0-12-227090-1. DOI: https://doi.org/10.1016/B0-12-227090-8/00375-4. URL: https://www.sciencedirect.com/science/article/pii/B0122270908003754.

[7] Code of Federal Regulations. *§ 86.1818-12 Greenhouse gas emission standards for light-duty vehicles, light-duty trucks, and medium-duty passenger vehicles. 40 CFR 86.1818-12*. 2005. URL: https://www.ecfr.gov/current/title-40/chapter-I/subchapter-C/part-86/subpart-S/section-86.1818-12.

[8] Jean Muhlbaier Dasch. 'Nitrous Oxide Emissions from Vehicles'. In: *Journal of the Air & Waste Management Association* 42.1 (1992), pp. 63–67. DOI: 10.1080/10473289.1992.10466971. eprint: https://doi.org/10.1080/10473289.1992.10466971. URL: https://doi.org/10.1080/10473289.1992.10466971.

[9] Ronald M. Dell, Patrick T. Moseley and David A.J. Rand. 'Chapter 4 - Development of Road Vehicles with Internal-Combustion Engines'. In: *Towards Sustainable Road Transport*. Ed. by Ronald M. Dell, Patrick T. Moseley and David A.J. Rand. Boston: Academic Press, 2014, pp. 109–156. ISBN: 978-0-12-404616-0. DOI: https://doi.org/10.1016/B978-0-12-404616-0.00004-9. URL: https://www.sciencedirect.com/science/article/pii/B9780124046160000049.

[10] Adam B Dempsey, Scott J Curran and Robert M Wagner. 'A perspective on the range of gasoline compression ignition combustion strategies for high engine efficiency and low NOx and soot emissions: Effects of in-cylinder fuel stratification'. In: *International Journal of Engine Research* 17.8 (2016), pp. 897–917. DOI: 10.1177/1468087415621805. eprint: https://doi.org/10.1177/1468087415621805. URL: https://doi.org/10.1177/1468087415621805.

[11] Pavlos Dimitriou and Rahat Javaid. 'A review of ammonia as a compression ignition engine fuel'. In: *International Journal of Hydrogen Energy* 45.11 (2020), pp. 7098–7118. ISSN: 0360-3199. DOI: https://doi.org/10.1016/j.ijhydene.2019.12.209. URL: https://www.sciencedirect.com/science/article/pii/S0360319920300124.

[12] C. P. Fenimore. 'Formation of nitric oxide in premixed hydrocarbon flames'. In: *Symposium (International) on Combustion* 13 (1971), pp. 373–380. DOI: https://doi.org/10.1016/S0082-0784(71)80040-1.

[13] Tim Franken et al. 'Modeling of Reactivity Controlled Compression Ignition Combustion Using a Stochastic Reactor Model Coupled with Detailed Chemistry'. In: *15th International Conference on Engines Vehicles*. SAE International, Sept. 2021. DOI: https://doi.org/10.4271/2021-24-0014. URL: https://doi.org/10.4271/2021-24-0014.

[14] P. Glarborg et al. 'Modeling nitrogen chemistry in combustion'. In: *Progress in Energy and Combustion Science* 67 (2018), pp. 31–68. DOI: http://dx.doi.org/10.1016/j.pecs.2018.01.002.

[15] D. S. Gray et al. *AMMONIA APPLICATION TO RECIPROCATING ENGINES. VOLUME 2*. CONTINENTAL AVIATION and ENGINEERING CORP DETROIT MI, 1967. URL: https://apps.dtic.mil/sti/pdfs/AD0706860.pdf.

[16] Christopher W. Gross and Song-Charng Kong. 'Performance characteristics of a compression-ignition engine using direct-injection ammonia–DME mixtures'. In: *Fuel* 103 (2013), pp. 1069–1079. ISSN: 0016-2361. DOI: https://doi.org/10.1016/j.fuel.2012.08.026. URL: https://www.sciencedirect.com/science/article/pii/S001623611200662X.

[17] Metin Gumus, Cenk Sayin and Mustafa Canakci. 'The impact of fuel injection pressure on the exhaust emissions of a direct injection diesel engine fueled with biodiesel–diesel fuel blends'. eng. In: *Fuel (Guildford)* 95.1 (2012), pp. 486–494. ISSN: 0016-2361.

[18] Dong Han, Yusen Liu and Zhen Huang. 'The Use of Ammonia as a Fuel for Combustion Engines'. In: *Engines and Fuels for Future Transport*. Ed. by Gautam Kalghatgi et al. Singapore: Springer Singapore, 2022, pp. 233–256. ISBN: 978-981-16-8717-4. DOI: 10.1007/978-981-16-8717-4_10. URL: https://doi.org/10.1007/978-981-16-8717-4_10.

[19] J.B. Heywood. *Internal Combustion Engine Fundamentals*. Automotive technology series. McGraw-Hill, 1988. ISBN: 9780071004992. URL: https://books.google.co.in/books?id=O69nQgAACAAJ.

[20] J.B. Heywood. *Soot Formation in Combustion*. Springer Series in Chemical Physics. Springer, Berlin, Heidelberg, 1994. ISBN: 978-3-642-85167-4. DOI: https://doi.org/10.1007/978-3-642-85167-4_10.

[21] S. Iavarone et al. 'A multiscale combustion model formulation for NOx predictions in hydrogen enriched jet flames'. In: *International Journal of Hydrogen Energy* 44 (2019), pp. 23436–23457. DOI: http://dx.doi.org/10.1016/j.ijhydene.2019.07.019.

[22] IEA. 'Global Energy Review 2021'. In: (2021). URL: https://www.iea.org/reports/global-energy-review-2021.

[23] IEA. 'Greenhouse Gas Emissions from Energy: Overview'. In: (2021). URL: https://www.iea.org/reports/greenhouse-gas-emissions-from-energy-overview.

[24] iiar. *Ammonia data book*. iiar, 2005. URL: http://web.iiar.org/membersonly/PDF/CO/databook_ch2.pdf.

[25] Yuki Ishimoto et al. 'Large-scale production and transport of hydrogen from Norway to Europe and Japan: Value chain analysis and comparison of liquid hydrogen and ammonia as energy carriers'. eng. In: *International journal of hydrogen energy* 45.58 (2020), pp. 32865–32883. ISSN: 0360-3199.

[26] Shuji Kimura et al. 'Ultra-Clean Combustion Technology Combining a Low-Temperature and Premixed Combustion Concept for Meeting Future Emission Standards'. In: *SAE 2001 World Congress*. SAE International, Mar. 2001. DOI: https://doi.org/10.4271/2001-01-0200. URL: https://doi.org/10.4271/2001-01-0200.

[27] T Kitamura et al. 'Mechanism of smokeless diesel combustion with oxygenated fuels based on the dependence of the equivalence ration and temperature on soot particle formation'. In: *International Journal of Engine Research* 3.4 (2002), pp. 223–248. DOI: 10.1243/146808702762230923. eprint: https://doi.org/10.1243/146808702762230923. URL: https://doi.org/10.1243/146808702762230923.

[28] Donggeun Lee and Han Ho Song. 'Development of combustion strategy for the internal combustion engine fueled by ammonia and its operating characteristics'. In: *Journal of Mechanical Science and Technology* 32 (2018), pp. 1905–1925. DOI: http://dx.doi.org/10.1007/s12206-018-0347-x.

[29] R. Lemaire et al. 'Experimental comparison of soot formation in turbulent flames of Diesel and surrogate Diesel fuels'. In: *Proceedings of the Combustion Institute* 32.1 (2009), pp. 737–744. ISSN: 1540-7489. DOI: https://doi.org/10.1016/j.proci.2008.05.019. URL: https://www.sciencedirect.com/science/article/pii/S1540748908000989.

[30] Michał T Lewandowski et al. 'Numerical investigation of glycerol/diesel emulsion combustion in compression ignition conditions using Stochastic Reactor Model'. eng. In: *Fuel (Guildford)* 310 (2022), p. 122246. ISSN: 0016-2361.

[31] C. Lhuillier et al. 'Combustion Characteristics of Ammonia in a Modern Spark-Ignition Engine'. In: *Conference on Sustainable Mobility*. HAL, Oct. 2019. DOI: 10.4271/2019-24-0237. URL: https://hal.archives-ouvertes.fr/hal-02322493.

[32] Hailin Li et al. 'The NOx and N2O emission characteristics of an HCCI engine operated with N-heptane'. In: vol. 134. Jan. 2007. DOI: 10.1115/ICEF2007-1758.

[33] Jing Liu et al. 'A new surrogate fuel for emulating the physical and chemical properties of RP-3 kerosene'. In: *Fuel* 259 (2020), p. 116210. ISSN: 0016-2361. DOI: https://doi.org/10.1016/j.fuel.2019.116210. URL: https://www.sciencedirect.com/science/article/pii/S0016236119315649.

[34] *LOGEengine*. LOGE AB. Lund, Sweeden. URL: https://logesoft.com/.

[35] *LOGEresearch*. LOGE AB. Lund, Sweeden. URL: https://logesoft.com/.

[36] *MANUAL – BOOK1, Thermodynamics and Chemical Kinetics*. LOGE AB. Lund, Sweeden. URL: https://logesoft.com/.

[37] *MATLAB version 9.10.0.1613233 (R2021a)*. The Mathworks, Inc. Natick, Massachusetts, 2021.

[38] Andrea Matrisciano et al. 'Development of a Computationally Efficient Tabulated Chemistry Solver for Internal Combustion Engine Optimization Using Stochastic Reactor Models'. In: *Applied Sciences* 10.24 (2020). ISSN: 2076-3417. DOI: 10.3390/app10248979. URL: https://www.mdpi.com/2076-3417/10/24/8979.

[39] Rakesh Kumar Maurya and Nekkanti Akhil. 'Development of a new reduced hydrogen combustion mechanism with NOx and parametric study of hydrogen HCCI combustion using stochastic reactor model'. eng. In: *Energy conversion and management* 132 (2017), pp. 65–81. ISSN: 0196-8904.

[40] F Mauss. PhD thesis. RWTH Aachen University, 1997.

[41] J. Mertens, R. Belmans and M. Webber. 'Why the Carbon-Neutral Energy Transition Will Imply the Use of Lots of Carbon'. In: *Journal of Carbon Research* (2020), pp. 2–3. DOI: https://doi.org/10.3390/c6020039.

[42] James A. Miller and Craig T. Bowman. 'Mechanism and modeling of nitrogen chemistry in combustion'. In: *Progress in Energy and Combustion Science* 15.4 (1989), pp. 287–338. ISSN: 0360-1285. DOI: https://doi.org/10.1016/0360-1285(89)90017-8. URL: https://www.sciencedirect.com/science/article/pii/0360128589900178.

[43] C. A. Mims et al. 'Radical Chemistry in Methane Oxidative Coupling: Tracing of Ethylene Secondary Reactions with Computer Models and Isotopes'. In: *The Journal of Physical Chemistry* 98.50 (1994), pp. 13357–13372. DOI: 10.1021/j100101a041. eprint: https://doi.org/10.1021/j100101a041. URL: https://doi.org/10.1021/j100101a041.

[44] Salah E. Mohammed et al. 'The effects of fuel-injection timing at medium injection pressure on the engine characteristics and emissions of a CNG-DI engine fueled by a small amount of hydrogen in CNG'. In: *International Journal of Hydrogen Energy* 36 (2011), pp. 11997–12006. DOI: http://dx.doi.org/10.1016/j.ijhydene.2011.05.110.

[45] Balaji Mohan, Wenming Yang and Siaw kiang Chou. 'Fuel injection strategies for performance improvement and emissions reduction in compression ignition engines — A review'. In: *Renewable and Sustainable Energy Reviews* 28 (2013), pp. 664–676. DOI: http://dx.doi.org/10.1016/j.rser.2013.08.051.

[46] A. Monyem, J. H. Van Gerpen and M. Canakci. 'THE EFFECT OF TIMING AND OXIDATION ON EMISSIONS FROM BIODIESEL–FUELED ENGINES'. In: *Transactions of the ASAE* 44 (2001), pp. 35–42. DOI: https://doi.org/10.13031/2013.2301.

[47] S Mosbach et al. 'Dual injection homogeneous charge compression ignition engine simulation using a stochastic reactor model'. In: *International Journal of Engine Research* 8.1 (2007), pp. 41–50. DOI: 10.1243/14680874JER01806. eprint: https://doi.org/10.1243/14680874JER01806. URL: https://doi.org/10.1243/14680874JER01806.

[48] Dustin Mulvaney. *Solar Power: Innovation, Sustainability, and Environmental Justice*. University of California Press, 2019. ISBN: 9780520963191. DOI: doi:10.1525/9780520963191. URL: https://doi.org/10.1525/9780520963191.

[49] Krishnamoorthi Muniappan, Sreedhara Sheshadri and Pavan Prakash Duvvuri. 'Numerical Analysis of the Effects of Direct Dual Fuel Injection on the Compression Ignition Engine'. In: *ACS Omega* 5.46 (2020). PMID: 33251440, pp. 30047–30058. DOI: 10.1021/acsomega.0c04434. eprint: https://doi.org/10.1021/acsomega.0c04434. URL: https://doi.org/10.1021/acsomega.0c04434.

[50] Gunnar Myhre et al. *Anthropogenic and Natural Radiative Forcing*. Jan. 2014.

[51] Yoichi Niki. 'Reductions in Unburned Ammonia and Nitrous Oxide Emissions From an Ammonia-Assisted Diesel Engine With Early Timing Diesel Pilot Injection'. In: *Journal of Engineering for Gas Turbines and Power* 143.9 (May 2021). 091014. ISSN: 0742-4795. DOI: 10.1115/1.4051002. eprint: https://asmedigitalcollection.asme.org/gasturbinespower/article-pdf/143/9/091014/6702657/gtp_143_09_091014.pdf. URL: https://doi.org/10.1115/1.4051002.

[52] Mohamed Nour et al. 'Experimental evaluation of the performance and emissions of a direct-injection compression-ignition engine fueled with n-hexanol–diesel blends'. In: *Fuel* 302 (2021), pp. 121–144. DOI: https://doi.org/10.1016/j.fuel.2021.121144.

[53] Manosh C. Paul. *Soot : Sources, Formation, and Health Effects*. Environmental Health - Physical, Chemical and Biological Factors. Nova Science Publishers, Inc, 2012. ISBN: 9781619429413. URL: https://search.ebscohost.com/login.aspx?direct=true&db=nlebk&AN=541119&site=ehost-live.

[54] K. A. Pedersen. 'Numerical investigation of the potential of novel fuels in clean combustion systems'. Project thesis. NTNU Norges Teknisk Naturvitenskapelige Universitet, 2021.

[55] William J. Pitz and Charles J. Mueller. 'Recent progress in the development of diesel surrogate fuels'. In: *Progress in Energy and Combustion Science* 37.3 (2011), pp. 330–350. ISSN: 0360-1285. DOI: https://doi.org/10.1016/j.pecs.2010.06.004. URL: https://www.sciencedirect.com/science/article/pii/S0360128510000535.

[56] Industrial Marine Power. *Wartsila Diesel Engine Details - Output Range - RPM*. https://www.industrialmarinepower.com/wartsila-diesel-engine-details--output-range--rpm/#. May 2013.

[57] Michael J. Prather et al. 'Measuring and modeling the lifetime of nitrous oxide including its variability'. In: *Journal of Geophysical Research: Atmospheres* 120.11 (2015), pp. 5693–5705. DOI: https://doi.org/10.1002/2015JD023267. eprint: https://agupubs.onlinelibrary.wiley.com/doi/pdf/10.1002/2015JD023267. URL: https://agupubs.onlinelibrary.wiley.com/doi/abs/10.1002/2015JD023267.

[58] Michel Prigent and Geert De Soete. 'Nitrous Oxide N 2 O in Engines Exhaust Gases-A First Appraisal of Catalyst Impact'. In: *SAE transactions* 98 (1989), pp. 281–291.

[59] Senthil Ramalingam et al. 'Effect of operating parameters and antioxidant additives with biodiesels to improve the performance and reducing the emissions in a compression ignition engine – A review'. In: *Renewable and Sustainable Energy Reviews* 81 (2018), pp. 775–788. DOI: http://dx.doi.org/10.1016/j.rser.2017.08.026.

[60] H. P. Ramirez L. et al. 'Kinetics of Oxidation of Commercial and Surrogate Diesel Fuels in a Jet-Stirred Reactor: Experimental and Modeling Studies'. In: *Energy & Fuels* 24.3 (2010), pp. 1668–1676. DOI: 10.1021/ef9015526. eprint: https://doi.org/10.1021/ef9015526. URL: https://doi.org/10.1021/ef9015526.

[61] Aaron J. Reiter and Song-Charng Kong. 'Combustion and emissions characteristics of compression-ignition engine using dual ammonia-diesel fuel'. In: *Fuel* 90.1 (2011), pp. 87–97. ISSN: 0016-2361. DOI: https://doi.org/10.1016/j.fuel.2010.07.055. URL: https://www.sciencedirect.com/science/article/pii/S001623611000414X.

[62] Kyunghyun Ryu, George E. Zacharakis-Jutz and Song-Charng Kong. 'Performance characteristics of compression-ignition engine using high concentration of ammonia mixed with dimethyl ether'. In: *Applied Energy* 113 (2014), pp. 488–499. ISSN: 0306-2619. DOI: https://doi.org/10.1016/j.apenergy.2013.07.065. URL: https://www.sciencedirect.com/science/article/pii/S0306261913006326.

[63] Lars Seidel et al. 'Comprehensive kinetic modeling and experimental study of a fuel-rich, premixed n-heptane flame'. In: *Combustion and Flame* 162.5 (2015), pp. 2045–2058. ISSN: 0010-2180. DOI: https://doi.org/10.1016/j.combustflame.2015.01.002. URL: https://www.sciencedirect.com/science/article/pii/S001021801500005X.

[64] K. P. Shrestha et al. 'An experimental and modeling study of ammonia with enriched oxygen content and ammonia/hydrogen laminar flame speed at elevated pressure and temperature'. In: *Proceedings of the Combustion Institute* 38 (2021), pp. 2163–2174. DOI: https://doi.org/10.1016/j.proci.2020.06.197.

[65] K. P. Shrestha et al. 'Detailed Kinetic Mechanism for the Oxidation of Ammonia Including the Formation and Reduction of Nitrogen Oxides'. In: *Energy Fuels* 32 (2018), pp. 10202–10217. DOI: https://doi.org/10.1021/acs.energyfuels.8b01056.

[66] Krzysztof Jan Siczek. 'Chapter 2 - Principles of valve train operation'. In: *Tribological Processes in the Valve Train Systems with Lightweight Valves*. Ed. by Krzysztof Jan Siczek. Butterworth-Heinemann, 2016, pp. 3–18. ISBN: 978-0-08-100956-7. DOI: https://doi.org/10.1016/B978-0-08-100956-7.00012-6. URL: https://www.sciencedirect.com/science/article/pii/B9780081009567000126.

[67] G. P. Smith et al. *GRI-Mech 3.0*. URL: http://combustion.berkeley.edu/gri-mech/releases.html (visited on 27th Apr. 2022).

[68] TargetTrainingCentre. *Target Global Energy Training*. https://www.targettrainingcentre.nl/news/special/. May 2022.

[69] Hanqin Tian et al. 'A comprehensive quantification of global nitrous oxide sources and sinks'. eng. In: *Nature* 586.7828 (2020), pp. 248–256. ISSN: 0028-0836.

[70] M.J. TINDAL and O.A. UYEHARA. 'Chapter Three - Diesel Engines'. In: *Internal Combustion Engines*. Ed. by CONSTANTINE ARCOUMANIS. Academic Press, 1988, pp. 101–155. ISBN: 978-0-12-059790-1. DOI: https://doi.org/10.1016/B978-0-12-059790-1.50009-2. URL: https://www.sciencedirect.com/science/article/pii/B9780120597901500092.

[71] Sthepen R. Turns. *An Introduction to Combustion - Concepts and Applications*. Second. McGraw-Hill series in mechanical engineering, 2000.

[72] *TUTORIAL LOGEENGINE EXPERT SYSTEM – Diesel*. LOGE AB. Lund, Sweeden. URL: https://logesoft.com/.

[73] UNFCCC. 'UNFCCC'. In: *Paris Climate Change Conference - November 2015*. UNFCCC, Dec. 2015. URL: https://unfccc.int/sites/default/files/english_paris_agreement.pdf.

[74] A Valera-Medina et al. 'Ammonia for power'. In: *Progress in Energy and Combustion Science* 69 (2018), pp. 63–102. ISSN: 0360-1285. DOI: https://doi.org/10.1016/j.pecs.2018.07.001. URL: https://www.sciencedirect.com/science/article/pii/S0360128517302320.

[75] Hai Wang and Michael Frenklach. 'A detailed kinetic modeling study of aromatics formation in laminar premixed acetylene and ethylene flames'. In: *Combustion and Flame* 110.1 (1997), pp. 173–221. ISSN: 0010-2180. DOI: https://doi.org/10.1016/S0010-2180(97)00068-0. URL: https://www.sciencedirect.com/science/article/pii/S0010218097000680.

[76] G. Woschni. 'A Universally Applicable Equation for the Instantaneous Heat Transfer Coefficient in the Internal Combustion Engine'. In: *National Fuels and Lubricants, Powerplants, Transportation Meetings*. SAE International, Feb. 1967. DOI: https://doi.org/10.4271/670931. URL: https://doi.org/10.4271/670931.

[77] J. A. Wünning and J. G. Wünning. 'Flameless oxidation to reduce thermal NO-formation'. In: *Progress in Energy and Combustion Science* 23 (1997), pp. 81–94. DOI: https://doi.org/10.1016/S0360-1285(97)00006-3.

[78] A. Yousefi et al. 'Effects of ammonia energy fraction and diesel injection timing on combustion and emissions of an ammonia/diesel dual-fuel engine'. In: *Fuel* (2021). DOI: https://doi.org/10.1016/j.fuel.2021.122723.

[79] Amin Yousefi et al. 'Effects of ammonia energy fraction and diesel injection timing on combustion and emissions of an ammonia/diesel dual-fuel engine'. In: *Fuel* 314 (2022), p. 122723. ISSN: 0016-2361. DOI: https://doi.org/10.1016/j.fuel.2021.122723. URL: https://www.sciencedirect.com/science/article/pii/S0016236121025886.

[80] Kesong Zhang et al. 'Numerical simulation of diesel combustion based on n-heptane and toluene'. In: *Propulsion and Power Research* 8.2 (2019), pp. 121–127. ISSN: 2212-540X. DOI: https://doi.org/10.1016/j.jppr.2019.01.009. URL: https://www.sciencedirect.com/science/article/pii/S2212540X19300094.

Appendix

A Calibration report

LOGE engine
Expert System

Combustion analysis report

Simulation Parameters

Simulation Setup

Number of Particles: 200

Time step size: 0.5 [CAD]

Number of consecutive cycles: 10

Initial crank angle: -140 [CAD ATDC]

Final crank angle: 130 [CAD ATDC]

Mixing model used: Hybrid Curl/EMST (DI)

Calculate Soot: No

Stochastic variation: Yes

Mixing time model: K-epsilon VVAstandard

Intake valve diameter: 0.028 [m]

Maximum intake valve lift: 0.009 [m]

Fuel injection pressure: 2e+08 [Pa]

Mean liquid fuel density: 850 [kg/m3]

Input Files Setup

Liquid properties: :/mixingtimetuning/FUEL_SPECIES_DATA_Diesel.TXT

Fuel evaporation rate: C:/Users/Kristerp/Documents/LOGEengine/DI-Tutorial/YAGA/fuelinject_PP_1_Case_1.txt

EGR file: C:/Users/Kristerp/Documents/LOGEengine/DI-Tutorial/YAGA/EGR_PP_1_Case_1.txt

Initial GasComposition: C:/Users/Kristerp/Documents/LOGEengine/DI-Tutorial/YAGA/GASCOMPOSITION_PP_1_Case_1.txt

InputRedkin mechanism: :/chem/InputRedKinMec_Diesel.txt

InputRedkin thermodata: :/chem/InputRedKinTherm_Diesel.txt

Engine Setup

Engine Type: Diesel engine

Engine Speed: 2000 [RPM]

Compression Ratio: 16.5

Bore: 0.08 [m]

Stroke: 0.096 [m]

Connecting rod length: 0.14 [m]

Cylinder bowl diameter: 0.044 [m]

Cylinder bowl volume: 2e-06 [m3]

Cylinder bowl depth: 0.0144 [m]

Exhaust gas recirculation: 34.2207 [%]

EGR type: Mole % to oxidizer

Genetic Algorithm Setup

Elite combinations kept per generation: 10

Maximum generations calculated: 20

Initial mutation chance for an individual: 30 [%]

Mutationmodifier for each generation: 83 [%]

Keep additional simulation files: No

Heat Transfer Setup

Wall temperature: 490 [K]

Piston head temperature: 0 [K]

System Setup

MPI version used: IntelMPI

MPI flags used:

Cylinder head temperature: 0 [K]

Model: Woschni

C1: 2.28

C2: 0.0035

Swirl ratio: 0

Ap0: 1.2

Run locally: Yes

Cores used per combination: 4

Number of simultaneous combinations: 2

LOGE engine
Expert System

Analysis Parameters

Parameter	Value	Analysed	Lower bound	Upper bound
EGR [%]	34.2207	No		
Start of vaporisation [CAD ATDC]		Yes	-1	2
Pressure at IVC [Pa]	162023	No		
Temperature at IVC [K]	385.823	No		
Piston head surface factor (AP0) [-]	1.2	No		
Woschni C1 [-]	2.28	No		
Woschni C2 [-]	0.0035	No		
Woschni Swirl ratio [-]	0	No		
Constant Tau used:		No		
K-Epsilon mixing time density factor [-]	1	No		
K-Epsilon mixing time dissipation factor [-]	1	No		
K-Epsilon mixing time squish factor [-]	1	No		
K-Epsilon mixing time injection factor [-]		Yes	0.005	0.1
K-Epsilon mixing time swirl factor [-]	1	No		
K-Epsilon mixing time factor [-]		Yes	1	15

Target Parameters

Parameter	Value	Tolerance [%]
Pressure point 1 [Pa]	6.37639e+06 [Pa] @ -1 [CAD ATDC]	5
Pressure point 2 [Pa]	6.12759e+06 [Pa] @ 5.65 [CAD ATDC]	5
Pressure point 3 [Pa]	8.11802e+06 [Pa] @ 14.55 [CAD ATDC]	5
Pressure point 4 [Pa]	5.03041e+06 [Pa] @ 26.44 [CAD ATDC]	5
Pressure point 5 [Pa]	2.58338e+06 [Pa] @ 42.33 [CAD ATDC]	5
Pressure point 6 [Pa]	1.24028e+06 [Pa] @ 63.59 [CAD ATDC]	5
Pressure point 7 [Pa]	651102 [Pa] @ 92.01 [CAD ATDC]	5
Pressure point 8 [Pa]	413209 [Pa] @ 130 [CAD ATDC]	5
Pressure point 9 [Pa]	8.6619e+06 [Pa] @ 12 [CAD ATDC]	5

LOGE engine
Expert System

Result table

The best 10 combinations are shown in the table:

Comb	SOV	kepsInjection	kepsVVAL2	kepsTau	p_1[%]	p_2[%]	p_3[%]	p_4[%]	p_5[%]	p_6[%]	p_7[%]	p_8[%]	p_9[%]	Tolerances achieved	Total error
100	-0.376998	0.0377661	2.15205	7.61862	0.274208	0.955959	4.70711	4.55917	0.573678	0.860396	1.50998	2.10789000000000003	0.030961999999999996	YES	15.579353
194	-0.416013	0.036884	2.31256	7.58711	0.273427	0.558905	2.62841	3.138309999999997	0.539204999999999	1.293910000000001	2.270580000000003	2.97382	2.00909	YES	15.685657
52	-0.228541	0.0422233	2.40751	7.77784	0.277323	1.03607	4.117719999999999	4.114870000000001	0.558912000000001	0.918825	1.702450000000002	2.34494	0.646914	YES	15.718024
72	-0.627439	0.0341369	2.19648	7.92493	0.281294	0.20695700000000003	1.58948	3.662	0.668745	1.49404	2.332	3.04142	2.56287	YES	15.838806
43	0.0028035	0.0566376	2.66562	8.09995	0.325096	0.20793999999999999	3.54497	4.896500000000005	0.846449	0.956322000000001	1.454289999999999	2.04409	1.66777	YES	15.9434270000000003
170	-0.439537	0.0368801	2.29335	7.6391	0.274069	1.01038	3.898560000000002	4.28871	0.823604	1.060649999999999	1.84953	2.42675	0.577519	YES	16.2097719999999997
188	-0.448683	0.0360708	2.40416	7.62497	0.307765	0.289987	4.21563	4.99909	0.715124	0.99632	1.564269999999998	2.17227	1.01122	YES	16.2716760000000003
124	-0.259697	0.047056	2.54984	7.75871	0.27132	0.48562900000000003	2.84516	4.18059	0.894828	1.26631	2.16234	2.766390000000003	1.50425	YES	16.376817
154	-0.614777	0.0346081	2.24739	7.70699	0.285348	0.77944	2.17153	3.053	0.953155	1.40063	2.362020000000002	3.0234	2.54959	YES	16.5781130000000002
133	-0.455028	0.036002	2.47308	7.55559	0.273264	1.57103	3.22912	4.24249	0.843747	1.12859	2.02702	2.70409	0.717457	YES	16.736808

LOGE engine
Expert System

Best combination: 100

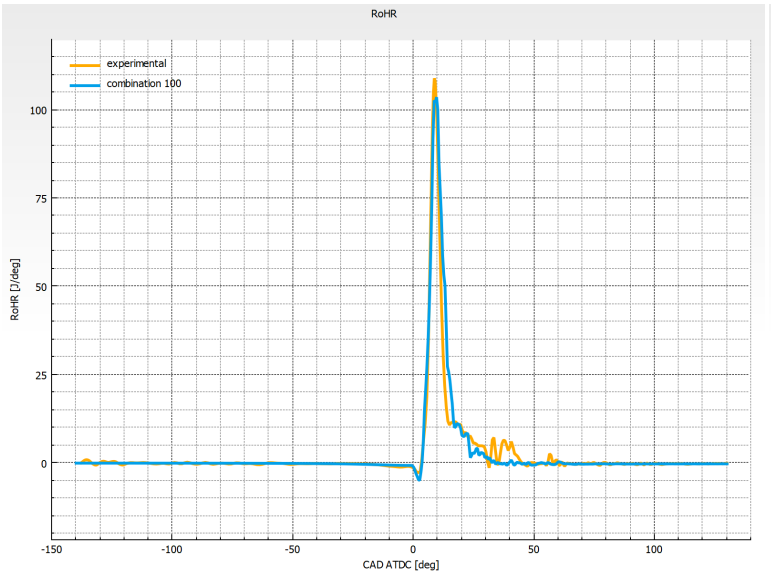

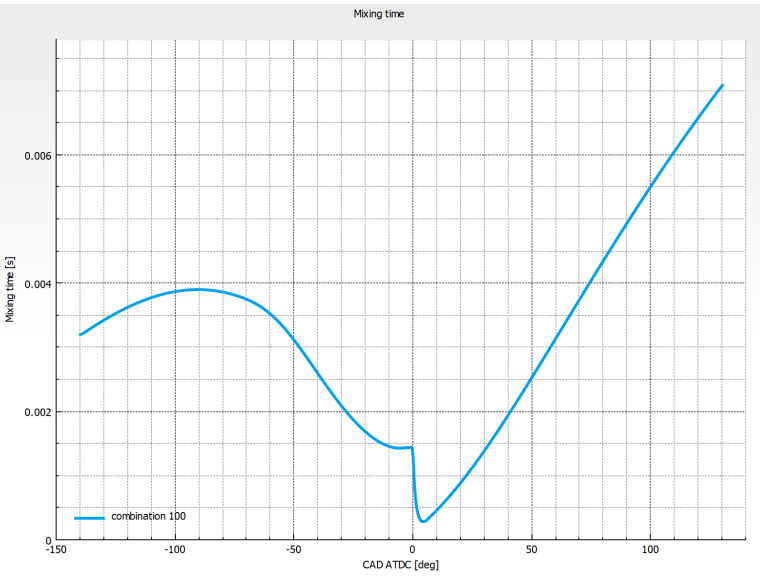

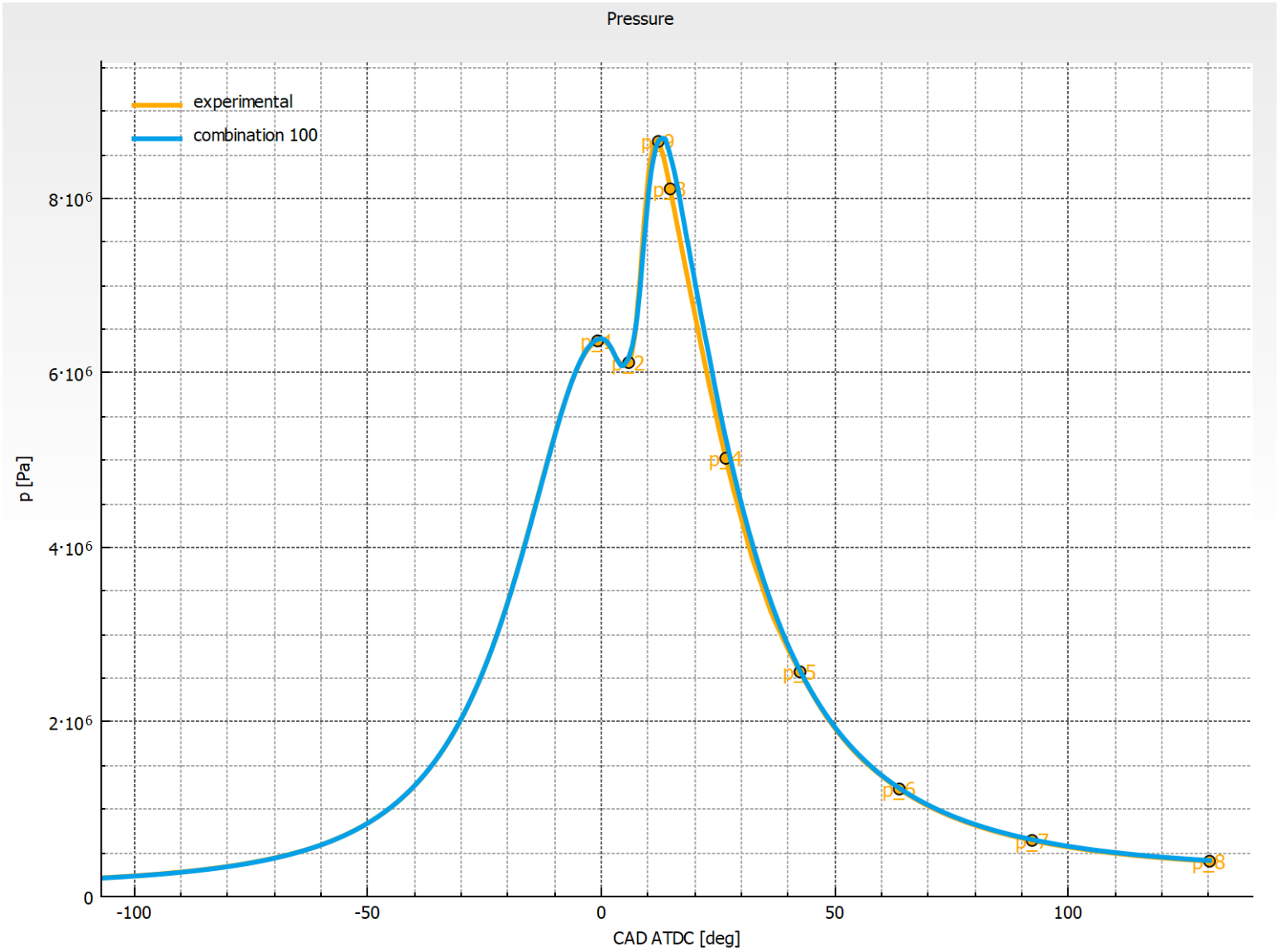
Pressure
experimental
combination 100
p_0
p_1
p_2
p_3
p_4
p_5
p_6
p_7
p_8
8·10^6
6·10^6
4·10^6
2·10^6
0
p [Pa]
-100
-50
0
50
100
CAD ATDC [deg]

B NO formation pathways

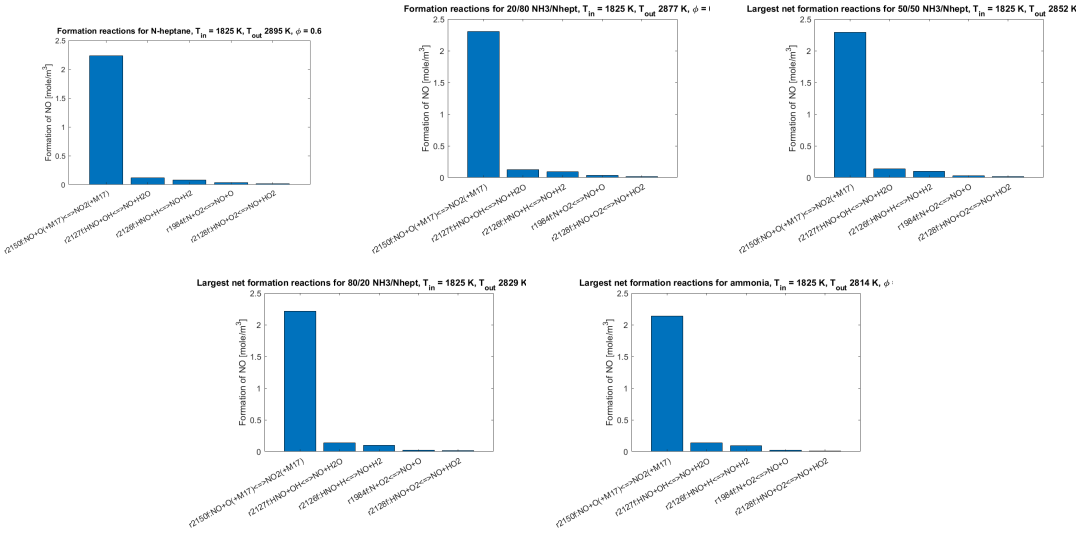

Figure 38: NO formation pathways for high temperature and an equivalence ratio of 0.6.

C NOx analysis in the ignition phase

D Dilution investigation

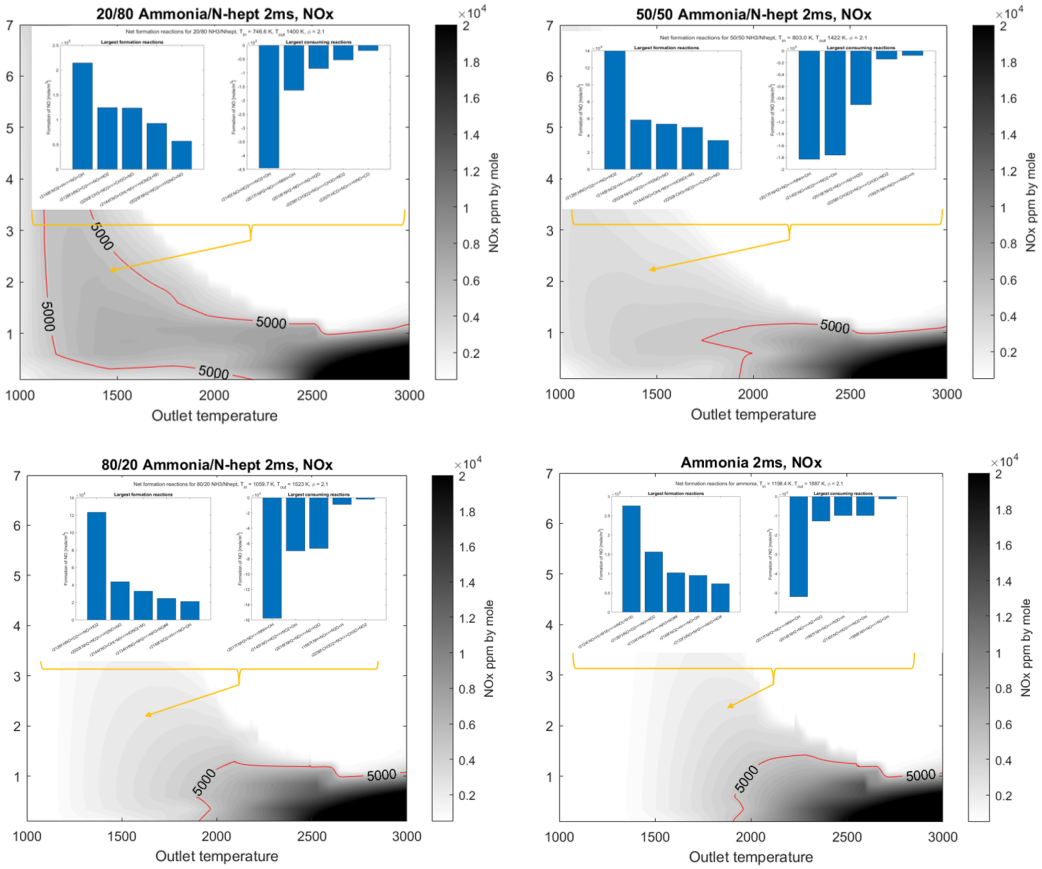

Figure 39: ϕ-T map with net NO formation pathways for five different cases at in uncomplete combustion zone.

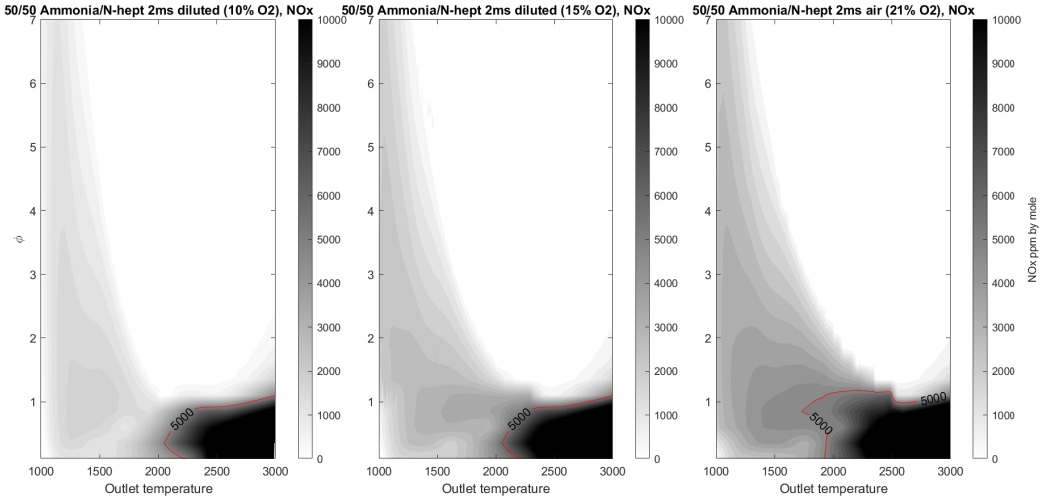

Figure 40: ϕ-T map with NOx emissions for three different dilution levels (21 % O_2, 79 % N_2,15 % O_2, 85 % N_2, 10 % O_2, 90 % N_2)

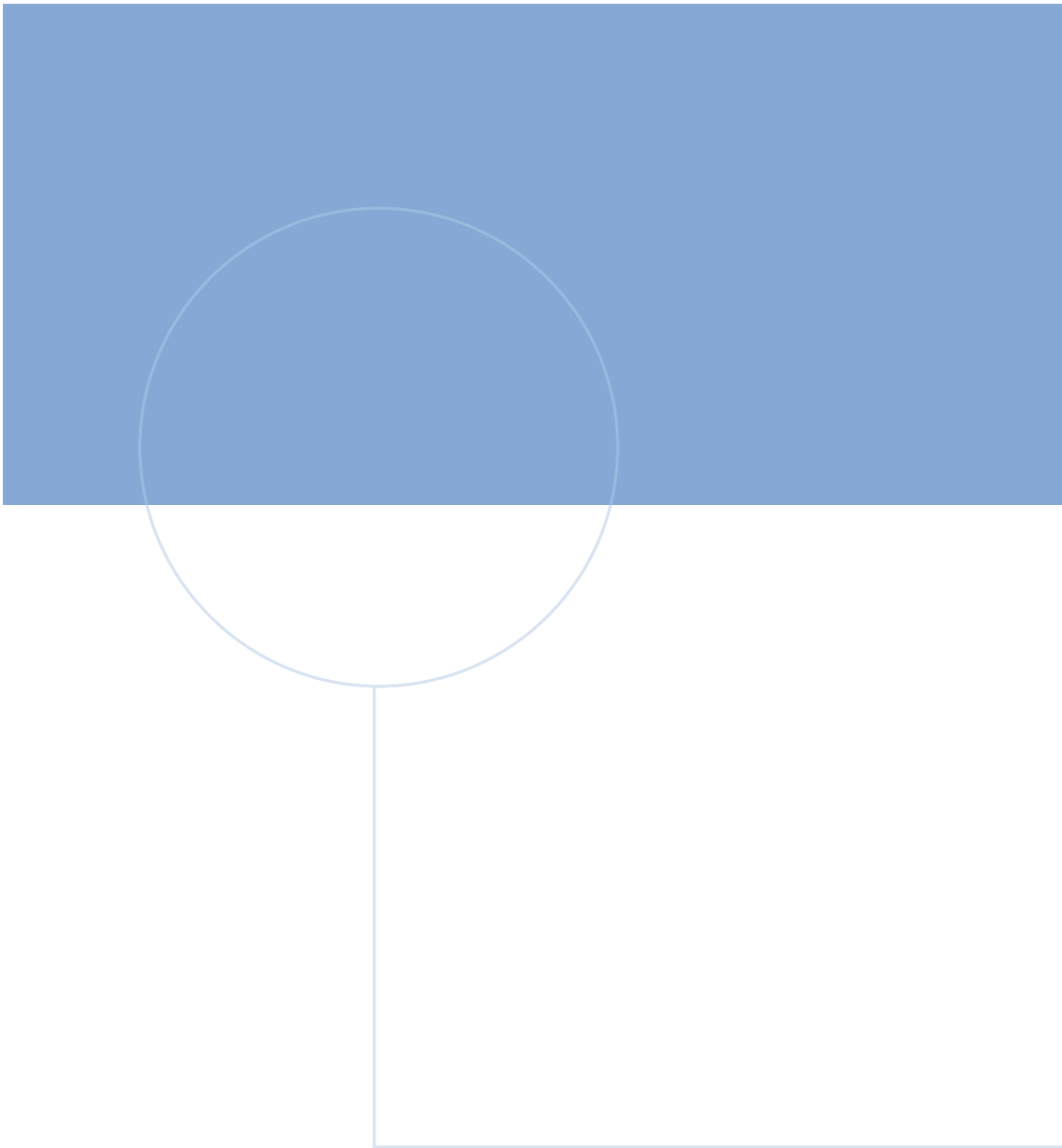

NTNU

Norwegian University of
Science and Technology